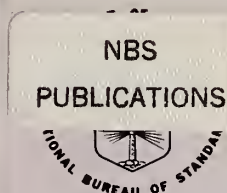


A11102 577875



NAT'L INST OF STANDARDS & TECH R.I.C.  
A11102577875  
Symposium on Optical/Technical digest -  
QC100 .U57 NO.720 1986 V1986 C.2 NBS-PUB

## ECIAL PUBLICATION 720

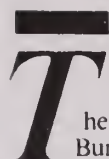
U.S. DEPARTMENT OF COMMERCE / National Bureau of Standards

# Technical Digest Symposium on Optical Fiber Measurements, 1986

Sponsored by the National Bureau of Standards  
in cooperation with the IEEE Optical Communications Committee  
and the Optical Society of America

QC  
100  
.U57  
No.720  
1986  
c.2





The National Bureau of Standards<sup>1</sup> was established by an act of Congress on March 3, 1901. The Bureau's overall goal is to strengthen and advance the nation's science and technology and facilitate their effective application for public benefit. To this end, the Bureau conducts research and provides: (1) a basis for the nation's physical measurement system, (2) scientific and technological services for industry and government, (3) a technical basis for equity in trade, and (4) technical services to promote public safety. The Bureau's technical work is performed by the National Measurement Laboratory, the National Engineering Laboratory, the Institute for Computer Sciences and Technology, and the Institute for Materials Science and Engineering.

### *The National Measurement Laboratory*

Provides the national system of physical and chemical measurement; coordinates the system with measurement systems of other nations and furnishes essential services leading to accurate and uniform physical and chemical measurement throughout the Nation's scientific community, industry, and commerce; provides advisory and research services to other Government agencies; conducts physical and chemical research; develops, produces, and distributes Standard Reference Materials; and provides calibration services. The Laboratory consists of the following centers:

- Basic Standards<sup>2</sup>
- Radiation Research
- Chemical Physics
- Analytical Chemistry

### *The National Engineering Laboratory*

Provides technology and technical services to the public and private sectors to address national needs and to solve national problems; conducts research in engineering and applied science in support of these efforts; builds and maintains competence in the necessary disciplines required to carry out this research and technical service; develops engineering data and measurement capabilities; provides engineering measurement traceability services; develops test methods and proposes engineering standards and code changes; develops and proposes new engineering practices; and develops and improves mechanisms to transfer results of its research to the ultimate user. The Laboratory consists of the following centers:

- Applied Mathematics
- Electronics and Electrical Engineering<sup>2</sup>
- Manufacturing Engineering
- Building Technology
- Fire Research
- Chemical Engineering<sup>2</sup>

### *The Institute for Computer Sciences and Technology*

Conducts research and provides scientific and technical services to aid Federal agencies in the selection, acquisition, application, and use of computer technology to improve effectiveness and economy in Government operations in accordance with Public Law 89-306 (40 U.S.C. 759), relevant Executive Orders, and other directives; carries out this mission by managing the Federal Information Processing Standards Program, developing Federal ADP standards guidelines, and managing Federal participation in ADP voluntary standardization activities; provides scientific and technological advisory services and assistance to Federal agencies; and provides the technical foundation for computer-related policies of the Federal Government. The Institute consists of the following centers:

- Programming Science and Technology
- Computer Systems Engineering

### *The Institute for Materials Science and Engineering*

Conducts research and provides measurements, data, standards, reference materials, quantitative understanding and other technical information fundamental to the processing, structure, properties and performance of materials addresses the scientific basis for new advanced materials technologies; plans research around cross-country scientific themes such as nondestructive evaluation and phase diagram development; oversees Bureau-wide technical programs in nuclear reactor radiation research and nondestructive evaluation; and broadly disseminates generic technical information resulting from its programs. The Institute consists of the following Divisions:

- Ceramics
- Fracture and Deformation<sup>3</sup>
- Polymers
- Metallurgy
- Reactor Radiation

<sup>1</sup>Headquarters and Laboratories at Gaithersburg, MD, unless otherwise noted; mailing address Gaithersburg, MD 20899.

<sup>2</sup>Some divisions within the center are located at Boulder, CO 80303.

<sup>3</sup>Located at Boulder, CO, with some elements at Gaithersburg, MD.

1155  
02100  
1057  
1172  
1986  
C12

# Technical Digest—Symposium on Optical Fiber Measurements, 1986

---

Digest of a Symposium sponsored by the  
National Bureau of Standards  
in cooperation with the  
IEEE Optical Communications Committee  
and the Optical Society of America

September 9-10, 1986  
National Bureau of Standards  
Boulder, Colorado 80303

Edited by  
G.W. Day  
D.L. Franzen

Electromagnetic Technology Division  
Center for Electronics and Electrical Engineering  
National Engineering Laboratory  
National Bureau of Standards  
Boulder, Colorado 80303



---

U.S. DEPARTMENT OF COMMERCE, Malcolm Baldrige, Secretary

NATIONAL BUREAU OF STANDARDS, Ernest Ambler, Director

Issued September 1986

Library of Congress Catalog Card Number: 86-600563

National Bureau of Standards Special Publication 720  
Natl. Bur. Stand. (U.S.), Spec. Publ. 720, 158 pages (Sept. 1986)  
CODEN: XNBSAV

U.S. GOVERNMENT PRINTING OFFICE  
Washington: 1986



## PREFACE

One might expect that, as a technology matures, associated measurement problems would be solved and research in those areas would diminish. That view is supported by examination of the programs for the annual Optical Fiber Communications Conference (OFC) and European Conference on Optical Communications (ECOC) which have shown a steady decline in the percentage of papers on measurement topics over the last 10 years. It is not supported by our experience with the Symposium on Optical Fiber Measurements. Rather, it appears that the need for a specialized meeting on the topic of measurements continues to grow.

We believe that the strength of this Symposium is best indicated by the number and quality of contributed papers. The number of papers submitted to the committee has grown by roughly 20 percent with each succeeding Symposium. Unfortunately, the time available for presentation could be increased at only half that rate. This year, only about 50 percent of the papers received by the program chairman could be accepted. Those that were accepted are diverse in both subject and origin. In only two technical areas, chromatic dispersion and joint characterization (including mode field diameter measurements), was it possible to schedule a full session on a single topic. In origin, there are 21 organizations in 9 countries represented in the program. Over 40 percent of the papers are from outside the U.S.

This Digest contains the text of all 34 papers presented (5 invited and 29 contributed). In addition to these formal presentations, two informal workshops were held. One, on "Components and Measurements for LAN's and Wide-band Premise Networks" was moderated by Allen Cherin of AT&T Bell Laboratories. The other, "Measuring the Future--Strategies for Upgradability" was moderated by Paul Reitz of Corning Glass Works. There is no written record of the workshops.

We continue to be indebted to the IEEE Optical Communications Committee and the Optical Society of America for their assistance in organizing this Symposium. The members of this year's committee, listed on the following page, have been especially helpful in providing timely reviews of manuscripts and other suggestions on the program.

G. W. Day  
D. L. Franzen  
Boulder, Colorado  
September 1986

#### SYMPOSIUM COMMITTEE

D. L. Franzen, NBS, General Chairman  
G. W. Day, NBS, Program Chairman  
A. H. Cherin, AT&T Bell Laboratories  
R. L. Gallawa, NBS  
P. Kaiser, Bell Communications Research  
F. P. Kapron, ITT  
T. Ito, NTT  
D. B. Payne, BTRL  
P. R. Reitz, Corning  
O. Szentesi, Siecor

## CONTENTS

	Page
Preface.....	iii
Conference Committee.....	iv
Status of single-mode fiber measurements (invited) William T. Anderson; Bell Communications Research.....	1
Study of algorithms used to fit group delay data for single-mode optical fibers W. A. Reed, D. L. Philen; AT&T Bell Laboratories.....	7
Chromatic dispersion in optical fibers: Comparison of measurements with models Leslie Button, Walter F. Love, Robert M. Hawk; Corning Glass Works.....	11
Accuracy of phase shift technique with LEDS for measuring total dispersion in singlemode fibers L. Bosselaar, G. Kuijt, J. F. van Luijk, P. Matthijsse Philips Glass.....	15
High speed and high accurate single-mode fiber dispersion measuring equipment using modified interferometric method Y. Namihiro, Y. Iwamoto; KDD.....	19
Chromatic dispersion measurements of single mode fibres in the 1.3 $\mu\text{m}$ and 1.55 $\mu\text{m}$ wavelength range by the wavelength temperature tuning technique Finn Mogensen, Hans Damsgaard, Ole Hansen; NKT Elektronik.....	23
Measurement of dopants in optical fibers by Raman scattering Dan L. Philen; AT&T Bell Laboratories.....	27
Utilizing cladding mode propagation to determine the refractive index profile of an optical fiber W. H. Hatton, E. L. Buckland, M. Nishimura; Sumitomo Electric Research Triangle.....	31
Determination of refractive-index distribution from near-field measurements in polarization maintaining fibres G. Coppa, P. Di Vita, M. Potenza; CSELT.....	35
Prism coupling technique: A novel method for measurement of propagation constant and beat length in single mode fibers K. Thyagarajan, M. R. Shenoy, M. R. Ramadas; Indian Institute of Technology.....	39
Characterization of optical fiber splices in the field (invited) Reinhard Engel, Siemans; Everett McNair, Siecor.....	43
Consistency of mode field diameter definitions for fibers with Gaussian and non-Gaussian field profiles in different measurement domains W. T. Anderson, J. P. Kilmer; Bell Communications Research.....	49
A new technique for mode field diameter determination by transverse offset measurements M. Calzavara, G. Coppa, P. Di Vita; CSELT.....	53

Joint losses as a function of offset and mode field diameters for dispersion-shifted and standard fibers and fiber combinations V. Shah, L. Curtis, W. C. Young; Bell Communications Research.....	57
A novel single-mode fiber splice alignment and loss measurement using local detection Ian A. White, Paul D. Ludington; AT&T Bell Laboratories.....	61
Fusion splicing of dissimilar fibers--A comparison of mode field diameter and cross correlation loss predictions with experimental results W. T. Anderson, A. J. Johnson, J. P. Kilmer, E. A. Thomas; Bell Communications Research.....	65
Stress-induced increases in interference effects at fiber joints and a method to eliminate interference effects in optical fiber measurements W. C. Young, V. Shah, L. Curtis; Bell Communications Research.....	69
Practical one-way-loss range for OTDRs M. C. Brain, E. A. Cottrell; British Telecom Research Laboratories.....	73
A new technique for the relative measurement of scatter levels in single mode fibers M. E. Fermann, S. B. Poole, D. N. Payne, F. Martinez; Southampton University.....	77
Mode field diameter effects on OTDR splice measurements Felix Kapron, Carrie Kozikowski, Ricky Crotts; ITT Electro-Optical Products Division.....	81
Multimode fiber systems characterization I. P. Vayshenker, D. R. Hjelme, A. R. Mickelson; University of Colorado.....	85
Single-ended bandwidth measurement for multimode optical fiber using far end pulse reflection Shin-ichi Furukawa, Katsuya Yamashita, Mitsuhiro Tateda, Yahei Koyamada; NTT.....	89
Effective fiber bandwidth in LED based systems Dieter Schickentanz, William S. Jackman; Siecor.....	93
Measuring 825 nm transmission on 1300 nm single-mode fibers Catherine M. Ragdale, Felix P. Kapron; ITT.....	97
Characterization of sources and detectors for optical fiber systems (invited) T. Ito, K. Kurumada; NTT.....	101
Characterization of specialty fibres and components (invited) D. N. Payne, S. B. Poole; Southampton University M. P. Varnham; British Aerospace R. D. Birch; Southampton University.....	107
Measurement requirements for waveguide electro-optic devices (invited) R. C. Alferness; AT&T Bell Laboratories.....	115



Practical upper limits to cutoff wavelength for different single mode fiber designs L. Wei, C. Saravanos, R. S. Lowe; Northern Telecom Canada Limited.....	121
New measurement technique for measurement of microbend losses in single mode fibers A. O. Garg, C. K. Eoll; Siecor.....	125
Predicting microbending losses in single-mode fibers Neil Kamikawa; Naval Ocean Systems Center Ching-Ten Chang; San Diego State University.....	129
On the numerical aperture of a single-mode fiber D. N. Christodoulides, L. A. Reith, M. A. Saifi; Bell Communications Research.....	133
Optical fibre far field ESI determination using the equalisation wavelength A. C. Boucouvalas, S. C. Robertson, J. Walker; GEC Research.....	137
Impact of reflection on the performance of single-mode fiber optic systems Shuenn Jyi Wang; Bell Communications Research.....	141
Spurious edge elimination for accurate glass geometry measurements Devon R. McIntosh, David A. Hall; Corning Glass Works.....	145
Index of Authors.....	149

Except where attributed to NBS authors, the content of individual sections of this volume has not been reviewed or edited by the National Bureau of Standards. NBS therefore accepts no responsibility for comments or recommendations therein. The mention of trade names in this volume is in no sense an endorsement or recommendation of the National Bureau of Standards.



# STATUS OF SINGLE-MODE FIBER MEASUREMENTS

by William T. Anderson  
Bell Communications Research

## 1. INTRODUCTION

Single-mode fiber manufacture has advanced dramatically over the past several years. Today, typical fibers approach the performance levels of the champion results reported only five years ago, with the attenuation approaching the theoretical minimum levels dictated by Rayleigh scattering. Consistent with the advance of the manufacturing state of the art, single-mode fiber measurements have advanced in ease and accuracy, and state of the art measurements which could be made only in the laboratory in the past are now being made in the factory and in the field. However, with these advances in the measurement state of the art, new problems have been discovered. In this paper, the current state of the art will be briefly reviewed with emphasis on measurements or specification issues where controversy still exists. In the following sections, the four major measurements will be covered: attenuation, dispersion, mode field diameter, and cutoff wavelength.

## 2. ATTENUATION

The measurement of attenuation is the oldest and, conceptually, the simplest of the single-mode fiber measurements. Three measurement techniques are commonly used. The most familiar of these is the cutback technique. Typically, a tungsten-halogen lamp and monochromator provide a low-power but wavelength-tunable source, and a lock-in amplifier is used for synchronous detection of the output of an unbiased PIN photodiode. The repeatability of the cutback technique is dependent primarily upon the ability to repeatably couple the fiber output to the detector. Standard deviations of .01 to .04dB and the dynamic ranges of 20 to 35dB are typical for this technique.

For installed spans or connectorized cables, a destructive technique such as cutback is inappropriate. In these cases, the attenuation by substitution or insertion loss techniques are commonly employed. The launch and detector coupling are made through connectors, and unlike the cutback technique, both launch and detect coupling must be accurately reproducible. Also, for an installed span the source and detector are separated so that either two detectors or a source with excellent long term stability are required. A systematic bias can be introduced by using two detectors which are not accurately cross-calibrated or by using fiber jumpers whose mode field diameters differ significantly from those of the fibers in the installed span. These factors clearly make the characterization of installed spans less accurate than the characterization of fiber and cable using the cutback technique.

A third commonly used attenuation measurement technique is backscatter, which employs an optical time domain reflectometer (OTDR). Unlike other measurement techniques, OTDRs can locate faults, measure splice losses, and resolve the attenuation coefficient throughout the installed span. OTDRs are also single-ended, so the measurement of installed spans requires only one craftsman rather than the two required by the substitution method. However, OTDRs have two significant disadvantages. First, the resolution of even the best and newest units is on the order of 100m, making it impossible to resolve the first one or two splices in an installed span. Second, OTDRs do not measure loss directly, but infer loss from the measured backscatter of the fiber. Differences in the backscatter capture coefficient along the span can produce inaccurate loss estimates, especially for mismatched fibers, and reports of splice gain are common. Averaging two bidirectional measurements can eliminate this effect, but only at the cost



of doubling the time and effort required to make the measurement.

While the measurement of attenuation is relatively straightforward, the specification of attenuation is complicated by the uncertainty of the wavelength of the sources. Based upon the typical wavelength ranges of currently used laser diodes, a wavelength "window" (e.g., 1285 to 1330nm) is often used as the basis for a specification on the allowable variation in the attenuation with wavelength (typically 0.1dB/km). However, with the advent of LEDs for subscriber loop applications and the possibility of wavelength division multiplexing in the future, a rigid window specification appears to be inadequate. Since the level of OH contamination in the fiber is typically the major limitation to the width of the low-loss window, a specification on the maximum loss at 1390nm may be more efficient than a multiplicity of windows for the multiplicity of possible sources. The specification and measurement of this "water peak" needs further study.

### 3. DISPERSION

The great information transmission capacity of single-mode fibers which makes them so attractive as a medium also makes the measurement of the information capacity very difficult. Since the major limitation in capacity for systems operating below tens of Gbit/sec is chromatic dispersion, indirect measurement techniques for determining the information transmission capacity by characterizing this change in group velocity with wavelength are often used. Two similar techniques are frequently employed: measuring the transit time of pulses at different wavelengths and measuring the phase shift of a modulated carrier at different wavelengths. The former approach may use a fiber raman laser<sup>[1]</sup> or multiple laser diodes<sup>[2]</sup> as the optical source, while the latter approach may employ either multiple laser diodes<sup>[3]</sup> or an LED and monochromator<sup>[4]</sup>. The directly measured delay data is usually too noisy or too discrete to allow numerical differentiation directly with acceptable accuracy, so the delay data is usually fitted to an analytical function, which can then be differentiated directly. However, there is some doubt about the validity of the three term sellmeier expansion which is most often used as a functional form for fitting delay data<sup>[5]</sup>. This is especially true of dispersion-shifted and -flattened fibers, for which no functional form is known *a priori*.

If instead of measuring group delay, one measured the change in group delay between two closely spaced wavelengths, then this differential delay would be an accurate approximation to the dispersion if the wavelength spacing were sufficiently small. A similar concept is used in differential spectroscopy. Two means of measuring differential delay are shown in figures 1 and 2. In the first method, an LED is used as a broad spectral source, and two closely spaced wavelengths are selected and detected. The phase difference is directly measured, and an accurate approximation to the dispersion is obtained without any assumptions about its spectral shape (except, of course, that the dispersion is slowly varying with wavelength). A second method employs a low frequency wavelength modulation on the output of the high frequency amplitude modulated LED, for instance by wobbling a monochromator grating<sup>[6]</sup>. This introduces a phase modulation in the output of the detector due to the variation in transit time in the fiber with wavelength, and this phase modulation is detected synchronously from the quadrature output of the high frequency mixer. This method offers more flexibility in choosing the spectral width and wavelength modulation width than does the other differential modulation technique.

The direct measurement of differential delay promises to eliminate the uncertainties of data fitting, although, in principle, similar benefits can be derived from the conventional delay measurement approach if the number of wavelengths is sufficiently large and the measurement error is suitably small.



Increasing the number of measurement wavelengths is feasible with either the fiber raman laser or the LED/monochromator, but not with multiple laser diodes. It may be possible to reduce the size and complexity of fiber raman sources by using non-silica raman fibers, which can be pumped with semiconductor lasers<sup>[7]</sup>.

The specification of dispersion has been a subject of recent controversy. The usual approach of specifying the maximum dispersion in a fixed wavelength window, similar to the specification of the wavelength variation of attenuation, is too inflexible to permit efficient system design using a multiplicity of possible sources, such as LEDs. For conventional step-index fibers, the dispersion is approximated by a sellmeier expansion. While this approximation may be too inaccurate for the measurement of dispersion, it may be sufficiently accurate for the specification of dispersion. The zero dispersion wavelength and the slope of the dispersion at the zero dispersion wavelength, used with the sellmeier approximation, have been proposed as the basis for the specification of dispersion. This method is more flexible than a window specification and permits the calculation of the dispersion over any desired wavelength window. However, there are questions about the accuracy and consistency of dispersion measurements made using the different techniques, and a round-robin series of measurements are planned to resolve this issue. For dispersion-shifted and -flattened fibers, for which no general functional form is known, a different method of specification is needed.

#### 4. MODE FIELD DIAMETER

In contrast to the difficult measurement of dispersion, the measurement of the mode field diameter is quite easy to implement. Perhaps it is too easy since there are so many proposed measurement techniques, and the challenge facing the industry is to ensure that all measurement techniques give consistent results for all fiber designs. Five techniques are currently being considered by the EIA and CCITT for standardization:

1. Scanning the fiber near fields by focusing a greatly magnified image of the fiber core either onto an infrared vidicon or onto the plane of a scanning small-area detector<sup>[8]</sup>.
2. Measuring the transmission through a splice as a function of offset, from which the two dimensional autocorrelation of the near fields can be obtained<sup>[9]</sup>.
3. Measuring the fiber far fields any of three ways:
  - a. Scanning a small area detector in the far field<sup>[10]</sup>.
  - b. Measuring transmission through apertures in the far field as a function of aperture radius<sup>[11]</sup>.
  - c. Measuring transmission past a knife edge in the far field as a function of lateral position<sup>[12]</sup>.

All of these techniques have certain advantages, and there appears to be little chance that any one of them will be widely accepted as a standard, or reference, technique by which the others could be judged. Therefore, consistency among the techniques is essential if the mode field diameter is to be used as a measure of the optical compatibility of two fibers.

The degree of consistency achievable with these five techniques is a direct result of the choice of a definition for the mode field diameter. Originally, the gaussian approximation, proposed by Marcuse<sup>[13]</sup> to explain single-mode fiber splice loss, was applied to data generated by the various measurements, but, since the fields of even a perfect step-index fiber are only approximately gaussian, small but systematic differences among the measurement techniques were observed for quasi-step index fibers, especially at longer wavelengths<sup>[14][15]</sup>. Differences of greater than 10% have been observed for non-step-index dispersion-shifted fibers<sup>[16]</sup>. Clearly, the gaussian approximation is not universally applicable.

An alternative definition based upon the second moment of the far fields, which is frequently called the "Petermann 2" definition<sup>[17][18]</sup>, can, in principle, solve this problem. Since the five measurements are related by several transforms to a good approximation, the second moment definition can be mapped from one measurement domain to another, and, in theory, consistency can be maintained. For example, the near fields, far fields, and autocorrelation are related by Hankel transforms. The far fields, knife edge scan, and variable aperture scan are related by Abel transforms. The knife edge scan and the autocorrelation function are related by the Fourier transform. Consistency between three of the five techniques has been demonstrated, and a round-robin measurement of non-step-index fibers, which is needed to confirm the applicability of this definition to all measurement techniques, is planned.

A consistent definition and improved measurement accuracy could lead to a more accurate specification of the mode field diameter. Since the specified mode field diameter is used to estimate the loss to be expected when dissimilar fibers are spliced, a more accurate specification would give a more accurate picture of the compatibility between fibers of different designs. Also, as splicing equipment and techniques improve, a larger fraction of the splice loss is attributable to fiber parameter mismatch, so a tighter tolerance on the variation of the mode field diameter may be appropriate.

## 5. CUTOFF WAVELENGTH

The concept of cutoff wavelength is deceptively simple. In theory, at wavelengths longer than the cutoff wavelength, the fiber supports only one mode (actually, a degenerate mode group). However, it is well known that the higher order modes become highly attenuated at wavelengths substantially below the theoretical cutoff wavelength. By convention, the "effective" cutoff wavelength is defined as the wavelength at which the higher order mode attenuation exceeds some chosen level and, therefore, higher order modes cease to propagate significant distances. This is a universally accepted definition for telecommunication systems, where the distances between mode coupling perturbations, such as splices, are typically on the order of hundreds of meters, and the adverse effects of multimode propagation, modal noise and distortion, can be avoided if the higher order modes are sufficiently attenuated. For short distance applications, such as fiber sensors, there may be different requirements.

The attenuation level which defines the cutoff wavelength depends upon the measurement technique. CCITT and EIA specify a measurement sample two meters long with a 28cm diameter loop<sup>[19]</sup>. The cutoff wavelength can be measured using two possible methods, as shown in figure 3. First, cutoff is identified as the wavelength above which a small diameter (typically 3 to 5 cm) loop changes the attenuation by less than 0.1dB (the bend reference method). Alternatively, cutoff is identified as the wavelength above which the transmission through the single-mode sample, when normalized by the transmission through a multimode reference fiber, approaches a linear region to within 0.1dB (the multimode reference technique). A round-robin measurement has verified that these two methods give approximately equal values for the cutoff wavelength<sup>[20]</sup>. Either of these methods equate cutoff with approximately 20dB of attenuation for the higher order mode, although this attenuation may be attributable to either the sample length or the bend, depending upon the fiber design.

These measurement conditions give a convenient and repeatable measurement, but the actual deployment conditions of the fibers will be different from those in this measurement. Since both fiber length and bending significantly alter the measured cutoff wavelength<sup>[21][22]</sup>, relating measurements made using this arbitrarily chosen length and bend condition do not relate simply to the design of telecommunications systems. To avoid modal noise and distortion, the attenuation of the higher order



mode must be large over the shortest distance between mode coupling perturbations, such as splices. While this distance is typically kilometers, it can be substantially shorter for jumpers and pigtails, for stub cables, or under certain difficult installation situations or for repair sections. A measurement method for determining the cutoff wavelength of cabled fiber, for which the user would specify a sample length and deployment condition consistent with his application, is under consideration. While the cable specification can be less conservative than the fiber specification, there is not universal agreement that a less conservative specification is desirable, especially when using LEDs with single-mode fibers. A better understanding of future applications in the subscriber loop is needed.

## 8. CONCLUSIONS

Single-mode fiber measurements continue to be developed and improved at a rapid pace. However, the performance of fibers and splicing equipment has also improved, and greater accuracy is required to characterize fibers and splices. Because of the high cost of installing, splicing, and testing single-mode fiber cables, their potentially high capacity is a compelling advantage since upgrading the capacity of an existing span may avoid additional construction. However, exploitation of this high capacity in the future or initial operation with LEDs may require utilizing fibers in wavelength regions which are not presently used. The uncertainty of possible future uses of the fiber complicates the measurement and specification of attenuation, dispersion, and cutoff wavelength. This uncertainty can only be resolved when the technology of optical systems, and especially that of the optical sources, is mature.

## REFERENCES

1. L. G. Cohen and C. Lin, *Applied Optics*, Vol. 16, p. 3136, 1977.
2. C. Lin et al, *Bell Syst. Tech. J.*, Vol. 62, p. 457, Feb. 1983.
3. K. Tatekura et al, *Tech. Digest, Symposium on Optical Fiber Measurements, 1984*, p. 119.
4. B. Costa et al, *Electron. Lett.*, Vol. 19, p. 1074, Dec. 1983.
5. F. P. Kapron and T. C. Olson, *Tech. Digest, Symp. on Optical Fiber Measurements, 1984*, p. 111.
6. A. G. Barlow and R. S. Jones, to be published.
7. H. Takahashi et al, *Optics Letters*, Vol. 11, No. 6, p. 383, June 1986.
8. Y. Murakami et al, *Applied Optics*, Vol. 18, p. 1101, 1979.
9. J. Streckert, *Opt. Lett.*, Vol. 5, p. 505, Dec. 1980.
10. K. Hotate and T. Okoshi, *Applied Optics*, Vol. 18, p. 3265, 1979.
11. E. Nicolaisen and P. Danielsen, *Electron. Lett.*, Vol. 19, p. 27, 1983.
12. W. G. Otten and F. P. Kapron, *Tech. Digest, OFC 86*, Paper TUL30.
13. D. Marcuse, *Bell Syst. Tech. J.*, Vol. 56, P. 703, 1977.
15. W. T. Anderson, *IEEE JLT*, Vol. LT-2, p. 191, April 1984.
15. D. L. Frantzen and R. Srivastava, *IEEE JLT*, Vol. LT-3, No. 5, Oct. 1985, p. 1073.
16. W. T. Anderson et al, measurement comparison to be published.
18. K. Petermann, *Electron. Lett.*, Vol. 19, p. 712, 1983.
18. C. Pask, *Electron. Lett.*, Vol. 20, p. 144, 1984.
19. CCITT Recommendation G.652 and EIA RS-455-80.
20. D. L. Frantzen, *IEEE JLT*, Vol. LT-3, No. 1, p. 128, Feb. 1985.
22. W. T. Anderson and T. A. Lenahan, *IEEE JLT*, Vol. LT-2, p. 238, June 1984.
22. V. S. Shah, *Tech. Digest, Symposium on Optical Fiber Measurements, 1984*, p. 7.

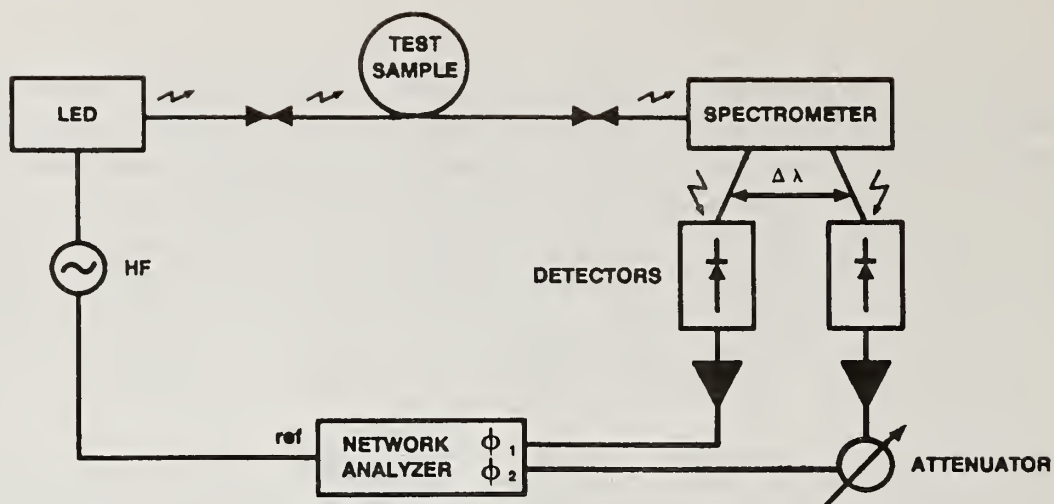


Figure 1- Differential Delay Dispersion Measurement

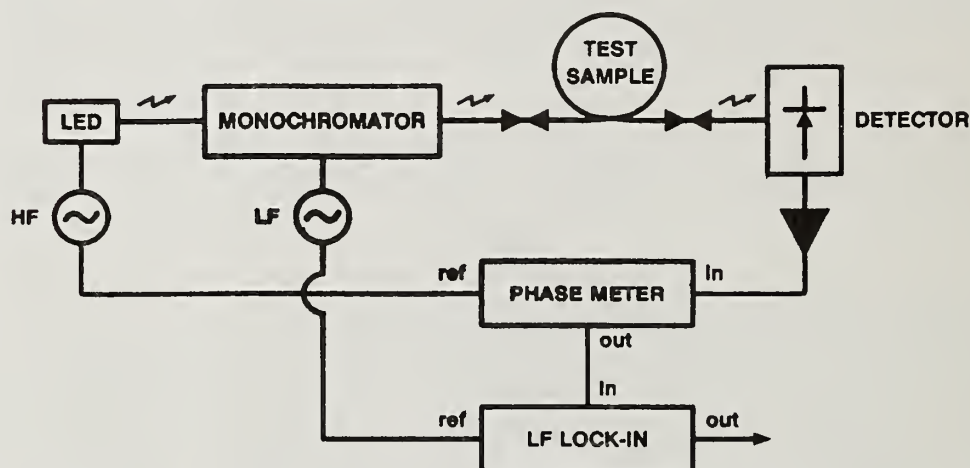


Figure 2- Double Modulation Dispersion Measurement

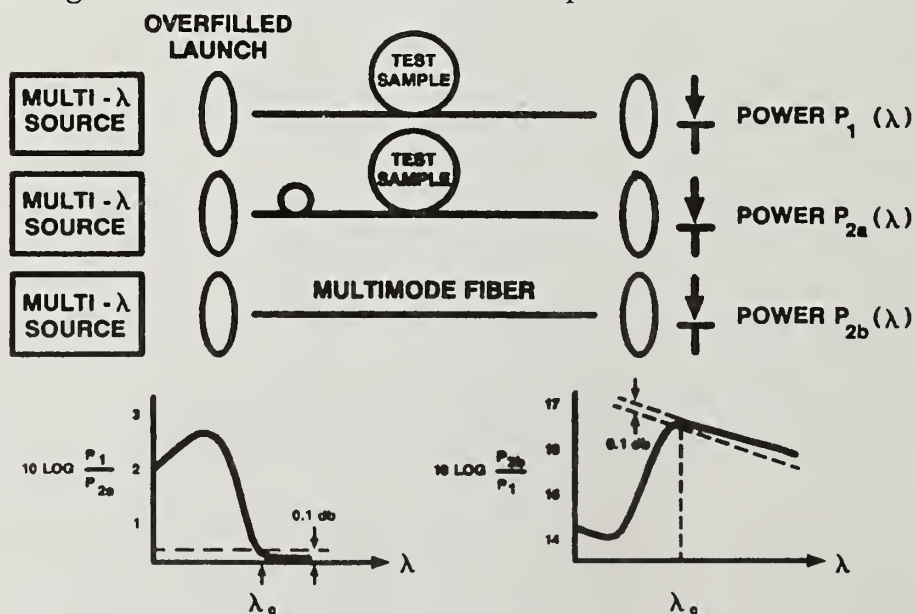


Figure 3- Cutoff Wavelength Measurement



## Study of Algorithms Used to Fit Group Delay Data for Single-Mode Optical Fibers

W. A. Reed  
AT&T Bell Laboratories  
Murray Hill, New Jersey

D. L. Philen  
AT&T Bell Laboratories  
Norcross, Georgia

### Introduction

The wavelength(s) of zero dispersion ( $\lambda_o$ ), and the slope(s) of the dispersion ( $S_o$ ) at  $\lambda_o$  are critical parameters in specifying the transmission properties of single-mode lightguides. The procedure used to calculate  $\lambda_o$  and  $S_o$  is to measure the relative group delay in the wavelength region of interest, fit an analytic function to the delay data, differentiate the function and calculate the dispersion using the fitted coefficients, calculate  $\lambda_o$  and  $S_o$  either from the coefficients directly or by interpolation.

Although several analytic functions have been used to fit the group delay data<sup>1</sup>, the EIA is proposing a three term Sellmeier equation for normal unshifted ( $\lambda_o \approx 1.3 \mu\text{m}$ ) fiber primarily because  $\lambda_o$  and  $S_o$  may be calculated directly from the fitted coefficients.

As single mode fibers are designed for operation at  $1.55 \mu\text{m}$  (dispersion shifted), operation at  $1.55 \mu\text{m}$  with reduced  $S_o$  (dispersion flattened), and with multiple dispersion zeros, the question arises whether the three term Sellmeier equation is adequate in all cases and, if not, is there a single equation which will satisfactorily fit the group delay of all fiber designs.

In this paper we present the results of fitting five different algorithms to group delay data for four different fiber designs. The group delay data used was both measured experimentally and calculated using computer aided modeling.

### Description of the Algorithms

The algorithms studied were selected because they are currently in use and have been studied by Kapron<sup>1</sup> for standard unshifted fiber.

The algorithms are as follows:

#### Three Term Sellmeier (S3)

$$\tau(\lambda) = c_1\lambda^{-2} + c_2 + c_3\lambda^2 \quad (1)$$

$$D(\lambda) = -2c_1\lambda^{-3} + 2c_3\lambda \quad (1a)$$

The data can be fitted using a linear least squares (llsq) fit;  $\lambda_o = (c_1/c_3)^{1/4}$  and  $S_o = 8c_3$ .

#### Five Term Sellmeier (S5)

$$\tau(\lambda) = c_1\lambda^{-4} + c_2\lambda^{-2} + c_3 + c_4\lambda^2 + c_5\lambda^4 \quad (2)$$

$$D(\lambda) = -4c_1\lambda^{-5} - 2c_2\lambda^{-3} + 2c_4\lambda + 4c_5\lambda^3 \quad (2a)$$

The data can be fitted using a llsq fit;  $\lambda_o$  and  $S_o$  are determined from interpolating the calculated dispersion.

### Three Term Power Series (P4)

$$\tau(\lambda) = c_2 + c_3(\lambda - c_1)^2 + c_4(\lambda - c_1)^3 \quad (3)$$

$$D(\lambda) = 2c_3(\lambda - c_1) + 3c_4(\lambda - c_1)^2 \quad (3a)$$

Although the data can be fitted using a llsq fit, to preserve the significance of  $c_1$  and  $c_3$ , a non-linear least squares (nllsq) procedure was used. In this form  $\lambda_o = c_1$  and  $S_o = 2c_3$ .

### Four Term Power Series (P5)

$$\tau(\lambda) = c_2 + c_3(\lambda - c_1) + c_4(\lambda - c_1)^2 + c_5(\lambda - c_1)^3 \quad (4)$$

$$D(\lambda) = c_3 + 2c_4(\lambda - c_1) + 3c_5(\lambda - c_1)^2 \quad (4a)$$

We fitted the delay data to the above equation using a nllsq fit although a llsq fit would also work using four coefficients and removing  $c_1$ . In either case  $\lambda_o$  and  $S_o$  must be obtained by interpolating the calculated dispersion.

### Log Term (Ln)

$$\tau(\lambda) = c_2 - c_3 c_1^2 \left( \frac{\lambda - c_1}{\lambda} - \ln \frac{\lambda}{c_1} \right) \quad (5)$$

$$D(\lambda) = c_3 \left( \frac{c_1}{\lambda} \right)^2 (\lambda - c_1) \quad (5a)$$

The data is fitted using a nllsq fit;  $\lambda_o = c_1$  and  $S_o = c_3$ .

For each equation that required finding  $\lambda_o$  and  $S_o$  by interpolation,  $\lambda_o$  was found approximately and the dispersion calculated for  $\Delta\lambda = 0.0001 \mu\text{m}$  around the approximate zero(s). Linear interpolation was then used between adjacent points to calculate  $\lambda_o$  and  $S_o$ . With the availability of inexpensive, fast microprocessors, any advantages of a linear vs. a non-linear fit or calculating  $\lambda_o$  and  $S_o$  from the fitted coefficients is negligible.

## Fiber Types Studied

Fibers exhibiting four basic types of dispersion were studied: a) standard unshifted ( $\lambda_o \approx 1.3 \mu\text{m}$ ) fibers with both matched and depressed claddings; b) dispersion shifted ( $\lambda_o \approx 1.55 \mu\text{m}$ ) fibers with triangular cores and both matched and depressed claddings; c) dispersion flattened ( $\lambda_o \approx 1.55 \mu\text{m}$ ,  $S_o$  reduced) fibers with triangular cores and depressed and multiple claddings; d) dual zero fibers of the quadrupedal clad design<sup>2</sup>. For each fiber type, the group delay was measured experimentally, and calculated using a computer aided modeling program. This was done to test the fitting procedures on data with and without "noise".

## Results

Tables I-IV summarize the results of fitting the five equations to the modeled data for the four fiber types. Fit indicates the algorithm used, npts is the number of points used in the fit, std. dev. is the mean square deviation,  $\lambda_o$  is the zero dispersion wavelength in microns, and slope is the dispersion slope at  $\lambda_o$  in ps/km-nm<sup>2</sup>. The data used to generate Tables I-IV were also reduced to 6 points about  $\lambda_o$  ( $\Delta\lambda = 0.01 \mu\text{m}$ ) and re-fitted since several commercially available dispersion test sets use six semiconductor lasers.

For standard unshifted fibers (Table I) all algorithms fit equally well in terms of  $\lambda_o$  and  $S_o$  except Ln which is slightly poorer. Over the restricted range of 6 points all algorithms fit well although S5 gives the smallest std. dev. When the experimental data is used the same conclusions are reached.

For the dispersion shifted designs (Table II) all five algorithms find  $\lambda_o$  correctly but S3 and Ln have slightly lower  $S_o$ 's and higher std. dev. When the number of points is reduced to 6 all algorithms work equally well. When the experimental data is used, S3, P4 and Ln give slightly less reliable values for  $\lambda_o$  and  $S_o$  with S5 and P5 giving consistently better results.

The results for the dispersion flattened design (Table III) are similar to those for the dispersion shifted design except that the error in  $S_o$  becomes magnified for S3 and Ln.

The group delays for the dual dispersion-zero design presents a problem for all of the algorithms. As can be seen in Table IV, S3 and Ln are unable to find two  $\lambda_o$ 's. Although P4, P5 and S5 all find two  $\lambda_o$ 's, none finds both values accurately. Of the three however, S5 comes the closest to the correct results.

### Summary

Based on the five algorithms tested in this study, we find that the three term Sellmeier (S3) is very adequate for fitting group delay data for standard unshifted fibers ( $\lambda_o = 1.3 \mu\text{m}$ ). However, in terms of a more general fitting equation that is applicable to a wide class of fiber types, we find that the 5 term Sellmeier equation (S5) gives consistently better results for all of the fiber designs tested using both experimental and modeled data. The 3 term Sellmeier (S3) and log (Ln) algorithms are inferior as a general equations. With the availability of inexpensive, fast microprocessors, the questions of linear and non-linear fits, and the ease of finding  $\lambda_o$  and  $S_o$  from the fitted coefficients is not a valid concern.

### References

- [1] Felix P. Kapron and Tom C. Olson, "Accurate Specification of Single-Mode Dispersion Measurements", NBS Symposium on Optical Fiber Measurements, 1984, pg. 111.
- [2] L. G. Cohen, W. L. Mammel, and S. J. Jang, "Low-Loss Quadruple-Clad Single-Mode Lightguides with Dispersion Below 2 ps/km-nm over the 1.28  $\mu\text{m}$ -1.65  $\mu\text{m}$  Wavelength Range," *Elect. Lett.* **18**, 1023-1024 (1982).

Table I  
Model Standard Unshifted Fiber ( $\lambda_o = 1.3113$ ,  $S_o = 0.0851$ )

fit	npts	std. dev.	$\lambda_o$	slope
S3	21	0.0279	1.3113	0.0851
S5	21	0.0000063	1.3113	0.0851
P5	21	0.111	1.3112	0.0857
P4	21	0.111	1.3112	0.0857
Ln	21	4.20	1.3105	0.0844

Table II  
Model Dispersion Shifted Fiber ( $\lambda_o = 1.5531$ ,  $S_o = 0.0589$ )

fit	npts	std. dev.	$\lambda_o$	slope
S3	16	0.749	1.5529	0.0571
S5	16	0.000882	1.5531	0.0589
P5	16	0.00262	1.5531	0.0589
P4	16	0.00233	1.5531	0.0589
Ln	16	1.77	1.5528	0.0560

Table III  
Model Dispersion Flattened Fiber ( $\lambda_o = 1.5622$ ,  $S_o = 0.0307$ )

fit	npts	std. dev.	$\lambda_o$	slope
S3	16	6.99	1.5621	0.0386
S5	16	0.00514	1.5622	0.0306
P5	16	0.0200	1.5625	0.0309
P4	16	0.0198	1.5625	0.0308
Ln	16	5.45	1.5621	0.0377

Table IV  
Model Dual Zero Fiber ( $\lambda_o = 1.4597$ ,  $1.6063$ ,  $S_o = 0.0336$ ,  $-0.0562$ )

fit	npts	std. dev.	$\lambda_o$	slope
S3	31	2360	1.4927	0.00931
S5	31	12.4	1.4606	0.0380
S5	31	12.4	1.6024	-0.0516
P5	31	91.1	1.4520	0.0386
P5	31	91.1	1.5996	-0.0386
P4	31	91.1	1.4520	0.0386
P4	31	91.1	1.5997	-0.0387
Ln	31	2310	1.4914	0.00965



## CHROMATIC DISPERSION IN OPTICAL FIBERS: COMPARISON OF MEASUREMENTS WITH MODELS

Leslie Button, Walter F. Love, Robert M. Hawk, Research and Development Division, Corning Glass Works, Corning, New York 14831

### INTRODUCTION

Chromatic dispersion is an important broadening mechanism for time dispersion in optical fibers. It is the limiting factor in LED-multimode systems and in single-mode systems apart from modal noise considerations. In this paper we present a comparison of time dispersion transmission measurements and refractive index data and models for both graded-index multimode fibers and single-mode fibers.

### EXPERIMENTAL METHOD

The time delay,  $\tau$ , was measured for fiber lengths,  $L$ , of 2 to 5 km over the wavelength range, 1.1 to 1.7  $\mu\text{m}$  using a fiber Raman laser system.<sup>1,2</sup> These data were fitted to  $\tau=A+B\lambda^2+C\lambda^{-2}$  for multimode fibers and unshifted single-mode fibers, SMF<sup>TM</sup>; whereas,  $\tau=a_0+a_1\lambda+a_2\lambda\ln\lambda$  was used for the dispersion-shifted single-mode fibers, SMF/DS<sup>TM</sup>, where  $\lambda$  is the wavelength of light. The chromatic dispersion,

$D$ , is readily obtained as  $D = \frac{1}{L} \frac{d\tau}{d\lambda}$ . A mode-scrambled launch is used to fully excite all modes in the multimode fibers. The precision in all cases is typically  $\sim 1$  nm.

The RNF index profile measurement<sup>3</sup> uses a He-Ne laser operating at 633 nm. The finite laser spot size gives an instrument resolution of 0.6  $\mu\text{m}$ . The measured index profile serves as input data to a computer program which numerically solves the scalar wave equation using the finite element method. Refractive index is required as a function of wavelength, viz.,  $n(\lambda)$ , and we have used the published work of Kobayashi<sup>4</sup>, Fleming<sup>5</sup>, and Shibata<sup>6</sup> in our comparisons for single-mode fibers.

### MULTIMODE FIBER RESULTS

Measurements of the zero dispersion wavelength,  $\lambda_0$ , are plotted versus an effective  $\Delta$  value based on far-field NA measurements for high-bandwidth graded index fibers and are shown in Fig. 1. The zero-doped value was obtained from

Malitson's index measurements of fused silica.<sup>7</sup> There is a high degree of correlation and a linear dependence up to approximately 2%. Thus,  $\lambda_0$  is shifting toward longer wavelengths with increasing germania doping.

The chromatic dispersion,  $D$ , has been calculated using the expression for  $\tau$  obtained by WKB analysis for  $\alpha$ -model index profiles.<sup>8</sup> Assuming equal mode excitation and a parabolic index profile, we obtain in agreement with Adams<sup>9</sup>,

$$D = \frac{2 M_1 + M_2}{3} + \frac{n_1 \Delta p}{3c\lambda} \quad (1)$$

where the material dispersion,  $M_i = -\frac{\lambda}{c} \frac{d^2 n_i}{d\lambda^2}$  and the subscript 1 and 2 refer to core and cladding. The profile dispersion parameter,  $p$ , is given by  $p \approx \frac{\lambda}{\Delta} \frac{d\Delta}{d\lambda}$  and  $c$  equals the speed of light.<sup>10</sup>

The profile dispersion term can be evaluated near 1300 nm, where  $p \approx 0.05$ , for  $\Delta \approx 0.01$  to give  $n_1 \Delta p / 3c\lambda = 0.63 \text{ psec nm}^{-1} \text{ km}^{-1}$ . At a slope of  $0.09 \text{ psec nm}^{-2} \text{ km}^{-1}$  ( $\text{GeO}_2\text{-SiO}_2$ ), this represents a 7 nm correction. Since the material dispersion varies linearly with wavelength near  $\lambda_0$ , Eq. 1 can be reduced to:

$$\lambda_0 = \lambda_0^{(2)} + \frac{2}{3} (\lambda_0^{(1)} - \lambda_0^{(2)}) - 7 \text{ nm} \quad (2)$$

Using the measurement results of Payne and Hartog<sup>11,12</sup> for  $\lambda_0$  versus mole %  $\text{GeO}_2$ -doped silica, we compute for 12 m%, corresponding to 0.20 transmitted NA,  $\lambda_0 = 1274 + 2/3 (1340 - 1274) - 7 = 1311 \text{ nm}$ . This agrees very well with our result shown in Fig. 1.

#### SINGLE-MODE FIBER RESULTS

Schematic diagrams of the index profiles for unshifted,  $\text{SMF}^{\text{TM}}$ , and dispersion-shifted,  $\text{SMF/DS}^{\text{TM}}$ , single-mode fibers are given in Fig. 2. The actual profiles for five of the former and four of the latter were measured at each end by the RNF method. These were entered as input data to a finite element solution of the scalar wave equation along with published index data.

The difference between the long-length measurements and the index-calculated

values for  $\lambda_0$ , viz.,  $\delta\lambda_0$ , are given in Table 1. The standard deviation about the mean value of  $\delta\lambda_0$  is denoted by  $\sigma_m$ . The best agreement is closest to Fleming for SMF<sup>TM</sup>. This is likely to shift towards the less dispersive index data of Kobayashi with deconvolution of the input spot size. This will be discussed in more detail later. For SMF/DS<sup>TM</sup>, the average agreement is better although there is more imprecision, viz.,  $\sigma_m$  is larger. This is understandable since the waveguide dispersion is dominant and small variations in index profile measurement give significant variations in  $\lambda_0$ .

A more detailed view of the difference between measured and calculated dispersion is given in Fig. 3 for SMF<sup>TM</sup> fibers. The shaded regions encompass  $\pm 1\sigma$  values.

### SUMMARY

We have compared long-length transmission measurements of chromatic dispersion for high-bandwidth graded-index multimode fibers and single-mode fibers with calculations based upon published index and dispersion data. We find very good agreement with University of Southampton results for the multimode case. For unshifted single-mode fibers, the agreement with calculation is best for Fleming's index data whereas for dispersion-shifted single-mode fibers agreement is good for all published index data considered, but the precision is less in this case.

### REFERENCES

1. L. G. Cohen and Chinlon Lin, IEEE J. Quantum Electronics QE14, 855 (1978).
2. W. F. Love, Proceedings of Sixth European Conference on Optical Communication, p. 113, York, U.K. (1980).
3. W. J. Stewart, Proceedings of Conference on Integrated Optics and Optical Communication, C2.2, Japan, 1977.
4. S. Kobayashi, S. Shibata, N. Shibata, and T. Izawa, Proceedings of Conference on Integrated Optics and Optical Communication, B8-3, Japan, 1977.
5. J. W. Fleming, Electronics Letters 14, 326 (1978).
6. N. Shibata, S. Shibata, and T. Edahiro, Electronics Letters 17, 310 (1981).
7. I. H. Malitson, J. Opt. Soc. Am. 55, 1205 (1965).
8. R. Olshansky and D. B. Keck, Applied Optics 15, 483 (1976).
9. M. J. Adams, D. N. Payne, F. M. E. Sladen, and A. H. Hartog, Electronics Letters 14, 64 (1978).
10. F. M. E. Sladen, D. N. Payne, and M. J. Adams, Electronics Letters 15, 469 (1979).
11. D. N. Payne and A. H. Hartog, Electronics Letters 13, 627 (1977).
12. M. J. Adams, D. N. Payne, F. M. E. Sladen, and A. H. Hartog, Electronics Letters 14, 703 (1978).



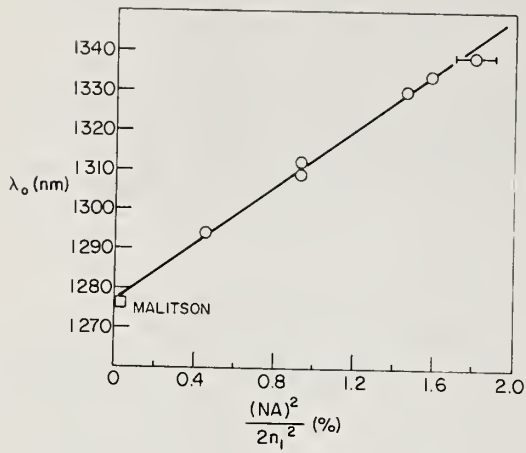


Fig. 1 Multimode fiber  $\lambda_o$  versus effective  $\Delta$  from  $\lambda_o$  far-field.

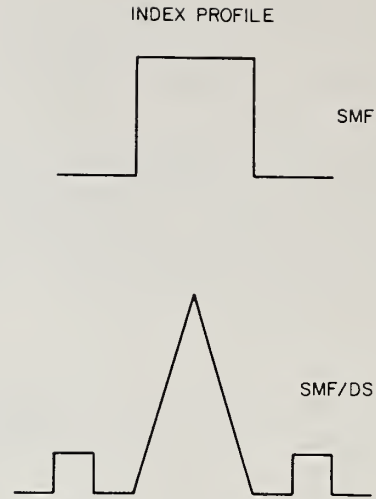


Fig. 2 Ideal index profiles for single-mode fibers.

TABLE I  
COMPARISON OF MODELS VS MEASUREMENTS

		KOBAYASHI	FLEMING	SHIBATA
SMF	$\delta\lambda_o$ (nm)	-16.4	-6.6	6.9
	$\sigma_m$ (nm)	2.3	4.0	2.6
SMF/DS	$\delta\lambda_o$ (nm)	-1.2	-1.2	+0.1
	$\sigma_m$ (nm)	4.7	9.3	5.4

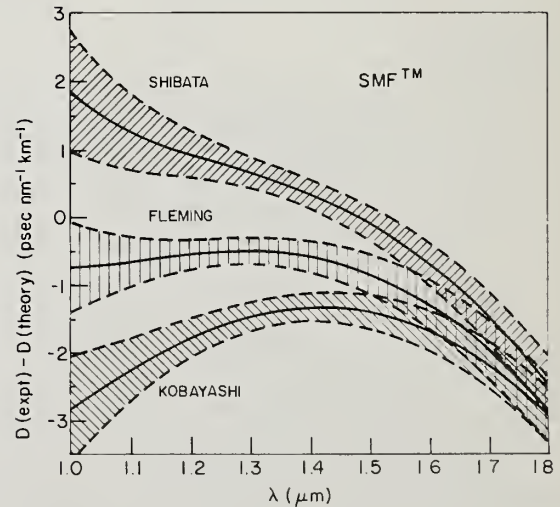


Fig. 3 Comparison of transmission measurements versus calculations for various index data.

# ACCURACY OF PHASE SHIFT TECHNIQUE WITH LEDS FOR MEASURING TOTAL DISPERSION IN SINGLEMODE FIBERS

L. Bosselaar, G. Kuijt, J.F. van Luijk, P. Matthijsse

Telecommunication fiber development - Philips Glass  
P.O. Box 218 - 5600 MD Eindhoven - The Netherlands

## 1. Introduction

The phase shift technique for measuring total dispersion coefficient has been described in several publications<sup>1,2</sup>. Main advantages of using LEDs are the compactness of the set-up and the possibility of measuring at many wavelengths with two sources only. In this summary the main effects determining the accuracy of this method are described. The results presented have been obtained as follows : A theoretical delay-time-versus-wavelength curve was calculated for depressed-cladding and for dispersion-flattened singlemode fibers<sup>3</sup>. This curve was disturbed with random noise and systematic errors. The disturbed curves were fitted through a limited number of points at several wavelengths with different types of curve-fits. The resulting dispersion coefficients at specific wavelengths were compared with the calculated exact values.

## 2. Random phase noise

This noise may have different sources, and will lead to a spread in the total dispersion measured. It was found that the spread in total dispersion coefficient increases linearly with the amplitude of the random noise for all the curve-fits. Tanaka<sup>2</sup> has found similar results.

## 3. Temperature changes

The group velocity of light in the fiber is temperature dependent<sup>4</sup>. The temperature coefficient is about  $30 \text{ ps km}^{-1} \text{ K}^{-1}$  for primary coated fibers. A change in temperature of the fiber during a measurement will consequently affect the total dispersion coefficient measured. For this error to be kept below  $0.1 \text{ ps km}^{-1} \text{ nm}^{-1}$ , the temperature change during a measurement should be less than about 1 K, dependent upon the temporal behaviour of this change (worst case; less than 0.1 K).

#### 4. Number of wavelengths at which phase shift is measured

The effect on the accuracy of the number of wavelengths measured has also been investigated by the method described in the introduction. The spread in the total dispersion coefficient of a depressed cladding singlemode fibre measured at 1330 nm ( $D_{1330}$ ) versus the number of points (N) at which the phase is measured is typically :

N	:	10	20	30	40
Spread in $D_{1330}$	:	0.2	0.06	0.04	0.02

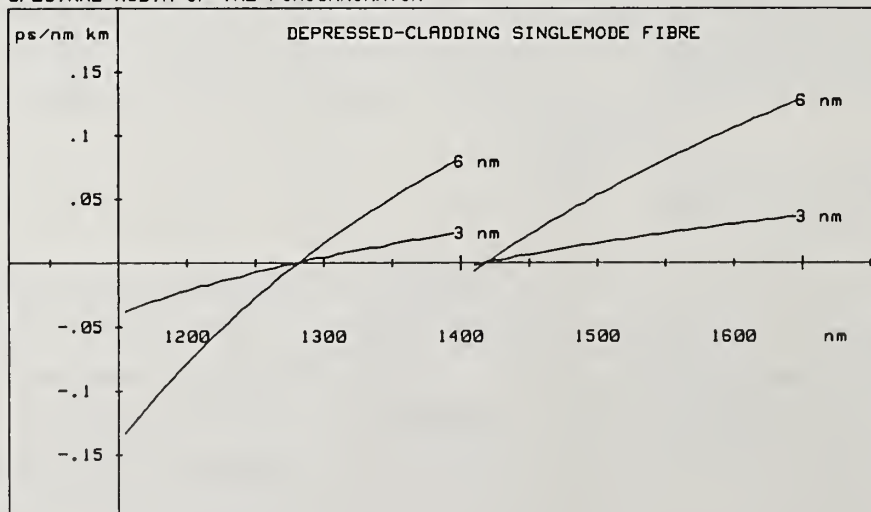
The table shows a nearly quadratic reduction in spread of  $D_{1330}$  with increasing N.

#### 5. Spectral width of monochromator

The spectral width of the monochromator will be chosen as high as possible to increase the received power and dynamic range. On the contrary the spectral width should be limited, for prevention of systematic error in the total dispersion coefficient measured. This systematic error has been calculated for two spectral widths of the monochromator, assuming there is one LED with a central wavelength at 1255 nm and one at 1540 nm. Fig. 1 shows the calculated error for the depressed-cladding singlemode fibre; fig. 2 shows this error for the dispersion-flattened singlemode fibre.

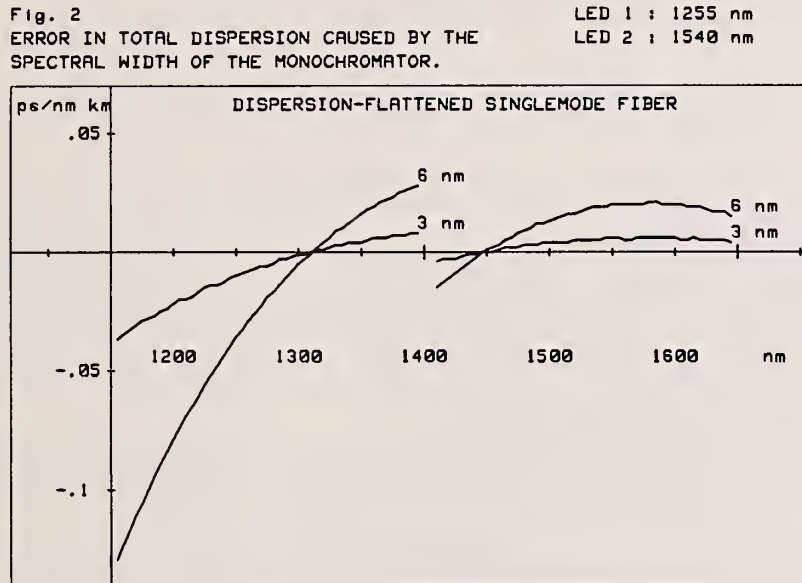
Fig. 1  
ERROR IN TOTAL DISPERSION CAUSED BY THE  
SPECTRAL WIDTH OF THE MONOCHROMATOR

LED 1 : 1255 nm  
LED 2 : 1540 nm





Figures 1 and 2 prove that the error in total dispersion is less than  $0.1 \text{ ps km}^{-1}\text{nm}^{-1}$  in the normally used transmission windows for a spectral width of the monochromator of 6 nm FWHM. As this error is systematic, it can be compensated for if some knowledge of the expected dispersive behaviour of the fibre is present.



## 6. Type of curve-fit

Among others the following fits with different numbers of coefficients have been tried for the disturbed delay-time-versus-wavelength points :

$$S(x) = s_1 + s_2x^2 + s_3x^{-2} + s_4x^4 + s_5x^{-4} \dots \quad \begin{array}{l} \text{(material dispersion fit,} \\ \text{based on Sellmeier's equation)} \end{array}$$

$$T(x) = t_1 + t_2(x-x_0) + t_3(x-x_0)^2 + t_4(x-x_0)^3 \dots \quad \text{(general Taylor series)}$$

The 5-coefficients Taylor fit ( $T_5(x)$ ) and the 5-coefficient material dispersion fit ( $S_5(x)$ ) were acceptable. Best results however, were obtained from the 3-coefficient material dispersion fit for the depressed-cladding singlemode fibre only and the 4-coefficient material dispersion fit for both types of fibres. The use of more coefficients caused oscillations in the dispersion curve.

The criteria for usefulness of a fit-curve were :

- 1) average deviation and spread of total dispersion coefficient for 1285, 1330 and 1550 nm
- 2) average deviation and spread of the wavelength of zero total dispersion ( $\lambda_0$ )
- 3) slope and its spread of total dispersion coefficient in  $\lambda_0$  (depressed-cladding singlemode fibre only)

## 7. Conclusions

- Measures for temperature stabilisation of the measured fibre must be taken into account.
- An increase in number of wavelengths at which the phase shift is measured, has a more favourable effect on the total accuracy of the measurement than an increase in precision of the measurement of the phase shift at one wavelength.
- Errors due to the non-zero spectral width of the monochromator normally are rather small.
- The 4-coefficient material dispersion fit yielded the best results of all fits tested for both depressed-cladding and dispersion-flattened singlemode fibres.
- The total accuracy of this method can be estimated as better than  $0.5 \text{ ps km}^{-1}\text{nm}^{-1}$  for standard production lengths of fiber in the 1300 and 1500 nm windows. Measuring results will be presented at the conference.

## References

1. B. Costa, D. Mazzoni, M. Puleo, E. Vezzoni, "Phase shift technique for the measurement of chromatic dispersion in optical fibers using LED's", IEEE journal of quantum electronics, vol. QE-18, no. 10, October 1982.
2. S. Tanaka, Y. Kitayama, "Measurement accuracy of chromatic dispersion by the modulation phase technique.", Journal of Lightwave Technology, vol. LT-2, no. 6, December 1984 p. 1040.
3. P.K. Bachmann et al., "PCVD DFSM-FIBRES: PERFORMANCE, LIMITATIONS, DESIGN OPTIMIZATION", 11th ECOC, VENECIA, 1985, Conf. Proc., P.197.
4. L.G. Cohen, J.W. Fleming, "Effect of temperature on transmission in lightguides", The Bell system technical journal, vol. 58, no. 4, p. 945-951, April 1979.

# HIGH SPEED AND HIGH ACUCURATE SINGLE-MODE FIBER DISPERSION MEASURING EQUIPMENT USING MODIFIED INTERFEROMETRIC METHOD

Y. NAMIHIRA, Y. IWAMOTO, T. MURAKAMI\* and S. AN\*

K D D Research & Development Laboratories,  
2-1-23 Nakameguro, Meguro-ku, Tokyo, Japan

(\*) SANTEC Corporation, Kamisue Komaki, Aichi, Japan

INTRODUCTION In the conventional interferometric chromatic dispersion measurement [1],[2],[3], the high speed measurement and compact arrangement could not be achieved. However, using modified interferometric method [4] with AC-modulation detection technique of the interference signal and interferometric filter instead of monochrometer, the high speed, high accurate and compact arrangement for single-mode fiber chromatic dispersion measuring equipment can be developed.

In this paper, the modified interferometric dispersion measurement in short length single mode fiber is presented.

MEASURING SYSTEMS Fig.1 shows a schematic diagram of the high speed and high accurate single-mode fiber dispersion measuring equipment (SANTEC SDA-6000) using modified interferometric method [4], and the appearance of the equipment is shown in Fig.2. The size of the equipment is about 905 (W) x 795(D) x 1100(H) (mm). The specifications of the measuring equipment are summarized in Table 1. As an optical source and detector, a 100-W halogen lamp and a InGaAs-APD were used. And, as a wavelength selector, the interferometric filter (FWHM  $\cong$  15 nm) was used to realize compact measuring equipment without using monochrometer. The dispersion equipment has a function of automatic control high speed signal processing sub-systems [4]. The input light is fed through the interferometric filter, and then launched into the lead single-mode fiber. After passing through the fiber, the light is devided into the input beamsplitter and launched into both arms of the Mach-Zehnder interferometer. A multi-reflection mirror was used in the interferometer reference arm in order to equalize the optical paths of the test fibers. The length of test fiber samples is about 1.300 (m)  $\pm$  5 (mm). A variable optical delay



line is placed in the reference arm of the interferometer. The principle of dispersion measurement is based on the conventional interferometric method [1],[2], however, in our modified interferometric measurement, in order to search the interference point in a short time, the optical path of the reference wave is modulated by actuating corner cuve with PZT at 60~100 Hz sinusoidal waves instead of optical chopper, and the modulated interference visivility fringe can be obtained [4]. A typical peak search pattern of the interference visivility fringe is shown in Fig.3.

#### RESULTS & DISCUSSIONS

The dispersion  $D = d\tau/d\lambda$  is obtained by least square fitting equation to be measured delay time  $\tau$  and differentiating it with respect to wavelength  $\lambda$ . Also, the dispersion slope is obtained as  $dD/d\lambda$ . The delay time and dispersion characteristics of the segmented-core dispersion shifted fiber (DSF) [5] as a function of wavelength are shown in Figs.4-(a) and (b), respectively. The delay time data (x) at 26 different wavelengths were measured by the modified interferometric dispersion measurement [4]. As a fitting equation [6],[7], the following three-term Sellmeier equation  $\tau_1 = A\lambda^2 + B + C\lambda^{-2}$  and the five term-Sellmeier equation  $\tau_2 = A\lambda^4 + B\lambda^2 + C + D\lambda^{-2} + E\lambda^{-4}$  and the Napierian logarithm expression  $\tau_3 = A + B\lambda + C\lambda \cdot \ln\lambda$  were used. Where, A, B, C, D, and E are coefficient of the delay time  $\tau$  fitting expressions. In the delay time curve-fitting expresions, the coefficients from A to E can be determined by RMS fitting to the experimental data. From Fig.4-(a), it is found that the fitting curves of  $\tau_2$  (—) and  $\tau_3$  (----) agree well with the experimental results (x) rather than that of  $\tau_1$  (---). The comparison of the three fitting expressions are summarized in Table 2. From Table.2, it is found that the meansquare fitness error and dispersion-slope of  $\tau_1$  is great different from that of  $\tau_2$  and  $\tau_3$ . It is considered that the lower-order Sellmeier equation of  $\tau_1$  is strongly dependent of the material dispersion, however, in the case of the DSF, the waveguide dispersion becomes greater than the conventional dispersion non-shifted fibers. Accordingly, the fitting expression of  $\tau_1$  does not agree with the measured values. Meanwhile, the results of  $\tau_2$  and  $\tau_3$  indicate almost the same values. At present, it is not concluded that which types of the fitting equation of  $\tau_2$

and  $\tau_3$  are the best fitting expression for the dispersion shifted fibers or not, and accordingly, the further study of the group delay fitting equations will be needed. Meanwhile, in order to confirm the measuring accuracy of the modified interferometric dispersion measurement, the comparison of the modified interferometric dispersion measurement and the conventional fiber Raman laser technique has been made, and the results are shown in Fig.5. In Fig.5, the dispersion of A-End (—), and B-End (.....) of short length (1.3 m) are good agreement with that of the fiber Raman laser technique (---) in the long length 8.323 (km) of triangular-DSF. The measured values of zero-dispersion wavelength ( $\mu\text{m}$ ), dispersion slope ( $\text{ps}/\text{nm}^2 \cdot \text{km}$ ) at zero dispersion wavelength in the modified interferometric measurement [A-End, B-End] and the conventional fiber Raman laser technique were [1.5000, 1.5008] and 1.5049, [ $59.36 \times 10^{-3}$ ,  $59.26 \times 10^{-3}$ ] and  $56.19 \times 10^{-3}$ , respectively.

CONCLUSIONS The high speed and high accurate single-mode fiber dispersion measuring equipment using modified interferometric method was developed. The total measuring time was about 11 (minute) in the  $1.2 \mu\text{m}$ ~ $1.7 \mu\text{m}$  wavelength regions. The measuring accuracy of chromatic dispersion of  $+ 0.2$  ( $\text{ps}/\text{nm} \cdot \text{km}$ ) was obtained. Also, it was found that the dispersion measurement of the interferometric method in short length fiber (1.3 m) is equivalent to that of the fiber Raman laser technique in long length fiber (8.323 km).

ACKNOWLEDGEMENTS The authors wish to thank M. Fujise and M. Nunokawa of KDD Labs., for their discussions, and M. Ichimura of SANTEC Corp. for his experimental support, and to Dr. H. Kaji, and Dr. T. Yamamoto of KDD Labs., for their encouragement.

#### REFERENCES

- [1] M. J. Saunders et al, Tech. Digest, NBS Symp. on Opt. Fiber Measurements, Boulder, CO, Oct., p.123, 1984
- [2] L. Oksanen et al., ibid, p.127, Boulder, 1984.
- [3] F. M. Sears et al, IEEE, vol. LT-2, No.2, p.181, 1984.
- [4] Y. Namiura et al, National Conv. Rec., IECE, No. 1025, 1986.
- [5] V.A. Bhagavatula et al., OFC'85, WD-3, p.94, SAN DIEGO, 1985.
- [6] L. G. Cohen, IEEE, Vol. LT-3, No.5, p.958, 1985.
- [7] R. A. Modavis et al., Tech. Digest, NBS Symp. on Opt. Fiber Measurements, Boulder, CO, Oct., p.115, 1984

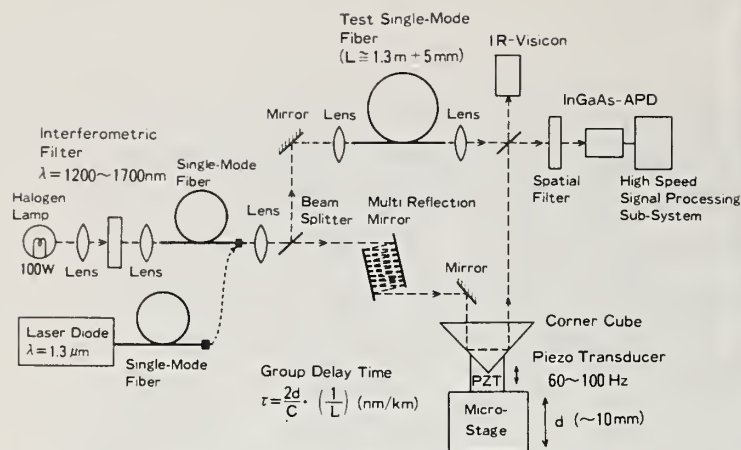


Fig.1 Schematic diagram of measuring equipment.

Table 1 Specifications of measuring equipment.

Optical source	Halogen Lamp (~100W)
Optical Detector	InGaAs-APD
Operating Wavelength	$\lambda = 1200 \sim 1700$ nm per 20 nm, 26 point
Measuring Accuracy	(Resolution) $\leq \pm 0.005$ (ps/m)
	(Dispersion $D \leq \pm 0.2$ (ps/km·nm)
	(Zero-Dispersion Wavelength) $\lambda_0 \leq \pm 0.2$ (nm)
Measuring Time at one point [Total]	~25 (sec) [~11 minute]

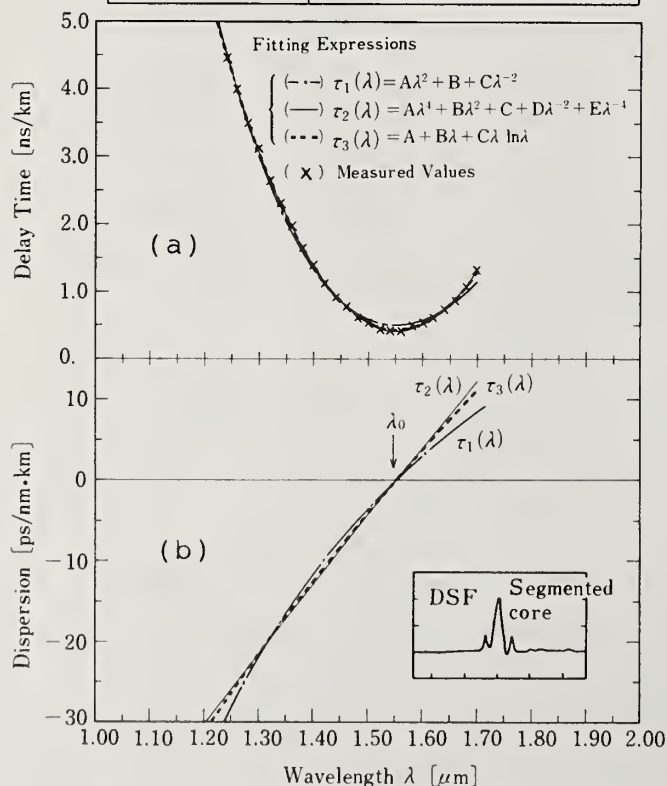


Fig.4 Delay time and dispersion characteristics as a function of wavelength.



Fig.2 Appearance of measuring equipment.

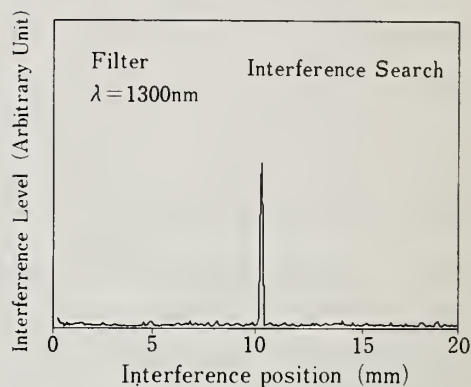


Fig.3 A typical peak search pattern of interference fringes.

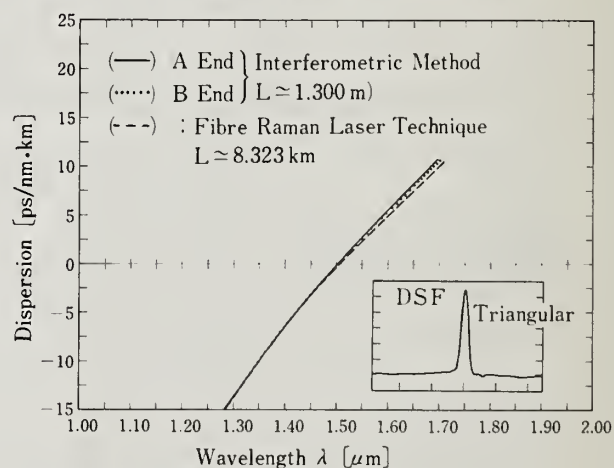


Fig.5 Comparison of modified interferometric dispersion measurement and fiber Raman laser technique.

Table 2 Comparison of fitting expressions.

Fitting Expressions	Zero-Dispersion Wavelength $\lambda_0$ [μm]	Dispersion Slope $dD(\lambda)/d\lambda \sim 10^{-3}$ (at $\lambda_0$ ) [ps/nm²·km]	Dispersion D (ps/nm·km) at $\lambda = 1.55 \mu\text{m}$	Fitting Mean-Square Error $\sim 10^{-3}$ (ns/km)²
$\tau_1(\lambda)$	1.5520	65.24	-0.1276	6.134
$\tau_2(\lambda)$	1.5525	82.26	-0.2084	0.620
$\tau_3(\lambda)$	1.5516	78.31	-0.1280	0.910



CHROMATIC DISPERSION MEASUREMENTS OF SINGLE MODE FIBRES IN THE 1.3  $\mu\text{m}$  AND  
1.55  $\mu\text{m}$  WAVELENGTH RANGE BY THE WAVELENGTH TEMPERATURE TUNING TECHNIQUE

Finn Mogensen, Hans Damsgaard and Ole Hansen  
NKT Elektronik, Brøndbyvestervej 95, DK-2605 Brøndby, Denmark

ABSTRACT

Highly accurate (0.5 ps/km for a 4 km length) delay vs. wavelength curves are presented for SM fibres in the 1.3  $\mu\text{m}$  and 1.55  $\mu\text{m}$  windows.  $\lambda_0$  is determined reproducibly with a relative accuracy of 0.02 per cent. An average  $\lambda_0$  value of 1312.8 nm with a standard deviation of 2.8 nm is determined from measurements on production fibres. The dispersion slope  $S$  is found to be 0.087 ps/km-nm<sup>2</sup> with a standard deviation of 0.003 ps/km-nm<sup>2</sup>.

INTRODUCTION

Various experimental techniques for measuring the dispersion properties of single mode fibres have been reported including Nd:YAG laser system (1), phase shift technique using light emitting diodes (LED's) (2), interferometric method (3) and series of laser diodes (LD's) (4).

In this paper chromatic dispersion measurements are presented for standard SM fibres and a dispersion shifted fibre with zero dispersion wavelengths around 1.3  $\mu\text{m}$  and 1.55  $\mu\text{m}$ , respectively. The fibres are manufactured by NKT Elektronik using the MCVD process.

EXPERIMENTAL PROCEDURE

The experimental set-up is illustrated in Fig. 1. Two LD's cover the wavelength range around 1.3  $\mu\text{m}$  and a third LD is used in the 1.55  $\mu\text{m}$  wavelength range. The wavelength tuning is obtained by temperature variation as described previously (5,6).

The delay vs. wavelength curves is measured using the phase shift technique. The fibre delay is measured relative to a short reference fibre in order to take into account any (temperature-dependent) delay variations in the LD's.

Two main error sources should be considered when using the experimental configuration shown in Fig. 1. The first is the temperature sensitivity of the fibre under test (the time delay will change approximately 40 ps/°C-km) and the second is the frequency stability of the signal generator.

In our experiments the influence of the two above-mentioned error sources was eliminated in one of two ways. Initially the fibre was isolated and temperature stabilized and the measurement time was short (around 10 min.). In this way accurate and reproducible results were obtained, however, the short measurement time limited the number of delay points which could be obtained. Later this was overcome by using a reference LD operating at a constant wavelength. By the inclusion of the reference LD the temperature stabilization of the fibre could be avoided and only short term stability was required for the signal generator.

## RESULTS AND DISCUSSION

Fig. 2 shows the relative time delay vs. wavelength measured on an 11 km long dispersion shifted SM fibre. The results were obtained within approximately 10 min. and no reference LD was applied. Measuring points have been fitted to the usual Sellmeier expression ( $a + b\lambda^2 + c\lambda^{-2}$ ). The maximum and the typical deviations between the fitted curve and the measurement points are 0.4 ps/km and 0.25 ps/km, respectively. The key parameters characterizing the chromatic dispersion are the zero dispersion wavelength  $\lambda_0$  and the slope  $S_0$  of the dispersion curve at this wavelength. From the fitted curve  $\lambda_0 = 1545.2$  nm and  $S_0 = 0.061$  ps/km-nm<sup>2</sup> were obtained.

The reproducibility of the measurement technique was verified by seven repeated measurements on the same 6.5 km length standard 1300 nm optimized SM fibre.  $\lambda_0$  was determined as 1310.5 nm with a standard deviation of 0.2 nm. The dispersion slope was found to be  $S_0 = 0.085$  ps/km-nm<sup>2</sup> with a standard deviation of 0.001 ps/km-nm<sup>2</sup>.

In order to evaluate the spread in the  $\lambda_0$  on the standard SM fibre from our production, time delay curves were measured for 13 different fibre samples. The average value of  $\lambda_0$  was found as 1312.8 nm and the standard deviation was 2.8 nm. The average value of  $S_0$  was determined as 0.087 ps/km-nm<sup>2</sup> with a standard deviation of 0.003 ps/km-nm<sup>2</sup>. The tested samples were from 1-7 km in length.

Finally Fig. 3 shows the delay curve for a 4 km long standard SM fibre measured using a reference laser. In this case a large number of points (28) were obtained. The maximum and the typical deviations between the fitted curve and the measurement points are 1.6 ps/km and 0.5 ps/km, respectively. In this example the chromatic dispersion characteristics were found to be  $\lambda_0 = 1312.0$  nm and  $S_0 = 0.090$  ps/km-nm<sup>2</sup>.

### CONCLUSION

Chromatic dispersion measurements based on the phase shift technique have been presented. LD's were used as light sources and wavelength variation was obtained through the temperature tuning effect.

$\lambda_0$  was determined with an accuracy of approximately 0.2 nm in the 1.3  $\mu$ m wavelength range yielding a relative accuracy of around 0.02 per cent.

For the standard SM fibre from our production the average value of  $\lambda_0$  was determined as 1312.8 nm with a standard deviation of 2.8 nm.

Relative time delay curves were presented both for the standard 1.3  $\mu$ m SM fibre and for a dispersion shifted fibre developed for the 1.55  $\mu$ m wavelength range. The reproducible and highly accurate ( $\sim 0.5$  ps/km) results confirm that the temperature tuning technique used here is an efficient alternative to other methods.

### REFERENCES

- (1) L.G. Cohen and C. Lin, Applied Optics 16, p. 3136 (1977).
- (2) B. Costa, M. Puleo, and E. Vezzoni, Electron. Lett. 19, p. 1074 (1983).
- (3) F.M. Sears, L.G. Cohen and J. Stone, J. Lightwave Tech. LT-2, p. 181 (1984).
- (4) C. Lin, A.R. Tynes, A. Tomita, P.L. Liu and D.L. Philen, Bell Syst. Tech. J. 62, p. 457 (1983).
- (5) T. Miyashita, M. Horiguchi and A. Kawana, Electron. Lett. 13, p. 227 (1977).
- (6) H. Damsgaard, O. Hansen and F. Mogensen, Submitted for publication.



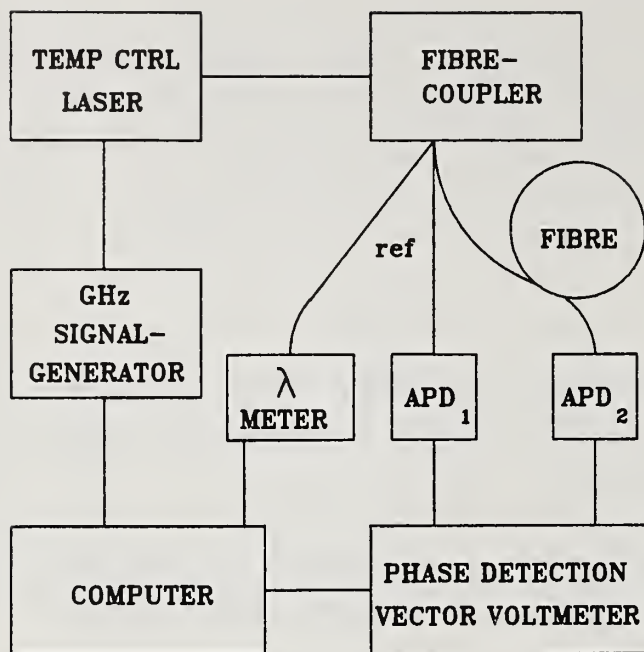


Fig. 1

Schematic of the experimental set-up.

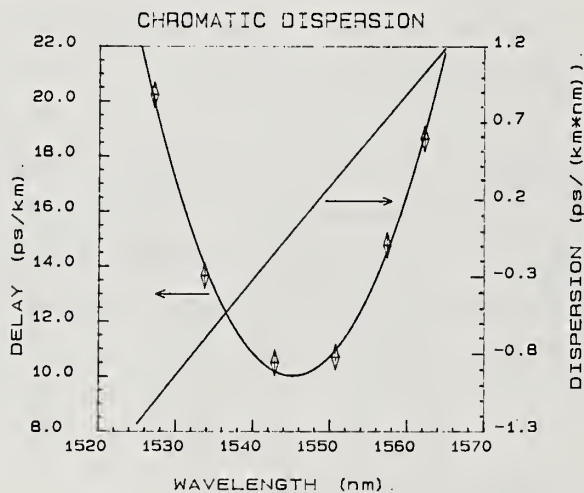


Fig. 2

Delay vs. wavelength measured for an 11 km long dispersion shifted SM fiber.  $\lambda_0 = 1545.2$  nm. Modulation frequency  $f_m = 500$  MHz.

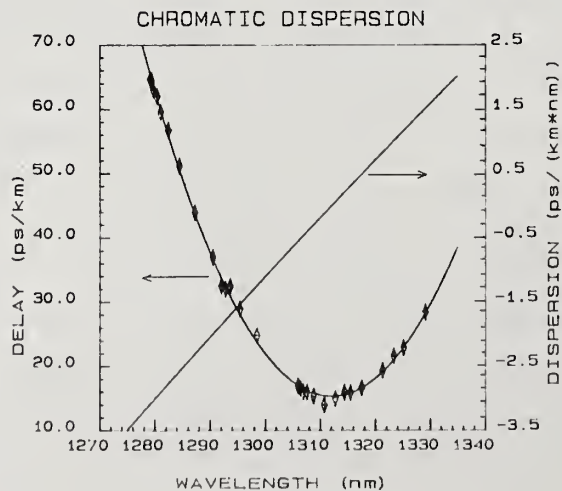


Fig. 3

Delay vs. wavelength measured for a 4 km long standard SM fiber.  $\lambda_0 = 1312.0$  nm. Modulation frequency  $f_m = 1$  GHz.



# MEASUREMENT OF DOPANTS IN OPTICAL FIBERS BY RAMAN SCATTERING

Dan L. Philen  
AT&T Bell Laboratories  
2000 Northeast Expressway  
Norcross, Georgia 30071

## INTRODUCTION

This paper describes a scattering technique that provides a new method for determining dopants in optical fibers. The measurement of the concentration levels of dopants used in optical fibers is difficult for several reasons. In the region of vibrational spectroscopy beyond  $2.5\text{ }\mu\text{m}$ , the fiber is opaque because of the silica lattice vibrations. In the region of electronic transitions, the fiber is also opaque because of strong UV band-edge absorptions. Unfortunately, for measurements in the region where the fiber is highly transparent, there are no strong optical absorptions (that is why the fiber is transparent). Measurements of dopant levels must then be done by "wet" chemical methods, or by exotic methods such as electron microprobe (X-ray emission).

A technique that has been used for bulk glass samples [1-4], and preforms [5,6], but has not found widespread application to optical fibers [7,8], is Raman scattering. Raman scattering is an inelastic scattering process where a small portion of the scattered light is shifted in frequency by an amount corresponding to the vibrational and rotational frequencies of the scattering medium. The Raman scattered light shifted to frequencies higher than the excitation is the anti-Stokes component, and those shifted to lower frequencies than the excitation is the Stokes component. The strength of the scattered light is given by  $m = \alpha F$ ; where  $\alpha$  is the polarizability of the molecule, and  $F$  is the electric field strength.

Raman scattering occurs at any excitation wavelength, so in principle any monochromatic excitation source can be used, but the intensity of the scattering increases with decreasing excitation wavelength, and the scattered information is contained within a smaller wavelength region. The scattered light is shifted in energy from the excitation line by an amount proportional to the vibrational frequency involved. Thus, a  $1500\text{ cm}^{-1}$  vibration would appear at 425.5 nm when excited by a 400 nm line (25.5 nm separation), but at 659.3 nm when

excited by a 600 nm line (59.3 nm separation). There is a compromise between the intensity of the scattering and the resolution from the excitation line that can be obtained with monochromators.

Since glasses are not good scatterers, sample size has been a problem when dealing with bulk samples. It is difficult to get enough glass material to interact with the excitation light and then efficiently collect the scattered light by a monochromator. Thus, complicated collection optics are generally required for studies on bulk samples. Optical fibers represent a solution to this difficulty because focusing the light into the small volume of the fiber core increases the electric field density, and scattering intensity is directly proportional to field strength. The excitation light is confined to the fiber core, so long interaction lengths are possible. Since the scattered light can be analyzed by forward scattering (as opposed to perpendicular scattering) sample sizes from a meter to several hundred meters are possible. Complicated light collection systems are not needed because the output end of the fiber can be placed at the entrance slit of the monochromator and all the forward scattered light detected.

## EXPERIMENTAL

A simple Raman scattering experiment is shown in Figure 1. Monochromatic light from a laser source is launched into the test fiber, and the scattered light exiting the fiber is directed into a double monochromator. The monochromator is scanned, starting near the excitation line, toward longer wavelengths. The vibrational bands of interest are observed displaced from the excitation line by the energy of the vibration. A photomultiplier is used as the detector and the output plotted on a strip chart recorder using phase sensitive electronics.

## RESULTS

In Figure 2 the observed Raman scattering bands for several experimentally determined vibrations are shown. The vibrational assignments are also shown in the accompanying table. Of particular interest is the vibration at  $1320\text{ cm}^{-1}$ , assigned to the P=O stretching vibration. The other observed transitions are broadened by the coupling of the vibration to the silica network. However, the P=O vibration is much sharper than the other observed vibrations because the P=O bond is a terminating link in the network. The oxygen is not a bridging

oxygen as in the Si-O-Si bridge, and thus the P=O vibration is not damped by the rest of the silica network, and appears as a sharp transition. Also, this vibration appears in a region where there is little other interference from other dopants. We have used the uniqueness of this line for quantitative analysis of phosphorus levels in test fibers down to 0.05 mole percent, and think that quantitative determinations could be made to significantly lower levels.

One advantage to this type of analysis is that the silica can be used as an internal calibration. Since silica is in such a great excess compared to the other dopants present, the silica scattering peaks at  $1060\text{ cm}^{-1}$  or  $1600\text{ cm}^{-1}$  can be used as internal standards and the unknown peaks compared to them. For the results presented here, the ratio of the scattering peaks was determined for a calibration sample analyzed by electron microprobe. Subsequent samples were then easily computed by determining the peak ratios and comparing them to the calibration sample. The sample peak ratios are independent of the sample size since we are comparing to a known silica reference within each sample. A larger sample (longer fiber length) does give increased signal to noise however, and data will be presented using a 5 mW He-Ne laser and 60 meters of sample.

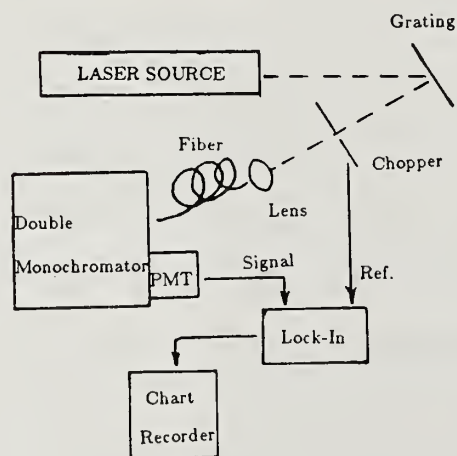
For most fibers, 10 meters of sample is enough, and a spectral scan requires about twenty minutes. Qualitative measurements are easily made for common dopants such as germania, phosphorus, fluorine, and boron, with quantitative determinations being only slightly more difficult. Quantitative measurements need suitable standards and peak-area determinations.

## CONCLUSIONS

Raman scattering is ideally suited to the study of optical fibers because (1) the excitation light is not confined to any particular region of the spectrum (2) sample size is greatly simplified since the light is confined to the fiber core, and (3) no complicated collection optics are needed. In addition, calibration samples need only be measured once since the ratio of peaks within the test sample may be used as an internal reference. Quantitative determinations of phosphorus levels have been made down to  $0.05 \pm 0.02$  mole percent using this technique. The determination of other dopants like fluorine, germania, and boron is also equally possible.

## REFERENCES

1. M. C. Tobin and T. Baak, "Raman Spectra of Some Low-Expansion Glasses," J. Opt. Soc. Am., **58**, 1459 (1968).
2. M. C. Tobin and T. Baak, "Raman Spectra of Vitreous  $B_2O_3$  and of Some  $B_2O_3-Al_2O_3$  Glasses," J. Opt. Soc. Am. **60**, 368 (1970).
3. F. L. Galeener, J. C. Mikkelsen, R. H. Geils, and W. J. Mosby, "The Relative Raman Cross Sections of Vitreous  $SiO_2$ ,  $GeO_2$ ,  $B_2O_3$ , and  $P_2O_5$ ," Appl. Phys. Lett., **32**, 34 (1978).
4. N. Shibata, M. Horiguchi, and T. Eda Hiro, "Raman Spectra of Binary High Silica Glasses and Fibers Containing  $GeO_2$ ,  $P_2O_5$ , and  $B_2O_3$ ," J. Non-Cryst. Solids, **45**, 115 (1981).
5. W. A. Sproson, K. B. Lyons, and J. W. Fleming, "Nondestructive Concentration Profiling of Fiber Optic Preforms by Analysis of Raman Spectra," J. Non-Cryst. Solids, **45**, 69 (1981).
6. P. Dumas, J. Corset, W. Carvalho, Y. Levy, and Y. Neuman, "Fluorine Doped Vitreous Silica Analysis of Fiber Optic Preforms by Vibrational Spectroscopy," J. Non-Cryst. Solids, **47**, 239 (1982).
7. G. W. Bibby and J. N. Ross, "Raman Spectra of Hydrogen Treated Optical Fibers," Electron. Lett., **20**, 182 (1984).
8. K. Noguchi, Y. Murakami, N. Uesugi, and K. Ishihara, "Raman Scattering Spectrum Analysis for Fluorine-Doped Silica Optical Fibers," Appl. Phys. Lett., **44**, 491 (1984).



Experimental Set-Up

FIGURE 1

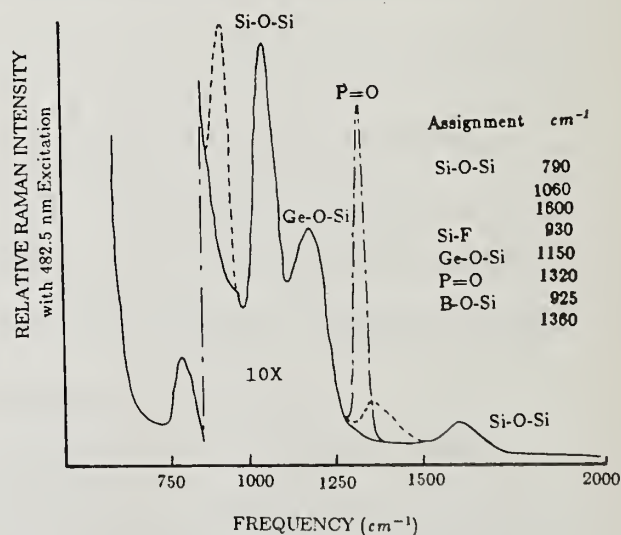


FIGURE 2



# UTILIZING CLADDING MODE PROPAGATION TO DETERMINE THE REFRACTIVE INDEX PROFILE OF AN OPTICAL FIBER

W.H. Hatton, E.L. Buckland and M. Nishimura

Sumitomo Electric Research Triangle, Inc.  
Research Triangle Park, NC 27709, USA

## 1. Introduction

A number of measurement techniques have been developed [1-2] in order to ascertain the refractive index profile of an optical fiber. For the most part, these measurement methods are associated with numerous drawback ( i.e. elaborate sample preparation, correction factors). The cladding mode near-field (CNF) technique has been developed in order to reduce the overall complexity of index profiling measurements. The CNF technique gives a direct measure of the refractive index profile, similar to the refractive near-field method[3-4], however, sophisticated optical and mechanical equipment are not necessary.

## 2. Principle of the CNF Technique

By surrounding an un-coated optical fiber with a material whose refractive index is less than the cladding ( for example air) light will not only propagate in the core, but also through the cladding region ( i.e. cladding modes). Consider the propagation of only cladding modes ( no modes bound by the core ) as shown in Figure 1. Utilizing Snell's law, light ray trajectories at the output end of the test fiber can be

described by

$$N_0 \cos \theta_1 = N(r) \cos \theta_2 \quad (1)$$

$$N(r) \sin \theta_2 = \sin \theta_3 \quad (2)$$

where  $N(r)$  is the local refractive index along the exit plane of the fiber, and  $N_0$  is the refractive index of the cladding. By combining equations (1) and (2), the angle at which light exits the fiber,  $\theta_3$ , can be uniquely related to a propagation angle of incidence  $\theta_1$ .

$$N(r)^2 - N_0^2 = -N_0^2 \sin^2 \theta_1 + \sin^2 \theta_3 \quad (3)$$

If uniform excitation of cladding modes exist then, from equation (3), the magnitude of  $N(r)$  at any radial position along the endface of the fiber determines the relationship between  $\theta_1$  and  $\theta_3$ . Assuming that  $N_0$  and  $\sin \theta_3$  are fixed, any variation in the fiber's refractive index profile will induce an equivalent change in  $\sin \theta_1$ . By examining the outputted intensity distribution with a detection system whose numerical aperture is limited (fixed at  $\sin \theta_3$ ), total power at any arbitrary point along the detected pattern will be directly related to  $\theta_1$ .

### 3. Description of CNF Measurement System

A schematic drawing of the measurement system is shown in Figure 2. Light from an intense optical source is focused along the glass/coating material interface of the test fiber. A small fraction of the power scattered at this interface will be coupled into the cladding region where for short lengths of un-coated

fiber, only cladding modes will be excited. The power outputted from the test fiber is projected onto a vidicon TV camera system where the total intensity profile is analyzed. The numerical aperture of the detection system is limited by an aperture, A1, placed directly behind lens L2. This position was chosen for convenience and is equivalent to positioning the aperture in front of the lens.

Preliminary laboratory results from the CNF technique have shown to be accurate when compared to data from other measurement methods. Three dimensional raster scans, as shown in Figure 3 for a polarization maintaining single mode fiber, are also easily obtained.

#### 4. Conclusion

A new method for accurately measuring the refractive index profiles of optical fibers has been developed. The cladding mode near-field technique has been shown to give a direct measure of the index profile without the requirement of elaborate test equipment, therefore, overall complexity of this type of measurement can be reduced.

#### References

- [1] D. Marcuse et al., Proc. of IEEE, 68, No.6, pp.666 - 688 (1980)
- [2] W.J. Stewart, IEEE Trans. Microwave Theory Tech., MTT-30, pp. 1439-1454 (1982)
- [3] W.J. Stewart, in Technical Digest of IOOC'77, paper C2-2 (1977)
- [4] K.I. White, Opt. Quant. Elec. , 11, pp 185-196 (1979)



Fig. 1 Propagation of cladding mode through an optical fiber

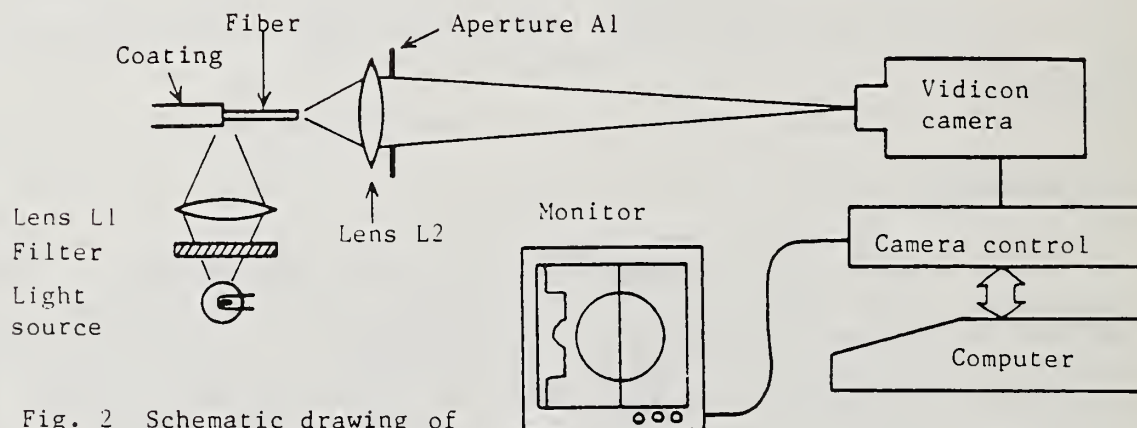
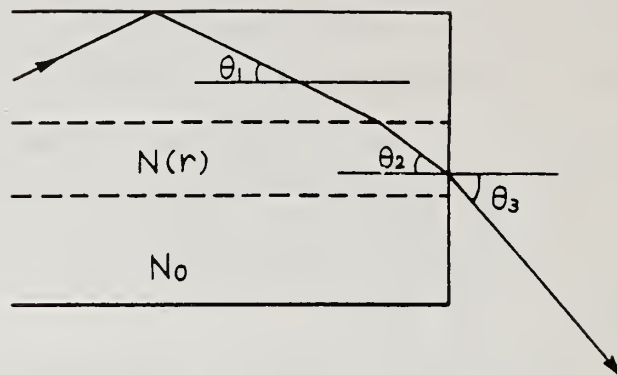


Fig. 2 Schematic drawing of CNF measurement system

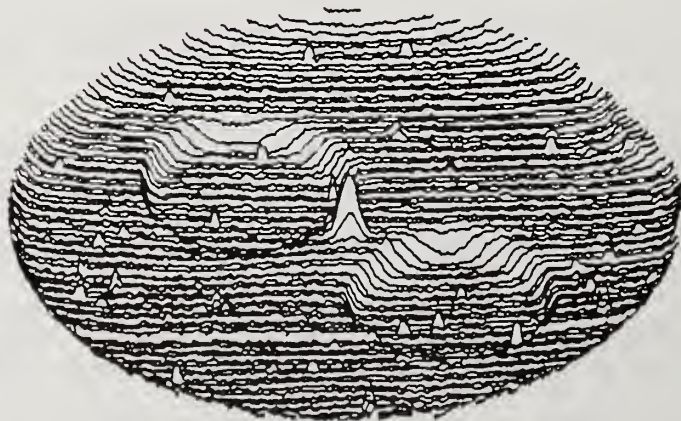


Fig. 3 Three dimensional raster scan of polarization maintaining single mode fiber

DETERMINATION OF REFRACTIVE-INDEX DISTRIBUTION  
FROM NEAR-FIELD MEASUREMENTS IN POLARIZATION MAINTAINING FIBRES

G. Coppa, P. Di Vita, M. Potenza

CSELT - Via G. Reiss Romoli, 274 - 10148 Torino (Italy)

Introduction

Polarization maintaining single-mode fibres are gaining increasing interest both in the field of sensors and in the field of communications. Their design is often based on azimuthally dependent refractive-index distributions: then these fibres can be characterized obtaining their two-dimensional refractive-index distribution.

In this contribution we propose an alternative method to the classical Refracted Near-Field technique [1], based on a numerical elaboration of the (Transmitted) Near-Field (TNF) intensity pattern of the fibre. This method has been already employed for circularly symmetric single-mode fibres and its effectiveness for one-dimensional index profiles has been proved [2]. However its extrapolation to two-dimensional index distribution measurements is not trivial, since the acquisition of a matrix of at least 50x50 TNF-points (with  $S/N > 30$  dB) is needed. This could be accomplished by a TV camera and a digitizing system, but the required performances are nearly at the limits of the available instrumentation. Otherwise a raster scanning of the measurement matrix could be performed by a photodiode. This leads to a considerably greater measurement time with respect to the one-dimensional case but it does not represent a particularly serious problem since available stabilized optical sources and precision motorized displacement scanning stages are required.

Moreover, the signal processing needs smoothing and differentiation algorithms which are substantially different owing to the two variables involved. Nevertheless the method is very convenient, since it requires a simple TNF set-up which is usually employed for the measurement of different parameters (e.g. mode field diameter or geometrical characteristics).

### Theory

The TNF-data processing is based on the fact that in single-mode fibres the intensity  $I(x,y)$  is proportional to the square of a component of the electromagnetic field  $E(x,y)$  which satisfies the following scalar wave equation:

$$\left(\frac{\partial^2}{\partial x^2} + \frac{\partial^2}{\partial y^2}\right)E(x,y) + \{[2\pi n(x,y)/\lambda]^2 - \beta^2\}E(x,y) = 0 \quad (1)$$

$n(x,y)$  being the refractive index distribution,  $\lambda$  the operating wavelength and  $\beta$  the mode propagation constant. Then it is possible to obtain the quantity  $\{[2\pi n(x,y)/\lambda]^2 - \beta^2\}$  from Eq. (1) directly, in terms of the measured field amplitudes. Since second derivatives have to be performed numerically on the measured data, these should be very accurate and a suitable smoothing procedure could be necessary. Absolute refractive-index differences and fibre NA's can be derived.

### Experimental results

The experimental apparatus is a standard TNF intensity scanning set-up with a dynamical range around 40 dB. The fibre under test is excited by an LED, its output end is magnified by means of a 0.65 NA objective and an x-y scan is performed by a moving photodiode in the image plane. A desk-top computer drives the displacement stages, acquires the TNF-data and processes them.



Figs. 1 to 3 show the results of the present method in some meaningful cases. In each figure the calculated refractive index distribution (a) and the TNF-pattern (b) for each fibre are reported. Fig. 1 concerns a circularly symmetric single mode fibre ( $\lambda = 1.3 \mu\text{m}$ ): the accuracy of the circular geometry confirms the good quality of the measurement procedure. Two fibres made in our laboratories are considered in Figs. 2 and 3 ( $\lambda = 1.5 \mu\text{m}$ ). The first one has an elliptical core with a remarkable dip in the centre that causes the field to break up into two peaks. Note how the depressed regions in the cladding are accurately evidenced by our algorithm. Finally Fig. 3 shows the characteristics of a square core fibre: though the structure is very complicated, an index distribution consistent with the original fibre design has been derived in this case too.

### Conclusions

A simple technique for the determination of two-dimensional refractive-index distributions in optical fibres has been proposed. It is based on a suitable elaboration of near-field measurement data. Experimental results have shown the accuracy and the reliability of the technique. This method can represent an useful tool of investigation for polarization maintaining optical fibres and, in general, for any non-circularly symmetric lightguides.

### References

1. W. J. Stewart, IOOC'77, Tokyo, Japan (1977), Tech. Digest, pp. 395 - 398.
2. G. Coppa et al., IOOC'83, Tokyo, Japan (1983), Tech. Digest, pp. 38-39.

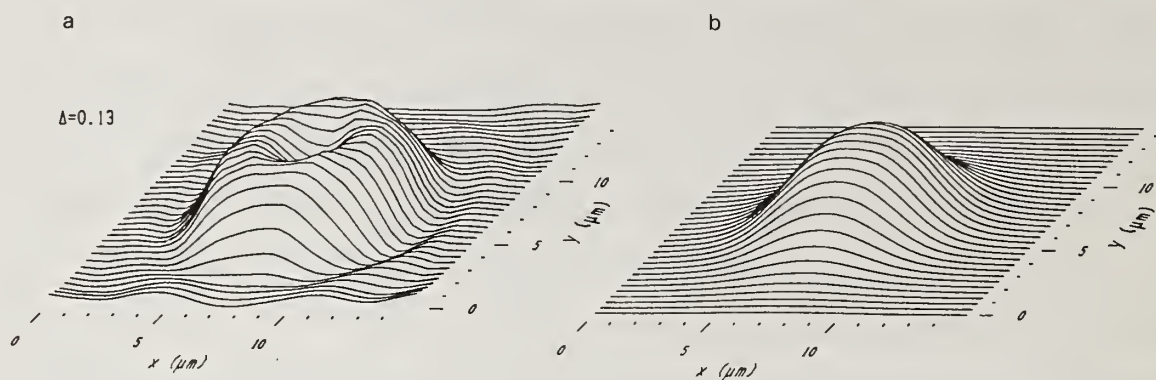


Fig. 1 Refractive index distribution (a) and two-dimensional near-field pattern (b) of a circularly symmetric fibre.  $\Delta$  is the maximum NA.

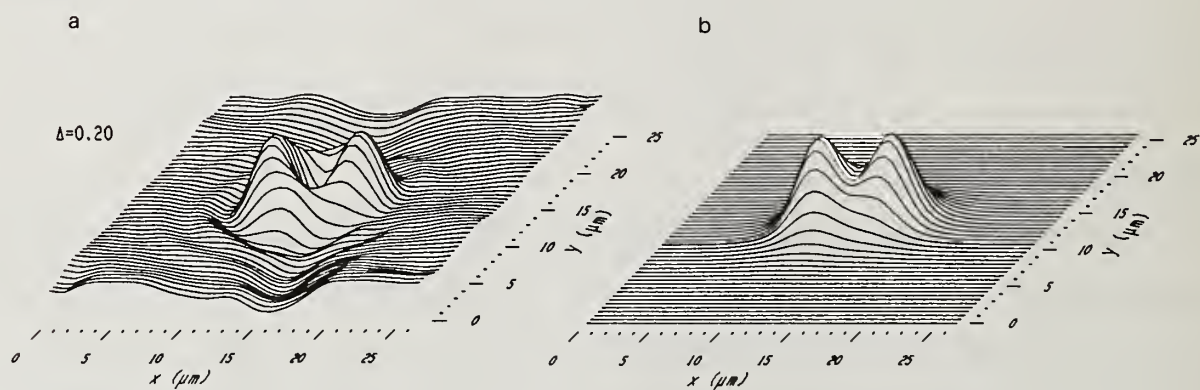


Fig. 2 The same as Fig. 1 but for an elliptical core fibre.

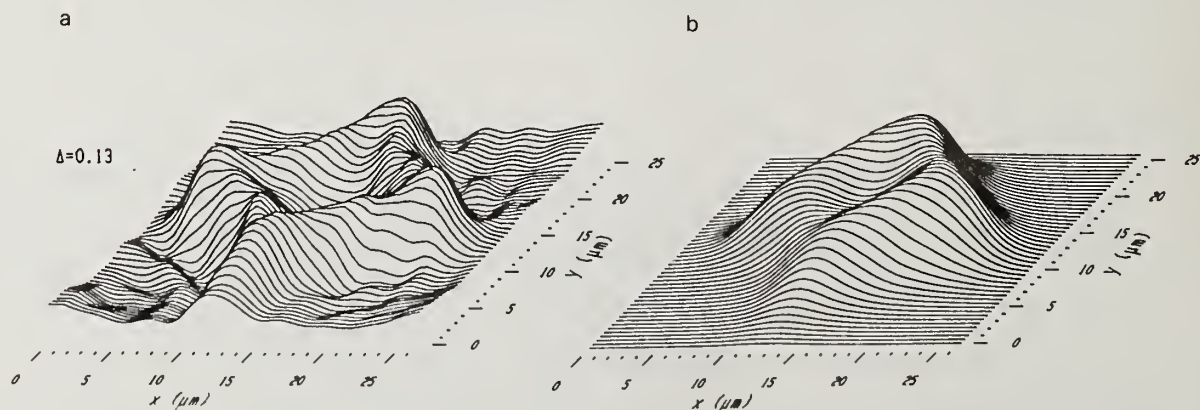


Fig. 3 The same as Fig. 1 but for a square core fibre.

Prism coupling technique: A novel method for measurement of  
propagation constant and beat length in single mode fibers

K.Thyagarajan, M.R. Shenoy and M.R. Ramadas  
Physics Department  
Indian Institute of Technology  
New Delhi 110016, INDIA

The prism-film coupling technique in integrated optics is a well-known technique for studying the mode spectra of planar optical waveguides. A prism whose refractive index is greater than or equal to the maximum refractive index of the waveguide is positioned close to the waveguiding structure; light incident on the base of the prism is coupled into the waveguide through the evanescent field in the intermediate layer. In a normal cladded fiber the modal field is not accessible from outside the fiber due to the large cladding thickness. However, if one can remove the cladding so as to be in the proximity of the core, it would be possible to couple light into (or out of) the fiber using this arrangement. Such a technique has been used earlier [1] to selectively excite particular groups of modes in a multimode fiber.

In this paper, we report preliminary investigations on the application of the prism-coupling technique to the measurement of the mode spectra of conventional and birefringent single mode fibers (SMF). Experimental results on the measurement of propagation constant in normal SMF, and the application of this technique to the measurement of beatlength on an elliptic core SMF, is presented.

In order to use the prism coupling technique, the cladding of the fibers were selectively removed using the standard polishing technique. Two single mode fibers, one from York



Technology (SM600) and the other from IIT (Tl601), having a cut off wavelength  $\sim 600$  nm were used in the experiment. The refractive index of the prism used was 1.5780. Light from a He-Ne laser was coupled into the fiber from one end and was decoupled using the prism placed on the polished surface. The propagation constant of the fiber mode can be determined by measuring the angle  $\theta$  at which the mode comes out of the prism (see Fig.1). The measured values of the propagation constants of the two fibers together with the calculated values using the fiber parameters given by the manufacturer and measured in the laboratory (for the IIT fiber) are given in table I. As can be seen the agreement is remarkably good; the slight difference can be attributed to the possible deviation of the prism lower surface from the plane tangent to the fiber's curvature, and also to the perturbation caused by the polishing operation. In the present experiment, however, the perturbation due to polishing is estimated to be small due to the observation that inspite of using an index matching liquid between the prism and the polished surface, complete decoupling of the mode was not possible which implies that a sufficient thickness of the cladding was still left.

In order to show the applicability of the technique to the measurement of beat length in birefringent fibers, we polished an elliptical core fiber (No.850417A- from Andrew Corporation) with its major axis perpendicular to the polished surface. Light from a He-Ne laser with the plane of polarization at  $45^\circ$  to the eigen polarization axes of the fiber was coupled into the fiber; the output consisted of two closely spaced m-lines separated by an angle of  $\sim 4'$ , and each one

was polarized, one with its plane of polarization parallel to and the other perpendicular to the polished surface. From the output coupling angles one can determine the difference in effective indices ( $\Delta n$ ) of the modes which would give us the beat length  $L_b$  according to the relation  $L_b = \lambda / \Delta n$ . The beat length of the same fiber was also measured independently using the Rayleigh scattering technique. The results of both these measurements are given in table II. As can again be seen, the agreement is very good.

The proposed novel technique should find applications in the measurement of the cut off wavelength in single mode fibers, the fiber dispersion characteristics, and can also be used to estimate the effect of polishing on the birefringence characteristics of single mode fibers [2].

The authors thank Dr. R.B. Dyott of the Andrew Corporation for providing samples of elliptic core fibers, and Professor A.K. Ghatak for constant encouragement.

#### References:

- 1 J.E. Midwinter, Optical Fibers for Transmission, John Wiley & Sons, New York (1979), p.208.
- 2 R.H. Stolen, 'Polishing-Induced birefringence in Single-mode fibers,' Applied Optics 25, 344 (1986).

Table I

Fiber type	$\beta/k_0$		
	Measured	Calculated from manufacturers data	Calculated from data obtained by RNF technique
ITT	$1.4592 \pm 0.0002$	1.45902	1.45927
York Technology	$1.4590 \pm 0.0002$	-	-

Table II

Fiber	Beat length measured using	
	Prism coupling	Rayleigh Scattering
Elliptic Core	$1.52 \pm 0.08$ mm	$1.5 \pm 0.01$ mm

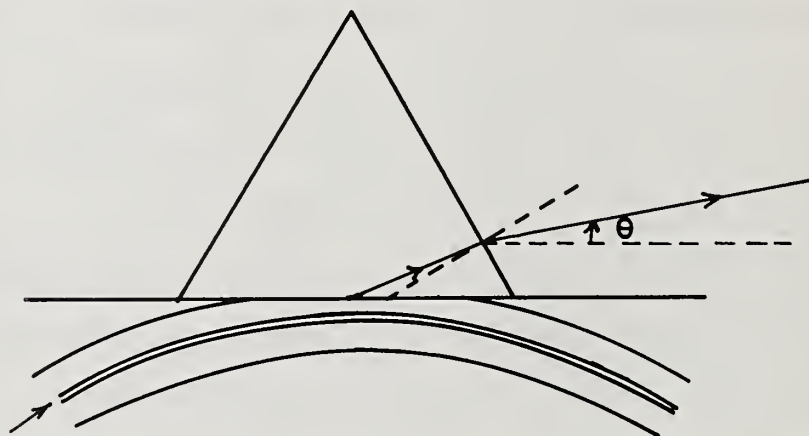


Fig.1



# CHARACTERIZATION OF OPTICAL FIBER SPLICES IN THE FIELD

Reinhard Engel  
Siemens AG,  
Munich, W Germany

Everett McNair  
Siecor Optical Cable  
Hickory, NC 28603

## I. INTRODUCTION

The objective of field splicing operations is to attain a permanent jointing which exhibits high strength and low loss. The generally recognized steps which must be accomplished to achieve this objective are; (1) precision alignment of the waveguides, (2) joining the waveguides, (3) permanent retention of the fiber's alignment and (4) an evaluation of the quality of the splice. This paper addresses field splice loss evaluation by reviewing the factors which contribute to splice loss and discussing some of the splice loss measurement methods that are currently being used in the field.

## II. SPLICE LOSS CHARACTERIZATION

Splice loss arises from both intrinsic and extrinsic factors. Loss attributed to intrinsic factors results from fiber-to-fiber parameter variations which occur during the manufacturing process. The degree to which intrinsic fiber parameters contribute to insertion loss at a splice can not be controlled or practically determined in the typical field environment.

Extrinsic contributors to splice loss are factors which can be directly influenced by the craftsperson or splicing technique. Lateral or axial misalignment of the fiber cores is the most significant extrinsic factor.

During the the splicing process the intrinsic and extrinsic losses are not additive. Instead they combine to yield a total loss which is less than their algebraic sum [1].

### III. Splice Loss Evaluation in the Field

Transmission Method. Fig. 1 illustrates a laboratory procedure for evaluating splice loss between dissimilar fibers. Before making the splice, the power, P1, transmitted through the first fiber is measured. After completing the splice a second power measurement, P2, is obtained in the immediate vicinity of the splice. The splice loss is then determined from

$$\text{Loss} = -10 \log P2/P1 \text{ dB} \quad (1).$$

This procedure is adaptable to the field environment but for multimode fibers, the location and the nature of the power source relative to the splice as well as the length (L2) of the fiber which follows the splice can affect the results obtained from transmission measurements [2]. For accurate splice loss measurements, the respective attenuation of the individual fiber lengths must be accounted for. In the field, this process requires a minimum crew size of three people. The uncertainties associated with cable losses can be eliminated by an ingenious but time consuming procedure known as presplicing [3], with a reported accuracy of +/- 0.02dB.

Local Detection. The use of local scattered light detection [4] reduces the overall splicing process to a two person operation and improves the speed with which two singlemode fibers can be aligned. Fig. 2 [4] provides a comparison of the alignment sensitivities achieved by far end transmission detection and local scattering detection methods. Splice loss is derived from a correlation between the amount of light coupled into the far end of one of the fibers and the amount of light that is locally detected at the splice point.

Optical Time Domain Reflectometry. Although the OTDR's accuracy is limited, splice loss can be easily evaluated by accessing only one

end of the jointed fibers. The OTDR measurement errors can be reduced, at the expense of productivity, by evaluating the splice from both directions and taking the mean of the results. Table 1 [5] shows the variances which can result from OTDR uni-directional measurements. An average directional splice loss difference of 0.20 dB was obtained from bi-directional measurements of 11 single mode splices. The maximum variance in measurements taken from opposite directions is 0.50 dB. The average of each series of uni-directional measurements compares favorably with the bi-directional average, illustrating that the uni-directional inaccuracies average out as the number of splice measurements increases.

Local Injection and Detection. The most reliable method of aligning fiber cores is the transmission method, because this measuring method duplicates the operating state of the fibers [6]. A prerequisite for its cost effective field application is the launching of light into the fiber core before the splice point and the extraction after the splice point. Application of bending couplers allows the injection of measuring light through the fiber cladding and coating into the fiber core directly at the splicer unit [7]. A local injection and detection system (Fig.3) simplifies the splicing process to a one-person one-location operation.

Some of the factors that affect measurement accuracy for single mode fibers are the measuring wavelength versus the cut-off wavelength for the fiber, amount of mode scrambling between the injection device and the splice, and the existence of cladding modes.

Given constant injection conditions, the extraction device detects the optical power level  $P_a$ , after the fiber ends have been fused. Using  $P_a$  and the ideal optical power level  $P_i$ , the splice loss is calculated



as 
$$\text{Loss} = -10 \log P_a/P_i \text{ dB} \quad (2).$$

$P_i$  is the level which could have been detected by the extraction device, if the splice had no loss. Therefore, the most accurate determination of the ideal level  $P_i$ , is a precondition for the calculation of splice loss.

One possible solution is to produce a reference splice by applying a drop of index matching fluid between the end faces of the fibers. This almost completely suppresses reflections caused by the air space between the fibers and perturbations due to angled end faces. After alignment in the lateral and axial directions, the power level at the detector corresponds so closely to the ideal level, that with identical single mode fibers the calculated splice loss has a typical margin of error of  $\pm 0.01 \text{ dB}$  [8].

When index matching fluid is not used, the opposing end faces form an optical resonator which reduces the optical transmission between the fiber ends by up to  $0.6 \text{ dB}$ , depending on the distance between the end faces. If the distance is greater than the coherence length of the measuring light, the interferences disappear and light transmission is only diminished by Fresnel reflection ( $0.3 \text{ dB}$ ), by the quality of the end faces and the gap between them (Fig. 4). If applied to identical single mode fibers, calculation of the ideal level according to the "gap" method for determination of the splice loss leads to a margin of error of  $\pm 0.08 \text{ dB}$  [9]. As in the case of the "wet" method, here too attenuation due to optical mismatching is not taken into consideration.

Much more accurate calculation of the ideal level, which also would take intrinsic losses into consideration, is expected from another "dry" method. With it, the interference response of the measuring light between the fiber end faces is used for calculation of the ideal level.

A maximum error of  $\pm 0.015$  dB is expected.

Direct Core Monitoring. The direct core monitoring [10],[11] splicing technique takes the approach of obviating splice loss measurements by addressing the accuracy with which fibers can be aligned solely by observation of the fiber cores. The estimation is based upon an analysis of the accuracy with which the fiber cores can be observed and manipulated to minimize alignment errors. Reportedly [10], a splice-loss standard of .2 dB can be guaranteed with 99 per-cent reliability when the observation detection accuracy is kept within 0.25  $\mu$ m.

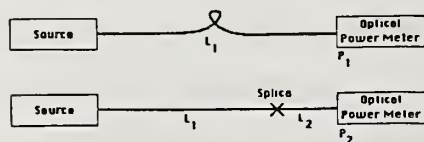
#### IV. SUMMARY

Field procedures for evaluating the quality of a splice must enhance the craftsperson's productivity as well as deliver the highest practical measurement accuracy. Ideally, the selected splicing technique is designed so that all four steps involved in the splicing operation can be performed by one individual located at the splice point. Local injection and detection systems offer this convenience and studies are on-going to further enhance the benefits of this technique.

#### REFERENCES

- [1] C.M. Miller, "Optical Fiber Cables and Splices," IEEE J. on Sel. Areas in Comm., Vol. SAC-1, No. 3, Apr. 1983; p. 536
- [2] R.B. Kummer, A.F. Judy, and A.H. Cherin, "Field and Laboratory Transmission and OTDR Splice Loss Measurements of Multimode Optical Fibers," Tech. Digest-Sym. Opt. Fiber Meas., 1982; pp. 109-121
- [3] Y. Kato, S. Seikai, and T. Tanifuji, "Arc-Fusion Splicing of Single-Mode Fibers: An Apparatus with an Automatic Core-Axis Alignment Mechanism and Its Field Trial Results," IEEE J. LW. Tech., Vol. LT-2, No. 4, Aug. 1984
- [4] C.M. Miller, "Local detection device for single-mode fiber splicing," Proceedings of OFC '82, paper THAA2
- [5] J. Lidh, "Splice losses: How measurements can mislead," Light-wave, The Jour. of Fiber Optics., June 1986;p. 47
- [6] T. Pavlopoulos, A. Lewis, M. McLandrich, "Simple method for permanently connecting single-mode fibers," Applied Optics, Vol. 16, No. 6, 1977; p. 1466

- [7] C. DeBlock, P. Matthyse, "Core Alignment Procedure for Single-Mode-Fibre Jointing," Elec. Ltrs., Vol. 20 No. 3, 1984; p. 109
- [8] Y.Kato, T. Tanifuji, M. Tokuda, N. Uchida, "New Optical Monitoring for Arc-Fusion Splice of Single-Mode Fibres and High-Precision Estimation of Splice Loss," Elec. Letters., Vol. 18, No. 22, 1982; p. 972
- [9] Y. Kato, S. Seikai, T. Tanifuji, "Arc-Fusion Splicing of Single-Mode Fibers: An Apparatus with an Automatic Core-Axis Alignment and its Field Trial Results," Jour. of LW. Techn., Vol. LT-2, No. 4, 1984; p. 442
- [10] O. Kawata, K. Hoshino, Y. Miyajima, M. Ohnishi, and K. Ishihara, "A Splicing and Inspection Technique for Single-Mode Fibers Using Direct Core Monitoring," IEEE J. LW. Tech., Vol. LT-2, No. 2, Apr. 1984.
- [11] O. Kawata, K. Hoshino, and K. Ishihara, "Low-Loss Single-Mode-Fibre Splicing Technique Using Core Direct Monitoring," Elec. Letters, Vol. 19, Nov. 24, 1983.



$$\text{Splice Loss} = -10 \log \frac{P_2}{P_1} \text{ dB}$$

Figure 1  
Laboratory Splice Loss Measurement  
for Dissimilar Fibers

SPICE NO.	VARIATIONS IN OTR MEASUREMENTS		ABSOLUTE DIFFERENCE	BIODIRECTIONAL
	MEASUREMENT DIRECTION >	MEASUREMENT DIRECTION <		
1	.31	.24	.07	.28
2	-.22	.28	.50	.03
3	.10	.04	.06	.07
4	.19	-.06	.25	.07
5	.00	.28	.28	.14
6	.17	.15	.02	.16
7	.10	.01	.09	.06
8	.27	-.15	.42	.06
9	.07	.08	.01	.08
10	.15	-.11	.26	.02
11	.00	.30	.30	.15
AVG	.104	.096	.205	.100

Sensitivity Comparison  
(Single Mode Fiber)

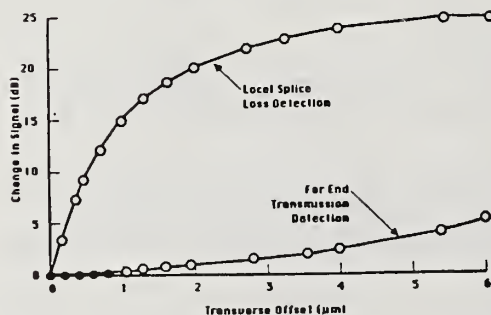
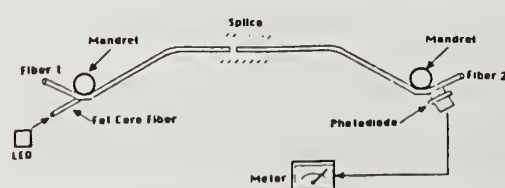


Figure 2



Local Injection and Detection System Principle

Figure 3

TABLE I  
VARIATIONS IN OTR MEASUREMENTS  
(From Ref. [5])

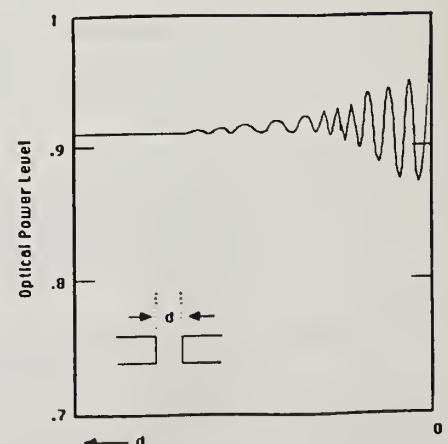


Figure 4



# CONSISTENCY OF MODE FIELD DIAMETER DEFINITIONS FOR FIBERS WITH GAUSSIAN AND NON-GAUSSIAN FIELD PROFILES IN DIFFERENT MEASUREMENT DOMAINS

by W. T. Anderson and J. P. Kilmer  
Bell Communications Research

## 1. Introduction

The Mode Field Diameters (MFDs) of two single-mode fibers can be used to predict the joint loss [1]. Controlling the MFD in manufacture will limit the intrinsic splice loss between two single-mode fibers from one supplier, and the differences between the MFDs of fibers from different manufacturers is a measure of the degree of compatibility between them. However, for the MFD to be of practical value as a predictor of fiber compatibility, the MFD measurements made by suppliers and users must be consistent for all fiber designs. Four measurement methods are commonly used: far-field scanning [2], measuring transmission through an offset joint [3], measuring transmission through apertures in the far-field [4,5], and far-field knife-edge scanning [6]. After years of debates in national and international standards organizations, none of these methods is universally accepted as a reference test method, nor is any method more or less fundamentally correct than the others. Therefore, consistency among the methods is especially important.

The MFD is computed from data generated by any of these measurement methods by applying a suitable definition. In this paper, we consider two different definitions. For the first generation of single-mode fibers, whose index of refraction profiles are nearly step-index, the field distributions are well approximated by gaussian functions [7]. It has been shown that, for the first generation of single-mode fibers, these gaussian definitions give consistent results among several of the measurement methods [8,9]. An alternative definition of the Mode Field Diameter is based upon the second moment of the far fields [10,11,12]. This second moment definition, which is often called the "Petermann 2" definition, is independent of the shape of the field distribution and, in principle, can be used to predict the joint loss between any two single-mode fibers of similar design. However, the applicability and consistency of this definition to the commonly used measurement methods has not been established, although a theoretical study [13] has shown that this definition is more consistent than the gaussian definition for fibers with non-step-index profiles.

The measurement methods are related to a good approximation by a number of transforms, as shown in Figure 1. Because of these transform relationships, theoretically or experimentally derived fields for any domain may be transformed into the other domains, and the MFDs which result from applying the two definitions in all five domains may be compared. In this manner, the degree of consistency among the measurement methods can be quantified, and a rational basis for the selection of a definition for the MFD can be established.

In section 2, MFD consistency is tested for a perfect step-index fiber using theoretically computed far fields. These results are verified using measured far fields for two commercially available nearly step-index fibers. In section 3, the MFD consistency is tested using the measured fields for a commercially available non-step-index dispersion shifted fiber. Finally, in section 4, conclusions are drawn.

## 2. Step-Index Fibers

The gaussian definition is applied to the four measurement methods as follows: far field- the overlap integral, offset joint- the  $1/e$  point, variable aperture- an integrated gaussian fit, and knife edge- an error function fit. For the second moment definition, moments can be used in all but the offset joint measurement, where the central curvature is needed.

The far fields of a step-index fiber can be expressed in closed form, so this is a logical starting point for the theoretical study. With a single integration or transformation of the far fields, the offset joint, variable aperture, or knife edge measurement can be simulated, and the consistency of the definitions can be tested by applying the definitions in each of the domains and comparing the resulting MFDs. Similarly, measured far field data for two approximately step-index fibers can be transformed into the other three domains and MFDs can be determined in an identical fashion. One of the two fibers is a depressed-cladding design manufactured using the inside process, and the other is a matched-cladding design manufactured using the outside process. When the second moment definition is applied to a set of transformed far field data, a consistent MFD value (to within 0.2%) is calculated in each domain. This is expected due to the portability of the moment definition. This moment MFD value is used as a gauge to compare the MFDs which result from applying the gaussian definition to the theoretical and experimental data for the two fibers at the two measured wavelengths in the four measurement domains. This is shown in figure 2. The gaussian MFDs are fairly consistent at 1300nm, but are less consistent at 1540nm where the field distributions are evidently somewhat less gaussian. Since the usual tolerance on the MFD is  $\pm 10\%$ , then differences of less than one or two percent are desirable. The theory and experiment are in good agreement considering that the fibers which were measured differed from an idealized step index profile.

## 3. Non-Step-Index Fibers

Far fields for a dispersion-shifted fiber [14] were measured. After transforming this data to the other three domains, MFDs were computed using both the gaussian and the second moment definitions. Results are shown in figure 3. The gaussian definition gives inconsistencies as large as 15%, while the second moment definition is consistent to within 0.2%. To verify that the second moment definition is a better predictor of splice loss, the autocorrelation function for this fiber is plotted in figure 4. Also plotted are the splice loss estimates resulting from both the second moment MFDs and the gaussian MFDs. Clearly, the second moment definition gives a superior estimate of splice loss.

## 4. Conclusions

For step-index fibers at 1300nm, either the gaussian or the moment MFD definition leads to consistency among the five measurement methods. However, for fibers with non-gaussian fields, the gaussian definition leads to inconsistencies as large as 15% between measurement methods. Furthermore, the gaussian definition does not lead to accurate predictions of splice loss. The next step in this study is a direct measurement comparison among the various methods to be certain that actual implementations yield the levels of consistency which the transforms have shown to be possible. Such a direct comparison will be presented in a forthcoming paper.

## REFERENCES

- [1] D. Marcuse, *BSTJ*, Vol. 56, No. 5, p. 703, 1977.
- [2] K. Hotate and T. Okoshi, *Applied Optics*, Vol. 18, No. 19, p. 3265, 1979.
- [3] J. Streckert, *Optics Letters*, Vol. 5, No. 12, p. 505, 1980.
- [4] E. Nicolaisen and P. Danielsen, *Electronics Letters*, Vol. 19, No. 1, p. 27, 1983.
- [5] D. K. Smith and R. A. Westwig, *Technical Digest*, OFC 85, Paper TuB2, 1985.
- [6] P. Samson, *Optics Letters*, Vol. 10, No. 6, p. 306, 1985.
- [7] D. Marcuse, *J Opt Soc Am*, Vol. 68, No. 1, p. 103, 1978.
- [8] W. T. Anderson and D. L. Philen, *IEEE JLT*, Vol. 1, No. 1, p. 20, 1983.
- [9] D. L. Frantzen and R. Srivastava, *IEEE JLT*, Vol. LT-3, No. 5, p. 1073, 1985.
- [10] K. Petermann, *Electronics Letters*, Vol. 19, No. 18, p. 712, 1983.
- [11] C. Pask, *Electronics Letters*, Vol. 20, p. 144, 1984.
- [12] W. T. Anderson, *IEEE JLT*, Vol. LT-2, No. 2, p. 191, 1984.
- [13] J. C. Auge and L. B. Jeunhomme, *Technical Digest*, SPIE Tech Symp, August, 1985.
- [14] T. D. Croft, J. E. Ritter, and V. A. Bhagavatula, *Technical Digest*, OFC 85, Paper WD2, 1985.

Figure 1

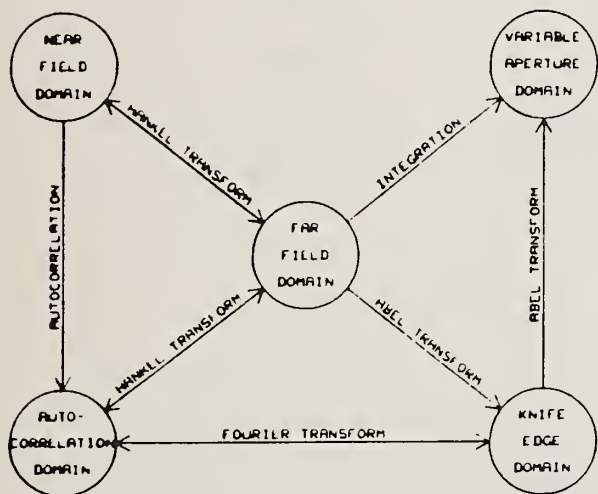


Figure 3

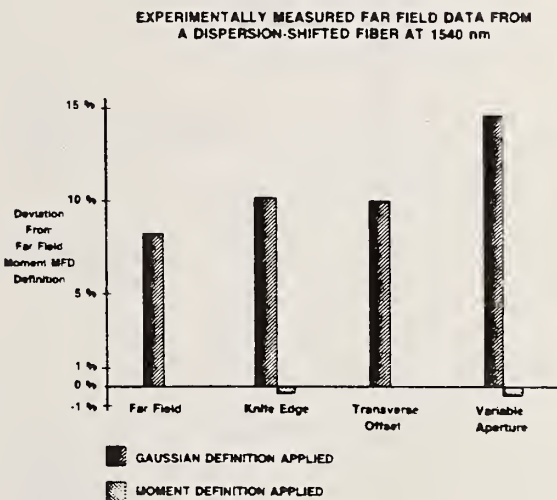
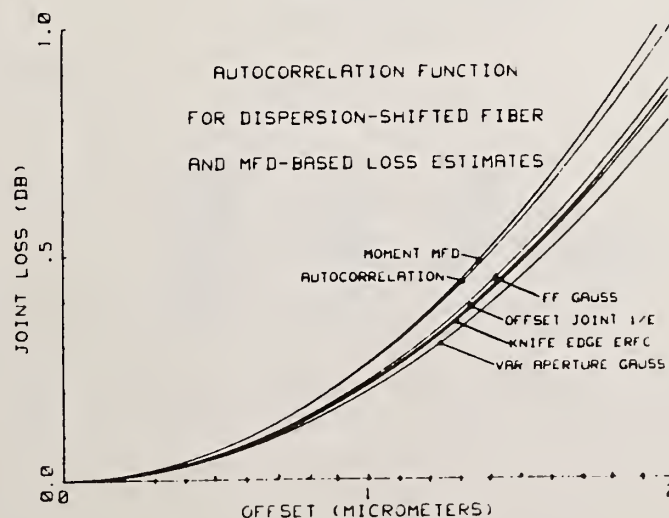


Figure 4





Deviation From Far Field Moment MFD Definition

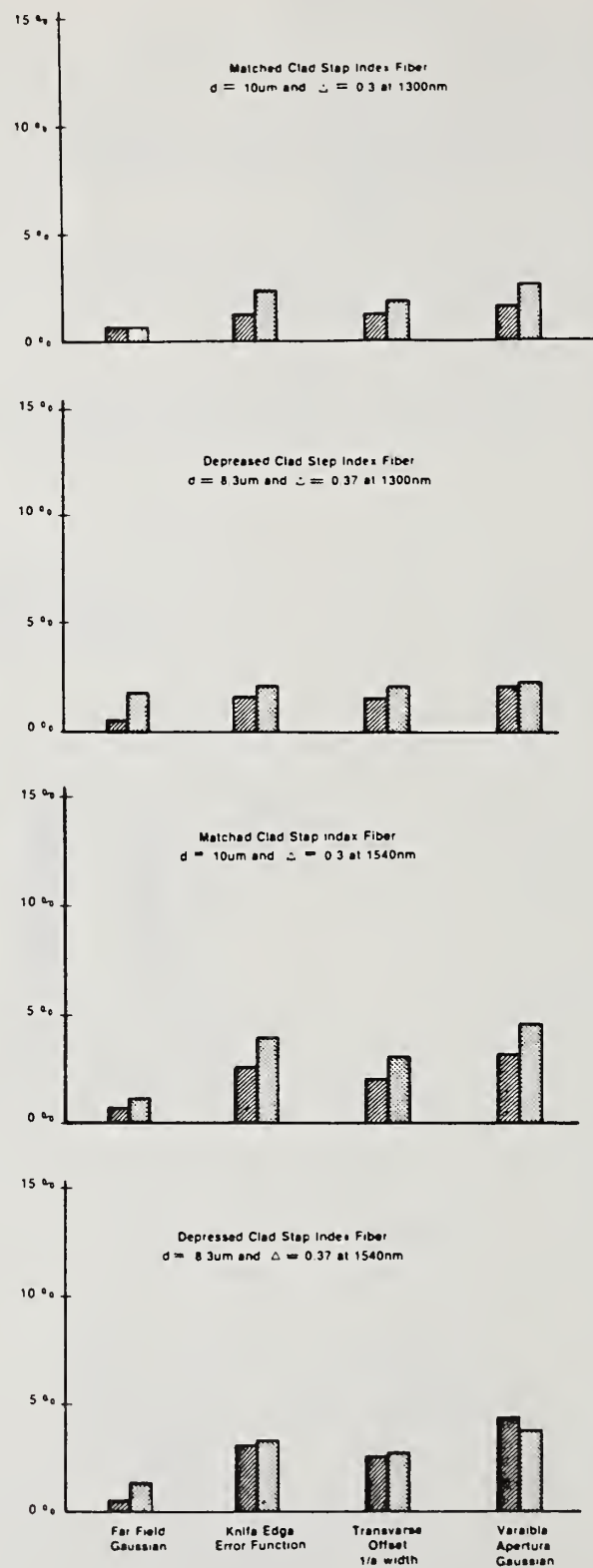


Figure 2

Theoretically Calculated Farfield Data  
 Experimentally Measured Farfield Data

A NEW TECHNIQUE FOR MODE FIELD DIAMETER DETERMINATION  
BY TRANSVERSE OFFSET MEASUREMENTS

M. Calzavara, G. Coppa, P. Di Vita

CSELT - Via G. Reiss Romoli, 274 - 10148 Torino (Italy)

Introduction. The problem of standardization of the mode field diameter (MFD) of single mode fibres is still debated. Different definitions of MFD are available with different meanings [1]. Among these the MFD  $d$  defined as the inverse of the r.m.s. width of the far-field distribution is finding an increasing interest.  $d$  can be evaluated in principle from far-field, from near-field and from transverse offset (TO) measurements. At present the last measurement technique seems the most critical. In fact calling  $P(u)$  the coupled power between the two fibre sections with a pure transverse offset  $u$ ,  $d$  is given by [2]:

$$(1) \quad d = 2[-2P(0)/P''(0)]^{1/2}$$

The most convenient way to calculate  $d$  consists in fitting the measured  $P(u)$  by a suitable function for  $u \ll d$  and applying Eq. 1 to the fitting function. This requires a lot of experimental points in the fit region. Although many practical problems of the TO technique have been overcome by the self-imaging version of the method [3] the need of submicron displacements still could represent a weakness of this technique with respect to the others. In this contribution we present some substantial improvements to the self-imaging TO technique that overcomes this weakness. The fitting procedure of the TO curve is also discussed and an effective algorithm is suggested.

Measurement technique. The chosen TO set-up (Fig. 1) is the self-imaging version further improved by a new optical component that simplifies the fibre

positioning procedure and improves optical resolution, and by introducing a fast scanning high-resolution measurement of TO curves.

The new optical component L (Fig. 1) is both reflective and refractive. It is obtained from a positive aplanatic meniscus lens, known also as Luboshez lens [4], by means of a partially reflecting metallic layer deposited on the concave surface. The Luboshez lens is able to make, in monochromatic light, an aberration free image of a pointlike object placed in the center of curvature of its concave surface. This concave surface is metallized and works as the spherical mirror used in the self imaging TO technique. Radiation from the fibre is partially reflected by the mirror and coupled back to the fibre itself to measure  $P(u)$ . Positioning of the fibre end in the mirror centre is accomplished observing the image formed by the part of light that crosses L. This also permits, e.g. in the case of elliptical core fibre, to control the orientation between the core axis and the scan direction. The aplanatism condition is satisfied at  $\lambda=633$  nm, because the alignment is performed with an auxiliary He-Ne laser beam. With component L the mirror NA can be very close to 1 (value attainable with a hemispherical concave surface). The observing optical system can be operated like a common high working distance microscope. The excitation of the fundamental mode and the measurement of the radiation coupled back is performed with the same apparatus described in [3]. A fast scan with 1024 points is performed by oscillating L at 60 Hz by a piezoelectric actuator. The signal from the detector and the sinusoidal signal (proportional to the mirror displacement) that drives the PZT high voltage amplifier are sent to the two input channels of a programmable digitizing oscilloscope, with 1024 points resolution. For an oscillation range of  $30\text{ }\mu\text{m}$  the average distance between two next points on the  $P(u)$  curve is about  $0.06\text{ }\mu\text{m}$ . Thus a high resolution, thanks to the very small scanning step, can be obtained. In addition a very high SNR is attainable, owing to the



possibility of high speed average. Finally a desktop computer acquires the two waveforms, provides  $P(u)$  and performs the elaboration.

Calculation of MFD. Fig. 2 shows the 80 experimental  $P(u)$  central points. The simplest fitting curve to these data is a parabola, but its parameters and hence  $d$  are heavily affected by the data errors when the number of experimental points is too small. To increase the number of fitted points it is necessary to use a larger  $u$ -range. But in this case  $P(u)$  can depart significantly from a parabola. However, considering that  $P(u)$  is approximately gaussian, we propose the following fitting function (Fig. 2):

$$(2) \quad P(u) = (A + Bu^2) \exp[-(2u/d_e)^2]$$

where  $d_e$  is the MFD obtained from the  $1/e$  points of the experimental  $P(u)$ ;  $A$  and  $B$  are the parameters to be determined by the fitting procedure. From Eqs. 1 and 2 one gets  $d$ . Fig. 3 shows the calculated  $d$ -value versus the number of fitted points. The first part of the curve, corresponding to few fitted points, is not reliable. On the other hand for very large number of points the curve becomes to drift. However, thanks to the chosen fitting function, a large central range (50-90 points) is left in which the obtained  $d$ -value is relatively constant, allowing a precise determination of the MFD. This could suggest an effective procedure for MFD evaluation. As a confirmation, a good agreement with the  $d$ -value obtained from a near-field measurement (dashed line) can also be observed.

#### References

1. G. Coppa et al., EFOC/LAN 85, Montreux (CH), 19-21 June 1985.
2. G. Coppa, P. Di Vita, CSELT Rapp. Tecn., Vol. 11 (1983), p. 427.
3. M. Calzavara et al., Electron. Lett., Vol. 22 (1986), p.144.
4. M. Herzberger, Modern Geometrical Optics, Interscience, 1958, p. 52.

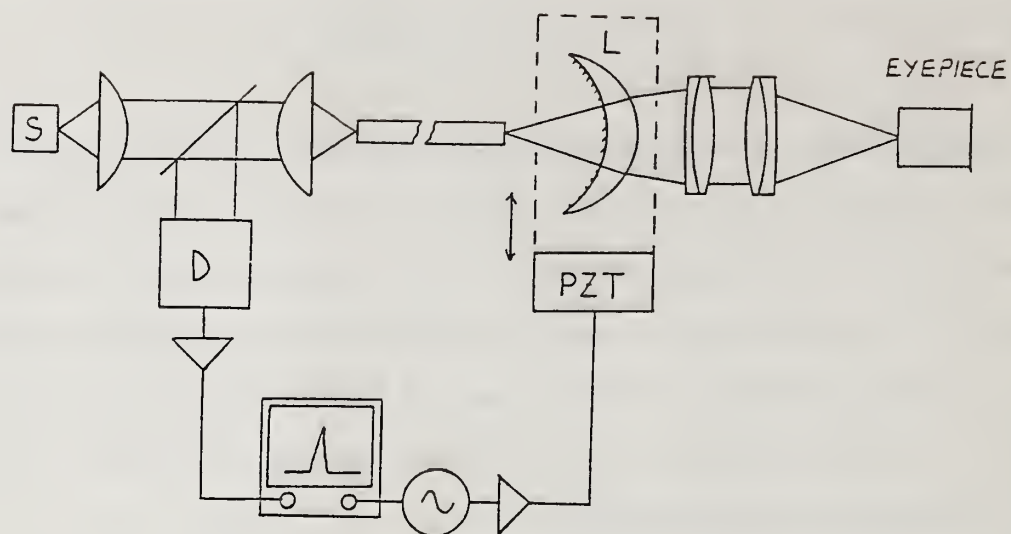


Fig. 1 - Schematic diagram of equipment

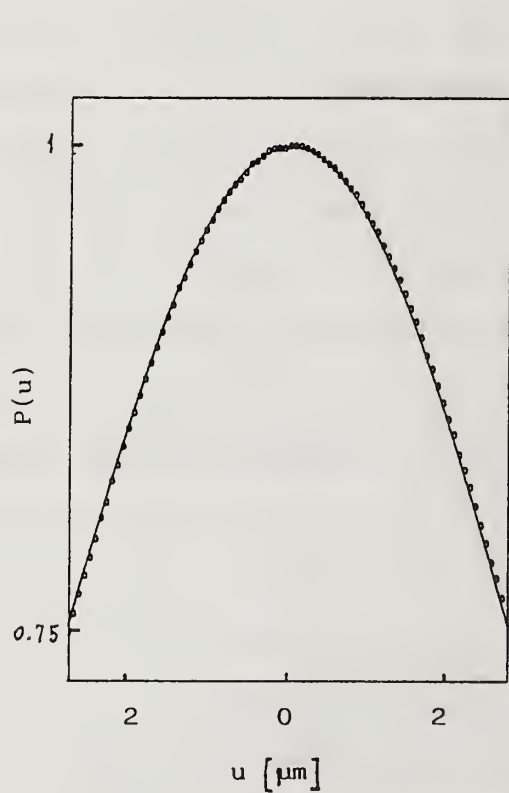


Fig. 2 - Experimental  $P(u)$  points (circlets). Fitting function according to Eq. 2 (full line)

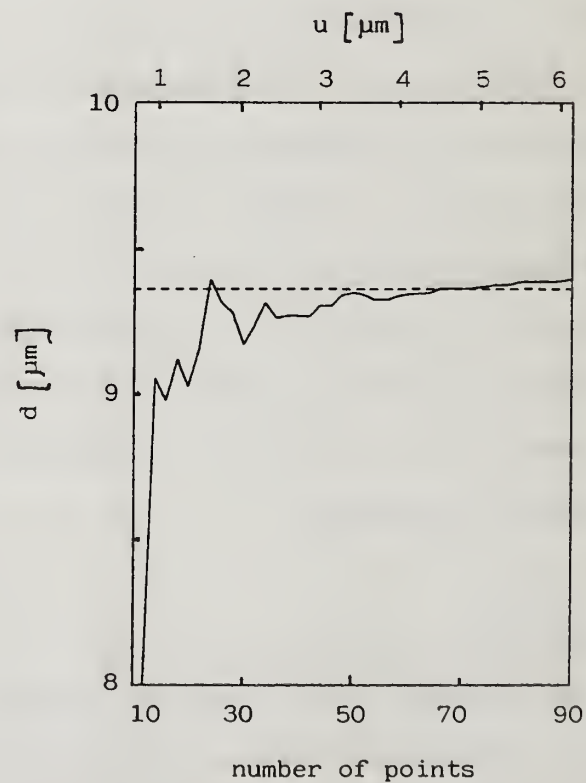


Fig. 3 -  $d$  evaluation versus the number of fit points

# Joint Losses as a Function of Offset and Mode Field Diameters for Dispersion-Shifted and Standard Fibers and Fiber Combinations

V. Shah, L. Curtis, and W. C. Young

Bell Communications Research, 331 Newman Springs Rd., Red Bank, NJ 07701-7020

## 1. INTRODUCTION

Recently, there has been increased interest in single-mode fibers having zero dispersion at 1550 nm because the spectral loss of the fiber has its minimum value near that wavelength. These fibers are called dispersion-shifted fibers, and have more complex index profiles than the standard fibers that have their zero dispersion wavelength at 1300 nm. Contrary to the case of standard fibers, the fields of such fibers are non-Gaussian in nature. And while the Gaussian approximation has been shown to give accurate results for the mode field diameter (MFD) of standard fibers,<sup>[1]</sup> for dispersion-shifted fibers, an alternate definition called "Petermann 2" based on the second-moment of the far field<sup>[2]</sup> has recently been shown to give consistent results for commonly used measurement techniques.<sup>[3]</sup>

In this paper, we present the results of the comparison between the measured values of the joint losses as a function of offset and a theoretical model, based on the Gaussian function of the offset. The comparison is performed on three fibers with different index profiles, two of which are standard matched cladding (MC) and depressed-cladding (DC) fibers, the third being dispersion-shifted (DS) fiber with a triangular core with a ring in the cladding region. Both the cases of identical and non-identical fibers (MFD's different) making up the joint are treated.

### MEASUREMENT OF THE MFD:

The MFD of the fibers were measured using the transverse offset method from which the mode field diameter was determined from the normalized curvature of the transmission coefficient as a function of offset at the point of zero offset. This definition has been shown to be equivalent to the second-moment of the far field definition.<sup>[1]</sup> This definition assumes identical fiber on both sides of the joint. We have extended this definition to include the measurement of the equivalent MFD of two non-identical fibers in a joint. It is defined to be  $2w_{eq} = 2/(\pi W_{eq})$  where, with  $F_1(q)$  and  $F_2(q)$  representing the far field amplitudes of fiber 1 and 2, respectively,

$$W_{eq}^2 = \frac{\int_0^{\infty} q^3 F_1(q) F_2(q) dq}{\int_0^{\infty} q F_1(q) F_2(q) dq} \quad (1)$$

$$\text{and } q = \frac{1}{\lambda} \sin \theta$$



The equivalent mode field radius (MFR) of non-identical fibers in the joint is then determined by the normalized curvature as discussed above. The results of these measurements are summarized in Table I. Numbers in parentheses in the table, are values of the equivalent MFR based on the Gaussian field assumption (i.e.,  $w_{eq}^G = \sqrt{(w_1^2 + w_2^2)/2}$ ).

#### COMPARISON OF THE JOINT LOSS MODEL WITH MEASUREMENT

The joint loss, as a function of transverse offset of fibers with non-Gaussian fields can be predicted by measuring the far fields and numerically evaluating the inverse Hankel transform<sup>[4]</sup>. As an alternative approach, in this study, a Gaussian function is used to model the joint losses of fibers (with non-Gaussian fields) as a function of transverse offset. The MFD based on the second-moment definition (or extension thereof for non-identical fibers) is used to characterize the Gaussian function used in the model. For standard fibers, loss (dB) due to mis-match =  $20 \log [(w_1^2 + w_2^2)/(2w_1 w_2)]$ ,  $w_1$  and  $w_2$  being the mode field radii of the fibers. For DS fibers, an overlap integral involving the far field amplitudes needs to be evaluated. This overlap integral has been shown to predict the loss due to mis-match with good accuracy<sup>[5]</sup>. In the absence of the far field data, in this paper, the measured value of the loss due to mis-match is used in the model.

Figures 1 and 2 show theoretical and measured joint loss vs offset at 1300 and 1550 nm for the MC and DS fibers, respectively. While the agreement between the measured and theoretical values is excellent for the standard fiber, for the DS fiber, there is good agreement for losses up to about 2 dB. For losses greater than 2 dB, the model predicts higher losses compared to the measured values.

The loss vs offset plot for MC/DS combination is shown in Fig. 3. It is evident that the model, using modified "Petermann 2" MFR ( $w_{eq}$ ) predicts joint losses with good accuracy at both wavelengths. Likewise, the same performance was observed for DC/DS and DC/MC combination.

Figures 4 and 5 show the loss vs offset plots at 1300 and 1550 nm, respectively, for MC fiber (curve A), DS fiber (curve B) and MC/DS combination (curve C). These three curves are measurement results. Curve D in both figures represents the calculation for MC/DS joint based on the theory developed in reference [6]. The loss in dB for the offset  $d$  is given, in this case, by<sup>[6]</sup>

$$\text{Loss} = 20 \log \left[ \frac{w_1^2 + w_2^2}{2w_1 w_2} \right] + 4.343 \left( \frac{d}{w_{eq}^G} \right)^2 \quad (2)$$

where  $w_1$  and  $w_2$  are measured MFR of individual fibers and  $w_{eq}^G$  is taken from the numbers in parenthesis in Table I. It is clear that this model overestimates the losses. The difference between the measured and calculated values, curves C and D for MC/DS joint, is smallest at zero offset and increases as the offset increases. The same performance holds for DC/DS combination.



## CONCLUSION

For both the cases of identical fibers (standard and dispersion-shifted) and DS/Standard fiber combination, a Gaussian joint loss model, characterized by the MFR based on the second-moment of far field (or its extension for non-identical fibers), was found to predict joint loss (at 1300 and 1550 nm), as a function of offset, within the range of practical interest with good accuracy. The difference between the measured and the theoretical loss value was less than .05 dB at 2 dB.

The authors would like to thank Corning Glass Works for providing the dispersion-shifted fiber used in this study.

## REFERENCES

- [1] W. T. Anderson, IEEE J. of Lightwave Tech., Vol. LT-2, No. 2, p. 191, 1984.
- [2] K. Petermann, Electron Letts., Vol. 19, No. 18, p. 712, 1983.
- [3] W. T. Anderson, et al., to be submitted for publication.
- [4] C. Pask, Electron Letts., Vol. 20, No. 3, p. 144, 1984.
- [5] W. T. Anderson, et al., submitted for publication.
- [6] D. Marcuse, BSTJ, Vol. 56, No. 5, p. 703, 1977.

TABLE I

Wavelength	Fibers					
	MC	DC	DS	DS/MC	DS/DC	DC/MC
1300 nm	4.95	4.50	3.33	4.45 (4.22)	4.3 (3.96)	4.72 (4.73)
1550 nm	5.70	5.15	4.26	5.31 (5.03)	4.95 (4.72)	5.37 (5.43)

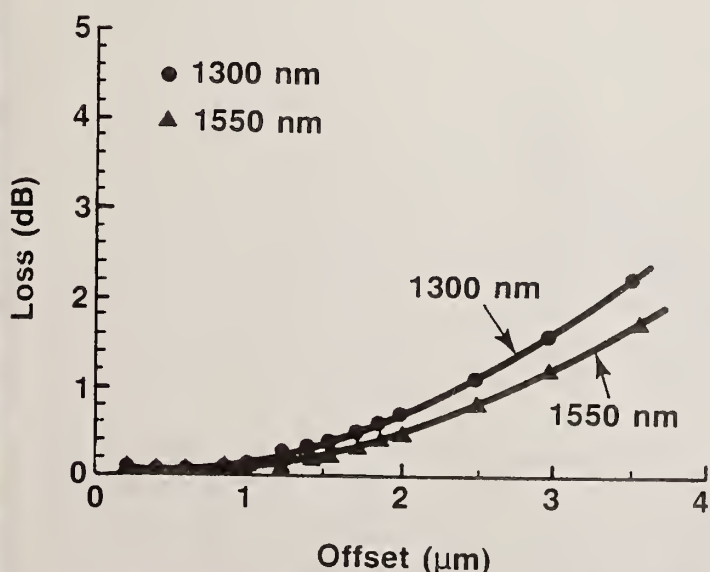


Fig. 1 Joint loss vs offset plot for MC fiber. Solid lines are theoretical calculations. ● and Δ represent measured values.

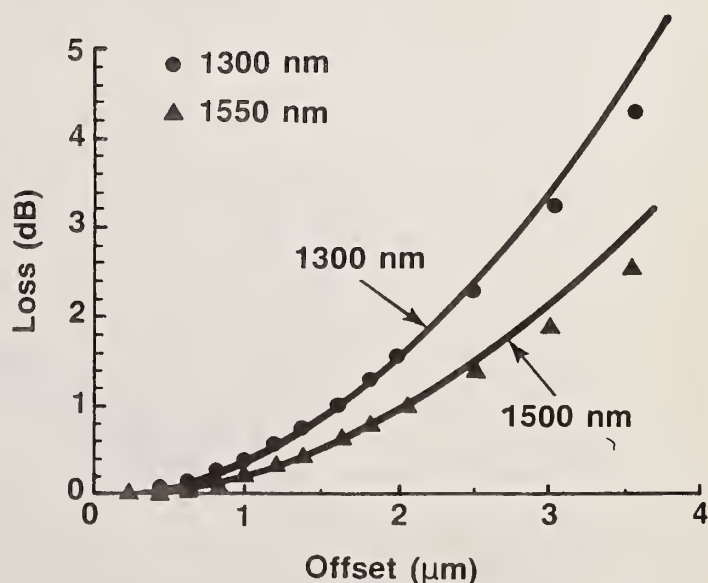


Fig. 2 Joint loss vs offset plot for DS fiber. Solid lines are theoretical calculations. ● and Δ represent measured values.

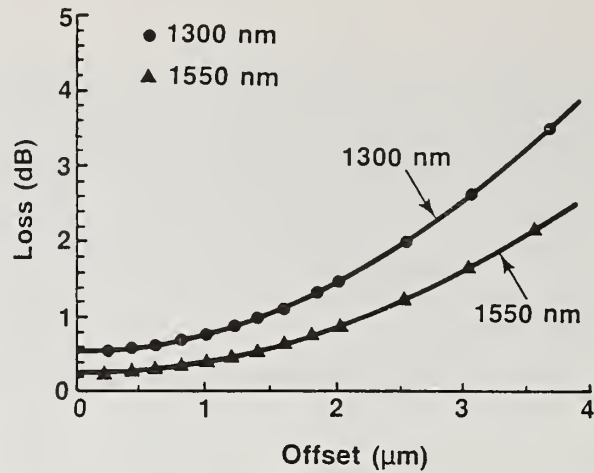


Fig. 3 Joint loss vs offset plot for MC/DS combination. Solid lines are theoretical calculations. • and  $\Delta$  represent measured values.

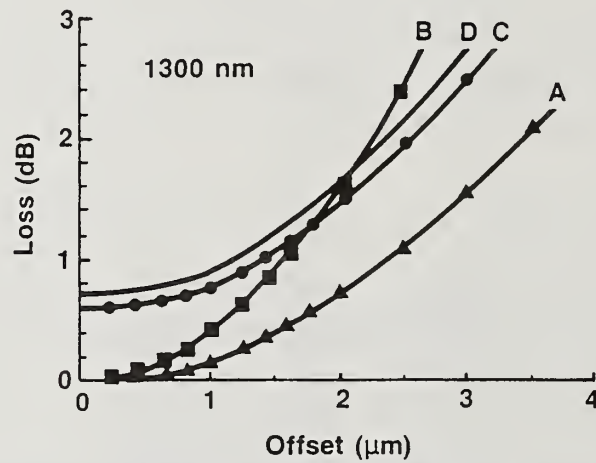


Fig. 4 Comparison of measured joint loss values with the theoretical model based on Eq. (2) at 1300 nm for MC/DS combination. Curves A, B and C are measurement results while D is theoretical curve.

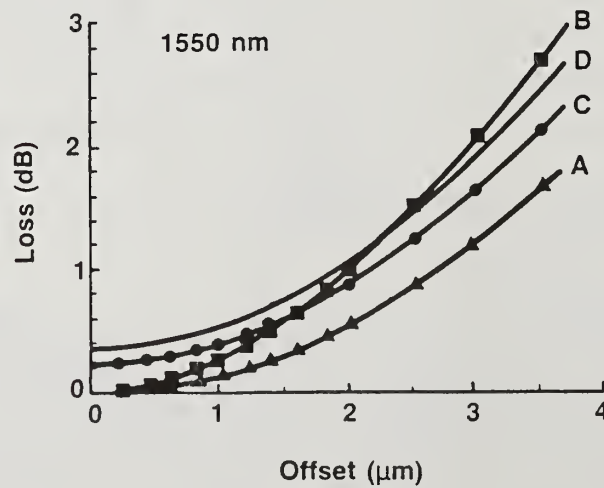


Fig. 5 Comparison of measured joint loss values with the theoretical model based on Eq. (2) at 1550 nm for MC/DS combination. Curves A, B and C are measurement results while D is theoretical curve.

# A NOVEL SINGLE-MODE FIBER SPLICE ALIGNMENT AND LOSS MEASUREMENT USING LOCAL DETECTION

Ian A. White and Paul D. Ludington†  
AT&T Bell Laboratories  
2000 Northeast Expressway  
Norcross, Georgia 30071  
(404) 447-2696

A mandrel-wrap local detector (MWLD) is described that is used to align single-mode (S-M) fiber splices to within 0.2  $\mu\text{m}$  and to accurately measure splice loss. A simple theoretical result for splice loss prediction from scattered power measurements is given and generally predicts splice loss within 10% when compared to far-end transmission measurements. Field results for some 10,000 splices, using this method, have yielded average losses of < 0.05 dB.

## INTRODUCTION

Local detection of power lost in S-M fiber splices can be used to assist in alignment of fiber cores during splicing and to determine splice loss. Many authors have reported the use of such local detection schemes.<sup>1-4</sup> The estimation of splice loss by these schemes is generally based on calibration of the splice loss versus detected power, and can be in error due to variations in the parameters of the receiving fiber. In this paper, we present a local detection system for the alignment of S-M splices, and a new theoretical calculation (using this locally detected scattered power) to accurately predict splice loss. This technique has been incorporated in the AT&T Technologies Single-Mode Bonded Splicing Apparatus.<sup>5</sup> More than 10,000 such splices have been successfully completed in the field with average losses of less than 0.05 dB.

## LOCAL DETECTION SYSTEM

In a S-M fiber splice, the power lost due to the splice is coupled into the radiation modes of the receiving fiber. By selectively detecting only this scattered power, without attenuating the fundamental mode, the fiber cores can be accurately aligned using the criterion of a minimum detected signal (null). In Figure 1, we illustrate the detection scheme using the mandrel wrap local detector (MWLD). A mandrel (radius 1.6 cm) is chosen to tap selectively the scattered power (from the splice) out of

---

†Now with Kodak Inc., Rochester.

the fiber, in the vicinity of the detector, without inducing any significant loss of the core power. A large area Ge detector (5 mm dia.) located tangential to the mandrel is used to detect the scattered power.

Highly accurate stepping motors (0.1  $\mu\text{m}$  step size) are used to align the fiber cores in both the horizontal and vertical directions with feedback provided by the MWLD. These accurate stepping motors are necessary for the loss evaluation discussed below. Figure 2 shows a typical scan profile in the horizontal direction for such a system superimposed on the refractive index profile of the receiving fiber. The sharp null, which is located at the center of the symmetric scan profile, corresponds directly to optimum splice alignment. (Note that the shape of the scan profile is related to the structure of the receiving fiber.)

#### THEORY OF LOCAL SPLICE LOSS MEASUREMENT

From the microbending theory of S-M fiber splicing,<sup>6</sup> more than 90% of the power lost from a splice with small amounts of offset and tilt, is coupled into the  $\text{LP}_{11}$  mode. By measuring the scattered power level in the null,  $P_1$ , and the power level,  $P_2$ , at some known offset from optimal alignment,  $r_0$ , and knowing that this power is in the same radiation mode for both offset positions it is easily shown that the splice loss at the optimally aligned position (null) is

$$\text{Loss (dB)} = 4.34 \left( \frac{r_0}{w_0} \right)^2 \left( \frac{\tilde{P}}{1-\tilde{P}} \right), \quad (1)$$

The effect of the variability of detected power levels due to fiber design variations and differences in the input power to the splice are eliminated since only the ratio of the detected power levels  $\tilde{P}$  is used in the loss calculation.

$$\tilde{P} = \frac{P_1}{P_2}. \quad (2)$$

The only constants in Eq. (1) are the known offset  $r_0$ , and the nominal mode field radius ( $w_0$ ) of the  $\text{LP}_{01}$  mode. The error in the loss calculation is a function of the variations in the value of  $w_0$ , which is typically well within 8% of nominal.



## SPLICE LOSS RESULTS

In Figure 3, the calculation of the splice loss of an optimally aligned splice using equation 1, is shown as a function of the choice of induced offset,  $r_0$ , from optimal alignment. For comparison, the loss of this splice using a conventional far end transmission measurement is also shown. For  $r_0 > 2 \mu\text{m}$  the perturbation analysis used to derive equation 1, begins to fail, resulting in erroneous predictions. Figure 4 shows a comparison of local loss predictions to far end measurements for the practical range of single mode fiber splices of 0 to 0.5 dB, illustrating that the local loss predictions are generally within 10% of the far end measured losses.

## APPLICATIONS AND CONCLUSIONS

This alignment technique and measurement procedure has been used in the AT&T Technologies Single-Mode Bonded Splicing Apparatus, for over 10,000 field splices with average losses of less than 0.05 dB. This technique is independent of the individual fiber parameters and accurately predicts loss.

## REFERENCES

1. C. M. Miller, Proc. OFC 1981, THAA2.
2. K. Kato, T. Tanifuji, M. Tokada and N. Uchida, Electronic Letters 18, 972 (1982).
3. T. Haibara, M. Matsumoto, T. Tanifuji and M. Tokuda, Optics Letters 8, 235 (1983).
4. C. M. De Blok and P. Matthijsse, Electronic Letters 20, 109 (1984).
5. M. R. Reynolds and P. F. Gagen, Proc. I.C.C., Amsterdam 1984.
6. I. A. White and J. F. Kuhl, Proc. I.O.O.C., Tokyo 1983.

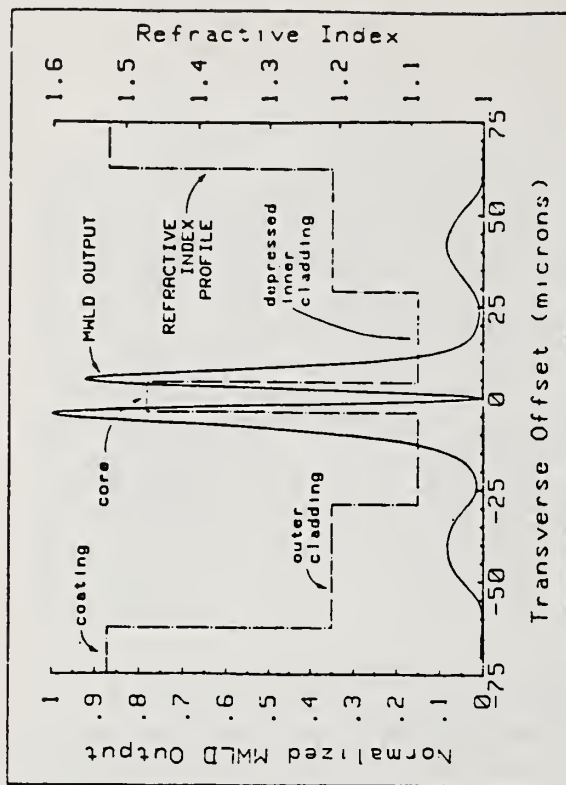


FIG. 2. Detected Power Scan Profile and the Refractive Index Profile of SMF.



FIG. 4. Comparison of Local Loss Predictions and Actual (Far-End) Loss Measurements.

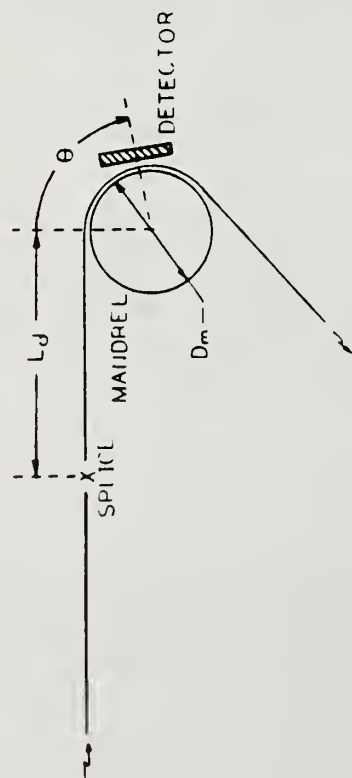


FIG. 1. MLD Geometry.

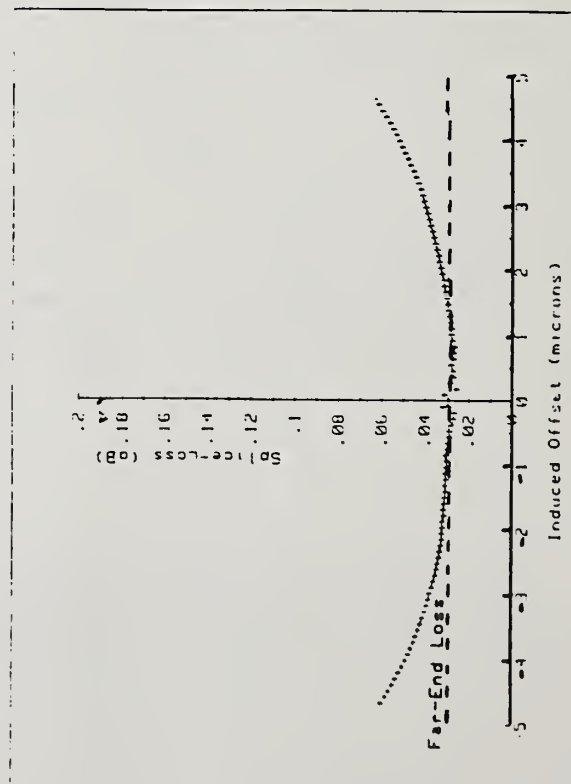


FIG. 3. Local Loss Predictions as a Function of the Choice of Induced Offset  $r_0$ .

# FUSION SPLICING OF DISSIMILAR FIBERS- A COMPARISON OF MODE FIELD DIAMETER AND CROSS-CORRELATION LOSS PREDICTIONS WITH EXPERIMENTAL RESULTS

by W. T. Anderson, A. J. Johnson, J. P. Kilmer, and E. A. Thomas  
Bell Communications Research

## 1. Introduction

In this paper, we report results from splicing single-mode fibers of different designs and attempt to interpret the results in terms of the degree of optical and physical compatibility between the fibers. When fusion splicing two single-mode fibers, a number of factors can contribute to the loss of the joint. While many of these factors relate to the fusion splicing machine and its operation, one factor over which the operator has no control is the degree of optical and physical compatibility of the two fibers. A wide range of designs are commercially available (matched and depressed cladding, conventional and dispersion-shifted) and two processes, each with several different implementations, are used to make the fibers (inside and outside deposition). Both design and process differences can affect the compatibility of two fibers with respect to fusion splicing.

Losses for butt-joint splices have been successfully predicted by the mode field diameter mismatch between the two fibers [1]. However, this single parameter, which defines the width of the fields, is adequate only if the field shapes of the two fibers are nearly identical. This limitation applies to both the gaussian mode field diameter definition [2] and to the recently proposed second-moment definition [3,4]. A more complex model, which is based upon the cross-correlation of the fields of the two fibers, has been used to predict butt-joint losses for fibers of dissimilar designs [5]. In this paper, loss measurements for fusion splices between three combinations of substantially dissimilar fibers are compared to three splice loss predictions: one based upon mode field diameter measurements with a gaussian definition, another based upon mode field diameter measurements with a second moment definition, and a third based upon field cross-correlation.

## 2. The Experiment

The electric arc fusion splicing machine used was microprocessor-controlled, and the arc settings were determined by trial and error by an experienced operator. Alignment of the two fiber ends was done visually using a 120x microscope. The alignment stages have minimum resolution of  $0.1\mu m$ . Power monitoring was not used. An arc time of 2.0 seconds, which allows for some self-alignment due to surface tension, was used for all splices. When used with fibers with nearly identical mode field radii, this technique produced splices below .02dB.

The splices involved four commercially available fibers. Three of them were conventional step-index single-mode fibers: a depressed-cladding inside process fiber ("DI"), a matched-cladding inside process fiber ("MI"), and a matched-cladding outside process fiber ("MO"). The fourth fiber was a commercially-available dispersion-shifted fiber [6] produced by the outside process ("SO"). Three combinations of these four fibers were studied: SO to MO, DI to MI, and SO to MI.

Two OTDRs were used to make initial loss measurements at both 1300 and at 1550nm. Because of the differences in fiber designs and the corresponding differences in backscatter capture coefficients, a difference in the OTDR readings taken in different directions was expected, but the average of the two OTDR readings taken in opposite directions gives an accurate measure of the splice loss. A series of splices were made and measured to determine the repeatability of the splices, and variations of less than 0.03dB were typical. After several splices, a joint whose loss was on the low side of this distribution was selected, and the sample was saved for a transmission measurement of the loss using the cutback technique. Enough slack fiber was saved so that the cutback measurement could be repeated twice in each direction, and the overall accuracy of the transmission measurement is estimated to be .02dB. The splice loss measurements for the three fiber combinations are shown in the table below.

Measured Splice Losses (+) or Gains (-) in dB							
Fiber Combination	Wavelength ( $\mu m$ )	OTDR Measurement			Transmission Measurement		
		Fwd	Rev	Avg	Fwd	Rev	Avg
SO - MO	1300	2.40	-1.47	.46	.413	.517	.46
	1550	1.73	-1.20	.26	.232	.263	.25
DI - MI	1300	0.93	-0.57	.18	.204	.199	.20
	1550	0.96	-0.62	.17	.201	.202	.20
SO - MI	1300	3.53	-1.68	.92	.973	.908	.94
	1550	2.65	-1.59	.53	.545	.464	.50

The averaged OTDR and transmission measurements agree well. The large directionality of the OTDR measurements was expected. However, the significant directionality observed for the transmission measurements of the first and third combination is surprising.

### 3. Splice Loss Prediction from Mode Field Diameter and Cross-Correlation

The mode field diameters of the four fibers were measured at the two wavelengths using the far field scan method [2]. Both the gaussian and the second moment definitions were used. The estimated splice loss is found from the two mode field diameters  $MFD_1$  and  $MFD_2$  as [1]

$$20 \log \left[ \frac{MFD_1^2 + MFD_2^2}{2 MFD_1 MFD_2} \right] \text{ dB}$$

The splice loss can also be predicted from the more complex cross-correlation, or overlap, of the fiber fields. Because of the Hankel transform relationship between the fiber near fields  $f(r)$  and the fiber far fields  $F(q)$ , the near-field cross-correlation and the far-field cross-correlation are identical [7], so the splice loss is predicted by



$$loss = 10 \log \frac{\left[ \int_0^{\infty} f_1(r) f_2(r) r dr \right]^2}{\int_0^{\infty} f_1^2(r) r dr \int_0^{\infty} f_2^2(r) r dr} = 10 \log \frac{\left[ \int_0^{q_m} F_1(q) F_2(q) q dq \right]^2}{\int_0^{q_m} F_1^2(q) q dq \int_0^{q_m} F_2^2(q) q dq} dB$$

where  $q = \frac{1}{\lambda} \sin \theta$  and the maximum scan angle  $\theta_m$  is chosen so that  $q_m = \frac{1}{\lambda} \sin \theta_m$  is large enough to accurately calculate the above integrals. The far field measurements were conducted over a range of  $\pm 25^\circ$ , but the 60dB dynamic range of the system limited the range of useful data for the step index fibers to about  $\pm 20^\circ$ . The far fields of each of the four fibers were measured twice, and the average of those two measurements are summarized below. The standard deviations were typically  $.04 \mu m$ .

Measured Mode Field Diameters (in $\mu m$ )				
Fiber	Gaussian MFD		Moment MFD	
	1300nm	1550nm	1300nm	1550nm
SO	6.82	8.86	6.54	8.18
MO	9.57	10.95	9.51	10.83
MI	11.07	12.21	10.70	11.83
DI	9.09	10.29	8.93	10.16

The MFD and cross-correlation predictions are compared to the measured splice losses below.

Splice Loss Predictions and Measurements (in dB)						
Fiber Combination	Wavelength $\mu m$	Predicted Splice Loss			Measured Splice Loss	
		Gaussian	Moment	Cross-cor	OTDR	Trans
SO - MO	1300	0.49	0.59	0.43	0.46	0.46
	1550	0.19	0.33	0.20	0.26	0.25
DI - MI	1300	0.17	0.14	0.16	0.18	0.20
	1550	0.13	0.10	0.10	0.17	0.20
SO - MI	1300	0.98	1.01	0.90	0.92	0.94
	1550	0.44	0.57	0.45	0.53	0.50

The differences between the three predictions and the two measured values are shown in the following table. Positive values indicate that the prediction is lower than the measured loss while negative values indicate the opposite.

Differences Between Loss Predictions and Measured Losses (in dB)							
Fibers	Wavelength $\mu m$	Gaussian MFD		Moment MFD		Cross-correlation	
		OTDR	Trans	OTDR	Trans	OTDR	Trans
SO - MO	1300	-.03	-.03	-.13	-.13	.03	.03
	1550	.07	.06	-.07	-.08	.06	.05
DI - MI	1300	.01	.03	.04	.06	.02	.04
	1550	.04	.07	.07	.10	.07	.10
SO - MI	1300	-.06	-.04	-.09	-.07	.02	.04
	1550	.09	.06	-.04	-.07	.08	.05

The cross-correlation prediction is systematically lower than the measured loss by 0.02 to 0.10dB. Since

these three fiber combinations are expected to be incompatible physically as well as optically, the predicted splice loss, which includes the effect of only optical incompatibility, should be somewhat smaller than the measured splice loss. Also, extrinsic factors, such as misalignment of the two fibers, will tend to increase the actual loss above the prediction. Considering that nearly identical fibers produced as much as 0.02dB loss using the same splicing machine and procedure, the cross-correlation prediction is reasonably consistent with the measured values. On the other hand, both of the mode field diameter predictions are neither consistently above nor below the measured values. Since a predicted loss which is higher than the loss actually observed (which would be negative in the above table) cannot be explained by extrinsic factors or physical incompatibilities, which can only increase the loss, these estimates are inconsistent with the measured values.

The predictions of the cross-correlation model are very consistent for the three splices. Since the first two combinations both involve fibers made using the same process and using similar dopants, these combinations were expected to be more physically compatible than the third combination, which involves two fibers from different processes and contain considerably different materials. If the different processes and materials significantly affected the fusion process, then the predictions, which include only optical compatibility considerations, would be worse for this combination than for the other two combinations. This expectation was not realized, and optical compatibility alone is sufficient to explain most of the observed loss. Also, the cross-correlation prediction is closer to the measured values at 1300nm than at 1550nm (average differences of .03dB versus .07dB). The reasons for this systematic difference are not known.

#### 4. Conclusions

The mode field diameter, which is a simple one parameter description of the field distribution, is not expected to accurately predict the loss of splices between fibers whose field shapes are substantially different. A more complex model seems to be necessary to predict the loss accurately. Additional work is required to verify the accuracy of this model with other fiber designs and to more fully understand the directionality which some splices exhibit. Also, a comparison of butt-joint splices with fusion splices could confirm the conclusion in this study that physical incompatibility contributes relatively little to the loss of fusion splices.

The authors wish to acknowledge the contribution of Corning Glass Works, who provided the sample of dispersion-shifted fiber used in this study.

#### REFERENCES

- [1] D. Marcuse, *BSTJ*, Vol. 56, No. 5, p. 703, 1977.
- [2] W. T. Anderson and D. L. Philen, *IEEE JLT*, Vol. 1, No. 1, p. 20, 1983.
- [3] K. Petermann, *Electronics Letters*, Vol. 19, No. 18, p. 712, 1983.
- [4] C. Pask, *Electronics Letters*, Vol. 20, p. 144, 1984.
- [5] J. C. Auge and L. B. Jeunhomme, *Technical Digest, SPIE Tech Symp*, August, 1985.
- [6] T. D. Croft, J. E. Ritter, and V. A. Bhagavatula, *Technical Digest, OFC 85*, Paper WD2, 1985.
- [7] W. T. Anderson, *IEEE JLT*, Vol. LT-2, No. 2, p. 191, 1984.

# STRESS-INDUCED INCREASES IN INTERFERENCE EFFECTS AT FIBER JOINTS AND A METHOD TO ELIMINATE INTERFERENCE EFFECTS IN OPTICAL FIBER MEASUREMENTS

W. C. Young, V. Shah, and L. Curtis

Bell Communications Research, 331 Newman Springs Rd., Red Bank, NJ 07701-7020

## INTRODUCTION

A common practice used in characterizing single-mode fiber systems, such as laser power measurements, bit-error-ratio measurements, and spliced fiber/cable loss measurements, usually employs the use of a "photon-bucket" (PB) type receiver jumper cable to access the fiber/cable ends. Typically, these PB jumpers consist of a length of multimode fiber with a sufficiently large core to collect all of the transmitted power from a single-mode fiber without regard to precision alignments. However, if other characteristics of these fiber joints are not controlled, a significant uncertainty in the measurements can be encountered. Our measurements show that for repeated measurements this uncertainty can result in loss variations as high as 1.14 dB. In this paper we describe the source of these loss variations and discuss techniques that can be used to minimize resulting measurement uncertainties.

## DISCUSSION

Practical consideration in measuring the optical power transmitted by a single-mode fiber dictates the use of a large-core fiber (multimode fiber) as a "photon-bucket" receiver. Using this MM fiber avoids the uncertainty, due to the required submicron alignment accuracies, in the loss of SM/SM fiber connectors. Furthermore, to increase their engagement/separation endurance level these SM/MM connections are designed to establish fiber endface separation. As a result of this separation and reflections from the fiber end faces, a Fabry-Parot etalon is formed at the joint. When excited with a coherent source, multiple-beam interference occurs,<sup>[1,2]</sup> as shown in Figure 1. The resulting interference effects cause large variations in transmitted power, as a function of fiber-to-fiber separation, as long as the separation is smaller than the coherence length of the source. With LEDs, the effect is significantly diminished with a separation of about 10 to 15 micrometers, whereas for a highly coherent source such as a laser, it persists for very large separations on the orders of 100  $\mu\text{m}$ , and beyond. Since a large percentage of measurements are made with laser sources, these effects can cause significant measurement uncertainties. Experimental measurements of these interference effects for SM/SM joints, using both a laser and a LED, are shown in Figure 2. The decrease in the mean transmitted power, with increasing separation, is due to the aperturing effect of the SM receiving fiber. In Figure 3 similar measurements are shown, but in this case we have used a SM/MM fiber joint. The receiving MM fiber was a 50/125 GI fiber. As can be seen in these figures, the variation in transmitted power, with laser sources, can be significant even for substantial separations. For the experimental results shown in Figures 2 and 3, the fiber endfaces



were polished, flat and perpendicular to the fiber axis within .2 degrees, using a one micron aluminum-oxide coated sheet of polyester. The polishing was performed dry with no lubrication. As previously reported, the maximum loss variation for air-gap joints having flat and parallel faces can be calculated from:

$$\text{variation} = -10 \log (1-4R) \quad (1)$$

$$R = \left( \frac{n-1}{n+1} \right)^2 \quad (2)$$

where  $n$  is the refractive index of the fiber.

For a refractive index of 1.46, typical for a fiber, theory predicts a maximum loss variation of 0.65 dB. However, experimentally, maximum variations of 0.90 to 0.95 dB were measured (Figures 2 and 3). To observe these higher values, the refractive index of the polished endfaces would have to be about 1.57. The possibility of the presence of a thin film of aluminum-oxide, which has a refractive index of about 1.6, after polishing was investigated with an SEM. However, no traces of such a film were found. Another cause which is more likely the reason for the high variation is that due to stresses induced during polishing the density of the glass surface increases, thus causing an increase in the refractive index. Previous work has shown that when silica glass was polished with red iron-oxide the index was increased from 1.46 to about 1.6<sup>[3]</sup>. Investigating the effect that different polishing techniques have on the maximum variation in loss (maximum change in the index of the surface), we were able to achieve a maximum variation of 1.14 dB by changing the rate and amount of polishing, while still using one micron aluminum-oxide grit. This loss would require a surface index of about 1.63. In contrast, when we used cleaved perpendicular faces, the maximum variation was 0.6 dB, which is expected for the refractive index of fused silica, namely 1.46.

Regardless of what effect the surface condition has on the index, a method to minimize the variations due to the interference effect is needed. We have achieved this minimization by introducing a face angle on the MM receiving connector. Measurements of transmitted-power-versus-separation for SM/MM joints, for MM fibers have various face angles are shown in Figure 4. The MM fiber was a 50/125 GI fiber. Based on these results, an appropriate face angle can be introduced, on the connector end, which significantly minimizes the interference effects in air-gap connectors. An alternate solution would be to use an index matching material in the joint but generally this approach has not been accepted as a practical solution due to problems such as contamination, handling, etc.<sup>[4]</sup>



In an experiment, we have used 50/125 GI fiber receiver jumpers, with a 5 degree face angle and a gap of about 25 microns, to measure end-to-end loss of 5 concatenated sections of SM fiber (about 35.7 km). The coupling loss of the SM/MM connectors ranged from 0.62 to 0.65 dB for repetitive measurements, in contrast to the range of 0 to 0.95 for parallel polished endfaces. For repeated end-to-end loss measurements, made in both directions through the fibers, loss measurements at 1300 nm ranged from 15.86 to 15.91 dB.

#### CONCLUSION

We have shown that interference effects in air-gap connectors can be affected by stresses induced in the fiber endface during polishing, and that by employing a face angle of  $5^\circ$  on a MM receiving test fiber, the maximum variation due to these interference effects can be reduced from .92 dB ( $0^\circ$  end face angle) to less than .05 dB. Finally, since a large reduction in the interference effect can easily be achieved by using the endface angle on MM fiber, the accuracy of optical fiber measurements can be substantially improved.

#### REFERENCES

- [1] W. C. Young et al., "A Transfer Molded Connector Biconic Connector with Insertion Loss Below 0.3 dB Without Index Match", Technical Digest, Sixth ECOC, U. York, 1980.
- [2] R. E. Wagner and C. R. Sandahl, "Interference Effects in Optical Fiber Connections", Applied Optics, Vol. 21, No. 8, pp. 1381, 15 April 1982.
- [3] L. Rayleigh, "The Surface Layer of Polished Silica and Glass with Further Studies of Optical Contact", Proc. Roy. Soc., A 160, pp. 507, (1937).
- [4] I. Sankawa et al., "Methods for Reducing the Fresnel Reflection in an Optical-Fiber Connector with Index Matching Material", Elect. and Comm. in Japan, Part 1, Vol. 69, No. 1, pp. 94, (1986).

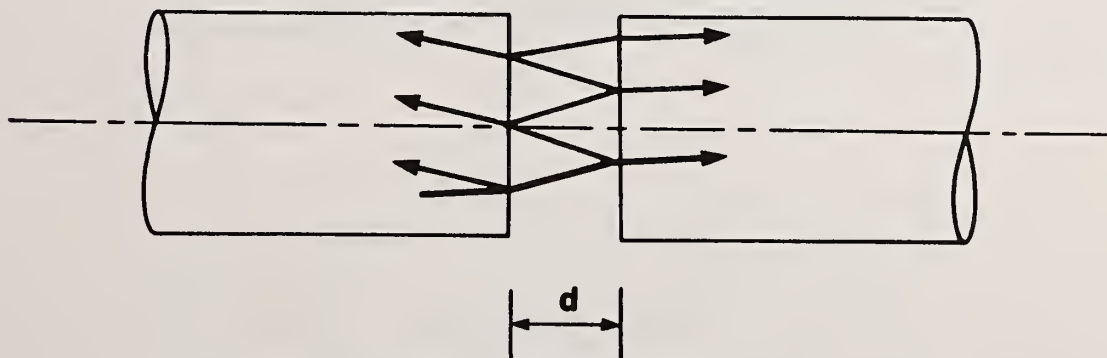


Fig. 1 Multiple-beam interference at a fiber joint.

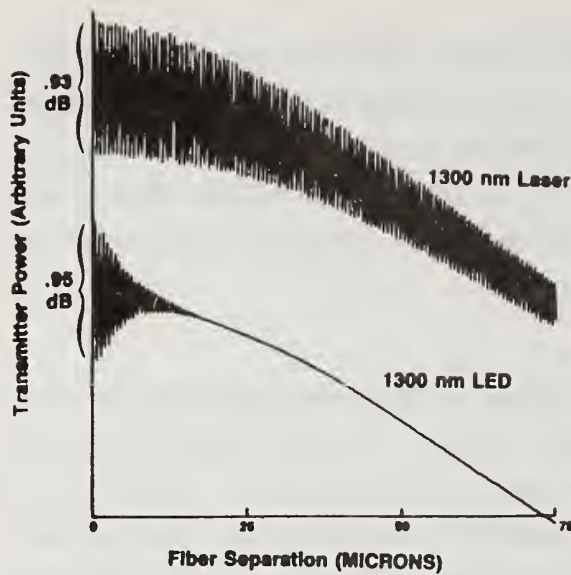


Fig. 2 Measured transmission fluctuation vs. fiber end face separation for a SM/SM joint.

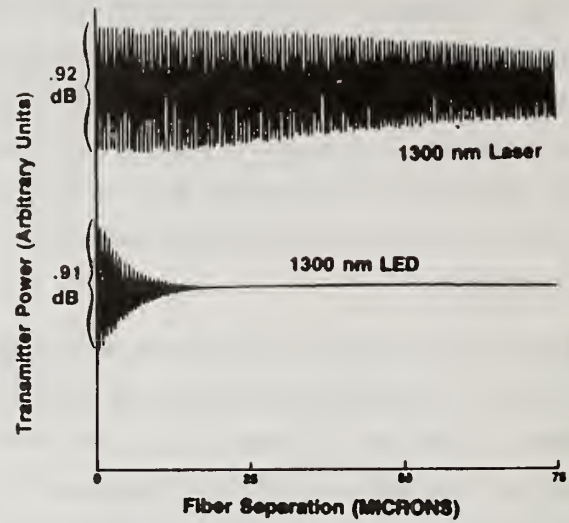


Fig. 3 Measured transmission fluctuation vs fiber end face separation for a SM/MM joint.

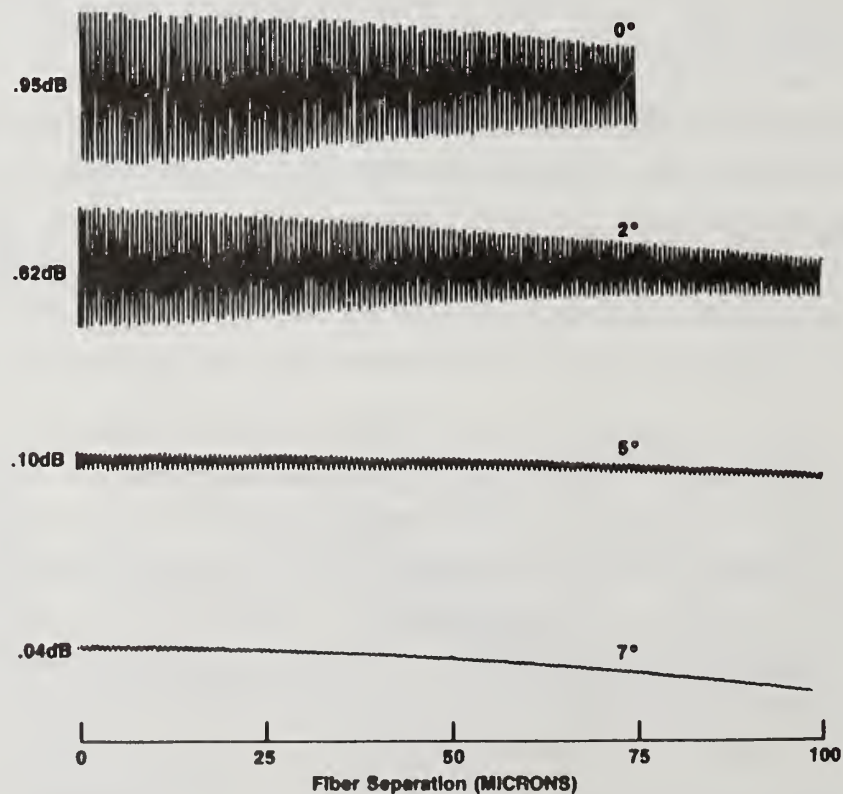


Fig. 4 Measured transmission fluctuation vs fiber end face separation for a SM/MM joint with a 1300 nm laser. The MM fiber end face in the joint is polished at different angles.

## PRACTICAL ONE-WAY-LOSS RANGE FOR OTDRs

M C Brain and E A Cottrell

British Telecom Research Laboratories

Martlesham Heath, Ipswich IP5 7RE, UK.

### Introduction

The method of detecting remote breaks in fibre transmission systems, by measuring backscattered optical power as a function of distance along the fibre [1], has made the Optical Time Domain Reflectometer (OTDR) an indispensable test instrument. In this paper, we show that the range of fibre loss over which breaks may be accurately located is less than the conventionally defined one-way-loss range. Our discussion is illustrated with measurements at 1.5  $\mu\text{m}$  over 100 km of commercial single mode fibre.

### Theory

An OTDR is shown schematically in Fig 1, and we develop the theory as follows. An optical pulse of peak power  $P_s$  from the laser is launched into the fibre via a directional coupler, and after a delay  $\tau$  a backscattered signal  $P_x$  is detected from a mean distance  $x$  into the fibre. The difference between  $P_s$  and  $P_x$  is determined by the total loss  $C$  in the coupling optics, the fibre loss  $2L_x$  incurred over the distance  $x$  on the outward and the return paths, and the reflection coefficient  $R$  for the signal backscattered in the vicinity of  $x$  within the capture angle of the fibre core [2, 3]. Thus,

$$2L_x = P_s - (R+C) - P_x \quad \text{dB} \quad (1)$$

The maximum range over which measurements can be made is reached when  $P_x$  approaches the noise equivalent power (NEP)  $P_d$  of the detector, although this can be improved by a factor  $5\log_{10}N$  ( $= \text{SNIR}/q$  [3]) by averaging  $N$  consecutive measurements. We thus arrive at a definition for the one-way-loss range  $L$  of an OTDR [3]:

$$L = [P_s - (R + C) - P_d + \text{SNIR}/q]/2 \quad (2)$$

This definition is convenient for comparing the performance of different OTDR instruments, but for practical measurements it must be noted that a limiting signal-to-noise ratio (SNR) of unity is implied by defining  $L$  in terms of the NEP of the detector. Close to this limit, where there is a high probability



of the signal-plus-noise being near zero, it would be impossible to locate accurately the position of a break giving little or no Fresnel reflection, since the logarithmic signal scale of a conventional backscatter trace would yield large negative-going spikes, which would mask the abrupt fall in signal expected at the break. The maximum actual fibre loss must therefore be less than  $L$ , by say  $M$  dB. The question arises, how large must  $M$  be?

If  $L_x$  in (1) is used to represent the new one-way-loss range, then

$$M = L - L_x = [P_x - P_d + \text{SNIR}/q]/2 = 5\log_{10}(I_x/\sigma) \quad (3)$$

where  $I_x$  is the postdetection photocurrent due to the backscattered signal from  $x$ , and  $\sigma$  is the postdetection RMS equivalent input noise current of the receiver. Thus  $I_x = \sigma 10^{M/5}$ . We now estimate the amplitude  $\Delta L$  of noise fluctuations on the backscatter trace by considering an envelope of  $\pm 2\sigma$  about the mean postdetection photocurrent; for Gaussian white noise, this envelope includes over 95% of the noise distribution. By a derivation similar to (3), we find:

$$\Delta L = 5\log_{10}[(I_x \pm 2\sigma)/I_x] = 5\log_{10}(1 \pm 2 \cdot 10^{-M/5}) \quad (4)$$

This is plotted in Fig 2 as a function of  $M$ , suggesting that a value of  $M$  greater than 1.5 dB is essential if large negative-going spikes are to be avoided, but a margin of 3 dB would reduce the  $-2\sigma$  deviation to -1.5 dB.

### Measurements

We now compare these predictions with practical measurements using a 1.5  $\mu\text{m}$  OTDR [4]. A semiconductor laser was used to launch 5  $\mu\text{s}$  pulses of peak power 7.6 mW at 1.535  $\mu\text{m}$  wavelength into commercial monomode fibre using a 3 dB single-mode fibre fused taper coupler. The fibre consisted of 19 lengths, fusion spliced to give a total length of 101.2 km with loss 22.8 dB. The receiver comprised a commercial InGaAs PIN photodiode (75  $\mu\text{m}$  diameter, 2.8 nA leakage, 1.08 A/W responsivity), followed by a transimpedance preamplifier with a silicon JFET input stage and a 10 Mohm resistor in the feedback loop. Single channel averaging improved the SNR to yield an expected one-way-loss range  $L = 16.3 + 2.5\log_{10}N$  dB, obtained from (1).

The implications of Fig 2 are demonstrated in Fig 3, which shows the  $\pm 2\sigma$  levels plotted about the measured backscatter traces for different

values of  $N$ . A one-way-loss range equal to the known fibre loss requires that 400 samples be averaged at each measurement point. The trace in Fig 3a was obtained with 1500 samples/point, suggesting a margin  $M$  of 1.4 dB, yet the location of the fibre end is obscured by the noise. When  $N$  is increased to 7500 samples/point (Fig 3b), the margin rises to 3.2 dB and the fibre end becomes distinct. Further increasing  $N$  to 75000 samples/point (Fig 3c) allows the fibre end to be characterised to an accuracy of  $\pm 0.3$  dB ( $\pm 2\sigma$  levels), corresponding to a margin  $M$  of 5.7 dB. In all cases the  $2\sigma$  envelope is a convincing fit to the measured trace. Furthermore, 7500 samples at a repetition rate of 900 Hz gives a measurement time of 8.3 seconds/point, which is acceptable for practical situations.

### Conclusion

We have demonstrated a break location capability over 100 km of commercial single mode fibre, using an OTDR operating at  $1.535 \mu\text{m}$  wavelength, assembled from commercial components. We have used these measurements to demonstrate that for accurate fibre end location in the absence of Fresnel reflection, the actual fibre loss should be  $\sim 3$  dB less than the one-way-loss range defined in terms of unity SNR. A margin of 5 dB allows the entire fibre to be characterised to better than  $\pm 0.5$  dB.

Acknowledgements: the authors thank the Director of Technology Applications, British Telecom, for permission to present this paper.

### References

- [1] C Y Boisrobert, Proc Topical Meeting on Optical Fiber Transmission, January 7 - 9 1975, Williamsburg Va, USA.
- [2] E Brinkmeyer, Electronics Letters, Vol 16 No 9, pp 329-330, 1980.
- [3] P Healey, J Lightwave Technology, Vol LT-3 No 4, pp 876-878, 1985.
- [4] E A Cottrell, M C Brain, Electronics Letters, Vol 22 No 8, pp 443-445, 1986.

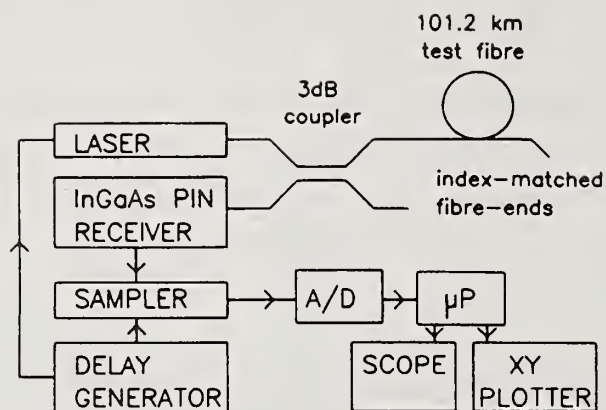


Fig 1. Schematic of OTDR equipment.

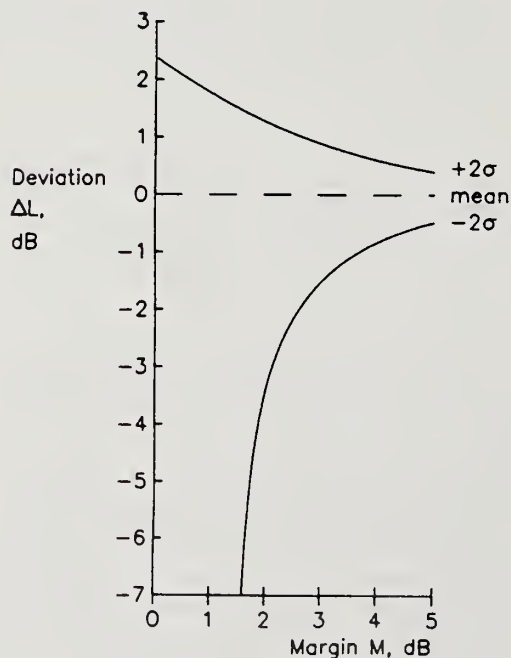


Fig 2. Deviation from mean backscatter level as a function of margin  $M$  between one-way-loss range  $L$  and actual fibre loss.

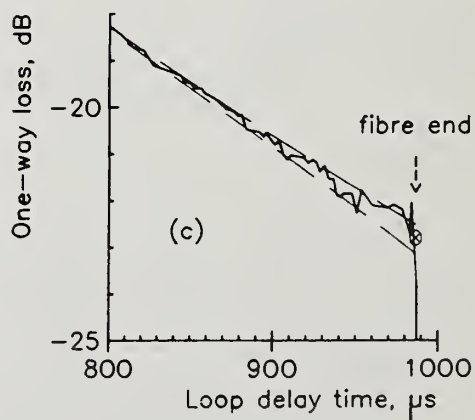
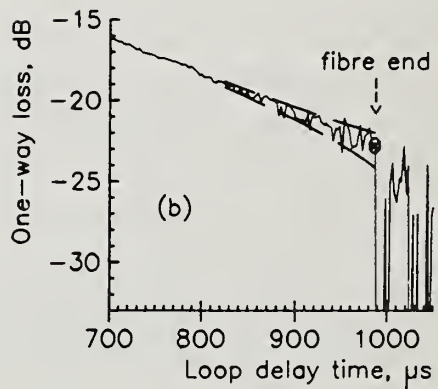
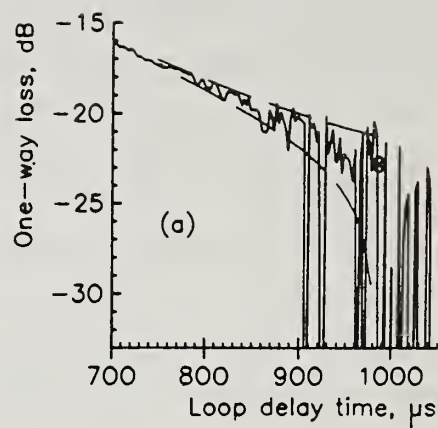


Fig 3. Plots of backscatter signal from the remote fibre end. The margin between the estimated one-way-loss range of the OTDR and the actual loss of the test fibre is:  
(a) 1.4 dB (unacceptable)  
(b) 3.2 dB (just acceptable for fault location).  
(c) 5.7 dB (accuracy  $\pm 0.3$  dB).



A NEW TECHNIQUE FOR THE RELATIVE  
MEASUREMENT OF SCATTER LEVELS  
IN SINGLE MODE FIBRES

M.E.Fermann, S.B.Poole, D.N.Payne, F.Martinez

Optical Fibre Group, Department of Electronics and Engineering, Southampton University, Southampton SO9 5NH

ABSTRACT

A new sensitive technique to separate scatter loss contributions from total fibre loss in single-mode fibres based on Optical Time Domain Reflectometry OTDR is described. Results for telecommunications-grade fibres with different  $\text{GeO}_2$  concentration in the fibre core are presented.

INTRODUCTION

The ability to measure relative scatter levels in single-mode fibres is essential for minimising fibre losses in telecommunications fibres operating in the 2nd and 3rd windows for optical communications. In this way fabrication processes can be optimised in response to small improvements in measured scatter levels. Surprisingly, there is no simple way in which this can be done with sufficient accuracy to suit current very-low fibre scatter losses.

We, therefore, describe a new technique which allows the separation of the Rayleigh scatter loss from the total loss in a single mode fibre. In this method, a reference fibre, the scatter loss of which may be determined by calorimetric techniques, is spliced to the fibre under investigation. The two fibres are then probed using OTDR. The backscattered light powers from each side of the splice are compared by using the test and reference fibres in turn as the launch fibre and from this the relative scatter losses of the fibres may be obtained. The technique is capable of determining very small changes in scatter from fibre to fibre and is, therefore, ideally suited to process control and optimisation.

## THEORY

It may be shown from ref.1 that, in the case of the single-mode step-index fibres operating around second-mode cutoff, the ratio of the scatter loss coefficients  $\alpha_t$  and  $\alpha_s$  of a test and a standard fibre is given by

$$\frac{\alpha_t}{\alpha_s} = \left( \frac{w_t}{w_s} \right)^2 \left( \frac{n_t}{n_s} \right)^3 \left( \frac{R_1}{R_2} \right)^{1/2}$$

where  $R_1 = P_{12}/P_{11}$  and  $R_2 = P_{21}/P_{22}$  are the ratios of the backscattered powers at the splice as defined in Figure 1;  $n_t$  and  $n_s$  are the core refractive indices, and  $w_t, w_s$  are the spot sizes of fibre t and s respectively. The spot sizes here are defined as the  $(1/e^2)$  power diameter of the Gaussian approximation to the power distribution of the fundamental mode in the fibre<sup>2</sup>. The ratio of the scatter losses between a test and a reference fibre may, therefore, be readily obtained from measurements of the relative backscattered power, fibre spot sizes and core refractive indices.

## MEASUREMENTS

The measurements were carried out at  $1.3 \mu\text{m}$  on a number of single-mode communication grade step index fibres, the parameters of which are summarised in Table 1. These fibres all had a  $\text{GeO}_2$ -doped core and a matched silica cladding, with the exception of fibre 5 which had a slightly depressed cladding. The fibres were fabricated using VAD and MCVD techniques. As a standard we used fibre 1, a low-loss fibre that exhibited a total attenuation of  $0.39 \pm 0.02 \text{ dB/km}$  at  $1.3 \mu\text{m}$ . The backscatter traces were obtained using commercial equipment operated with a resolution of 40 and 75 metres. The spot sizes were measured using a transverse offset technique.

## RESULTS AND DISCUSSION

The ratio  $\alpha_t/\alpha_s$  is plotted in Fig.2 as a function of numerical aperture NA. The accuracy obtainable for these ratios is limited by the accuracy of the spot size measurements. The resulting errors in the scatter loss ratios

were about 5% and are indicated in the Fig.2 with error bars. Assuming a scatter loss of silica of 0.3 dB/km at 1.3 $\mu$ m, differences of less than 0.015 dB/km in scatter loss may be detected.

As expected, the Rayleigh scatter loss increases proportional to NA<sup>4</sup> and this goes some way to explain the commonly-observed higher attenuation of fibres with high NA. Surprisingly, the manufacturing process does not have a measurable effect on scatter loss. The measured variations in total fibre losses are greater than would be expected solely due to changes in NA and are due to OH<sup>-</sup> peaks and process imperfections.

The measurement technique described here may be applied to any type of single mode fibre, provided an expression for the relative backscatter capture fractions of the fibres is computed. Thus triangular core, depressed-clad or even W-fibres could be measured.

#### CONCLUSIONS

We have described a new sensitive technique for the measurement of relative scatter losses in single-mode optical fibres. As an indication of the use of the method, results showing the measured increase in scatter loss with increase in NA have been presented.

#### ACKNOWLEDGEMENTS

The authors would like to thank Pirelli General plc and York VSOP for supplying fibres. We would also like to thank York Technology Ltd. for valuable assistance with the spot size measurements. The work was carried out under the JOERS programme. A readership (DNP) and Research Fellowship (SBP) were provided by Pirelli General plc.



## REFERENCES

1. A.H.Hartog and M.P.Gold. "On the theory of backscattering in single-mode optical fibres." Journal of Lightwave Technology, Vol.LT-2 (2), 76-82, 1984.
2. D.Marcuse. "Gaussian approximation of the fundamental modes in graded index fibres", J.Opt.Soc., Vol.68, pp.103-109, 1978.
3. York Technology FQm 1000.
4. H.Murata, S. Inao, Y.Matsuda, and T.Kuroha, "Optimum design for optical fibre used in optical cable system", Proceedings, 4th European Conference on Optical Communications, Genoa, pp.242-248, 1978.

Fibre Number	Spot-size $\mu\text{m}$	Cut-off nm	Total loss dB/km	$\alpha_t/\alpha_s$	NA	Manufacturing process
1	11.0	1250	0.39	1	0.10	VAD
2	9.8	1250	0.54	1.08	0.12	VAD
3	9.5	1250	0.54	1.10	0.12	VAD
4	8.5	1200	0.6	1.09	0.13	MCVD
5	6.3	1250	0.7	1.23	0.17	MCVD
6	7.6	1200	0.5	1.15	0.15	MCVD

Table 1. Fibre parameters.

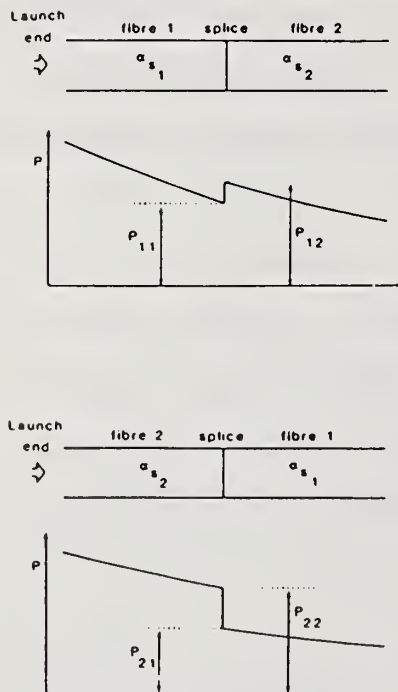


Fig.1 Definition of Parameters.

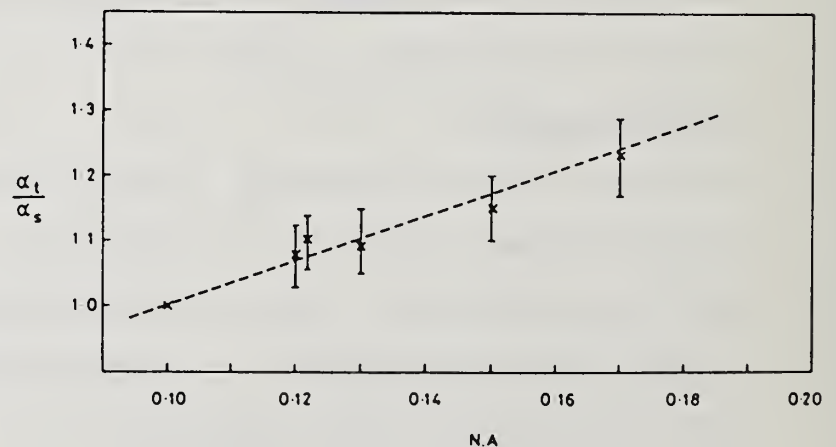


Fig.2 Rayleigh Scattering in Single-Mode fibres as a function of NA.

## MODE FIELD DIAMETER EFFECTS ON OTDR SPLICE MEASUREMENTS

Felix Kapron, Carrie Kozikowski, and Ricky Crotts

ITT Electro-Optical Products Division  
7635 Plantation Road  
Roanoke, VA 24019-0065

### Abstract

It is shown that OTDR measurements will give erroneous results on splice or connector losses that are due primarily to a difference in the mode field diameters of the joined fibers. A new simple formula gives an improved estimate of loss.

### Splice Real Loss and OTDR

Within a splice or connector, let  $2w_1$  and  $2w_2$  be the mode diameters of the input and output fibers, respectively. Define a relative mismatch  $R$  equal to the ratio of the mode diameter difference divided by the mode diameter average:

$$R = 2(w_1 - w_2)/(w_1 + w_2) \quad (1)$$

The resulting power transmittance [1] can be rewritten as a loss

$$\begin{aligned} \text{dB}(R) &= 20 \log_{10} \left( 0.5 \left[ (w_1/w_2) + (w_2/w_1) \right] \right) \\ &\approx 4.343 R^2 \text{ for } |R| < 0.8 \end{aligned} \quad (2)$$

By convention here, an OTDR signal drop is considered positive. The OTDR signal suffers the splice loss twice, but since the scale is typically halved in dBs, the bidirectional average, equal to (2), is automatically included.

### OTDR Apparent Loss

The OTDR signal level depends on the product of the overall scattering coefficient and the backscatter capture fraction. For single-mode fiber, the latter varies as [2]  $(\lambda/w_0)^2$ . Hence, if the mode diameter  $2w_0$  decreases across a splice, compared with its value for input fiber 1, there will be a corresponding increase in backscattered signal level in output fiber 2. This means that the splice loss as seen by the OTDR will appear to reduce by the backscatter ratio in halved dB's:

$$\begin{aligned} B(R) &= 5 \log_{10} (w_2/w_1)^2 \\ &\approx -4.343 R \text{ for } |R| < 0.35 \end{aligned} \quad (3)$$

From (2) and (3), the OTDR apparent loss is then

$$\begin{aligned} L(R) &= dB(R) + B(R) \\ &= 4.343 (R^2 - R) \end{aligned} \quad (4)$$

Since  $|R| < 1$ , the backscatter effect due to mode diameter mismatch overwhelms the loss effect due to the same cause. Figure 1 schematically shows the result (4) that differs depending upon the OTDR direction; a positive R will product apparent 'gain'. Bidirectional averaging naturally produces the best estimate of real loss:

$$0.5 [L(R) + L(-R)] = dB(R) \quad (5)$$

### Experiment

Gaussian mode diameters were obtained at 1300 nm on both ends of spooled fibers using the knife-edge technique [3]. Fiber pairs were purposefully selected to give mode diameter mismatches over a broad  $\pm 16\%$  range, and were spliced via core position monitoring in an arc fusion machine. The recoated splice was prooftested.

First, OTDR measurements were taken in both directions. The splice was then cut off the spools, leaving 5 m of fiber on each side of the splice. The true splice loss was measured by cutback in each direction. The spooled fibers were respliced and remeasured several times for the same mode diameter mismatch, and all readings were recorded in the accumulated data.

Figure 2 shows the correlation between measured bidirectional averages of cutback loss (which showed little directional dependence) and OTDR apparent loss (which showed much). Figure 3 displays the directional OTDR apparent splice loss correlated with mode diameter mismatch; the best fit line to the data is given. In view of the data scatter common to splice measurements, both Figures agree reasonably with predicted results. Any small offsets are likely due to directional imperfections in the splice procedure, exclusive of mode diameter mismatch.

### Conclusions

The effect of mode diameter mismatch on both splice loss and OTDR loss has been accounted for. The former can be predicted from the latter. Eliminating the relative mismatch R between (2) and (4), or Figures 2 and 3, gives the real loss estimate

$$dB(R) = (4.343/2) + L - [(4.343/2)^2 + 4.343 L]^{1/2} \quad (6)$$

Care must be taken to include the sign of the OTDR loss L.



Finally, a mode diameter tolerance in terms of OTDR deflection is much tighter than one based on real loss. For example from (4), an OTDR reading  $L(R) = 0.3$  dB corresponds to a mode diameter mismatch of  $R = -6.5\%$ . This yields a real power loss (2) of only  $dB(R) = 0.018$  dB.

### References

- [1] For example, W. Anderson and D. Philen, J. Lightwave Tech. LT-1 20 (March, 1983). An older definition of mode field radius is used.
- [2] A. Hartog and M. Gold, J. Lightwave Tech. LT-2, 76 (April, 1984). The V-value and older 'NA' terms must be simplified.
- [3] W. Otten and F. Kapron, OFC '86, paper TUL30 (February, 1986); also submitted, with T. Olson, to J. Lightwave Tech.

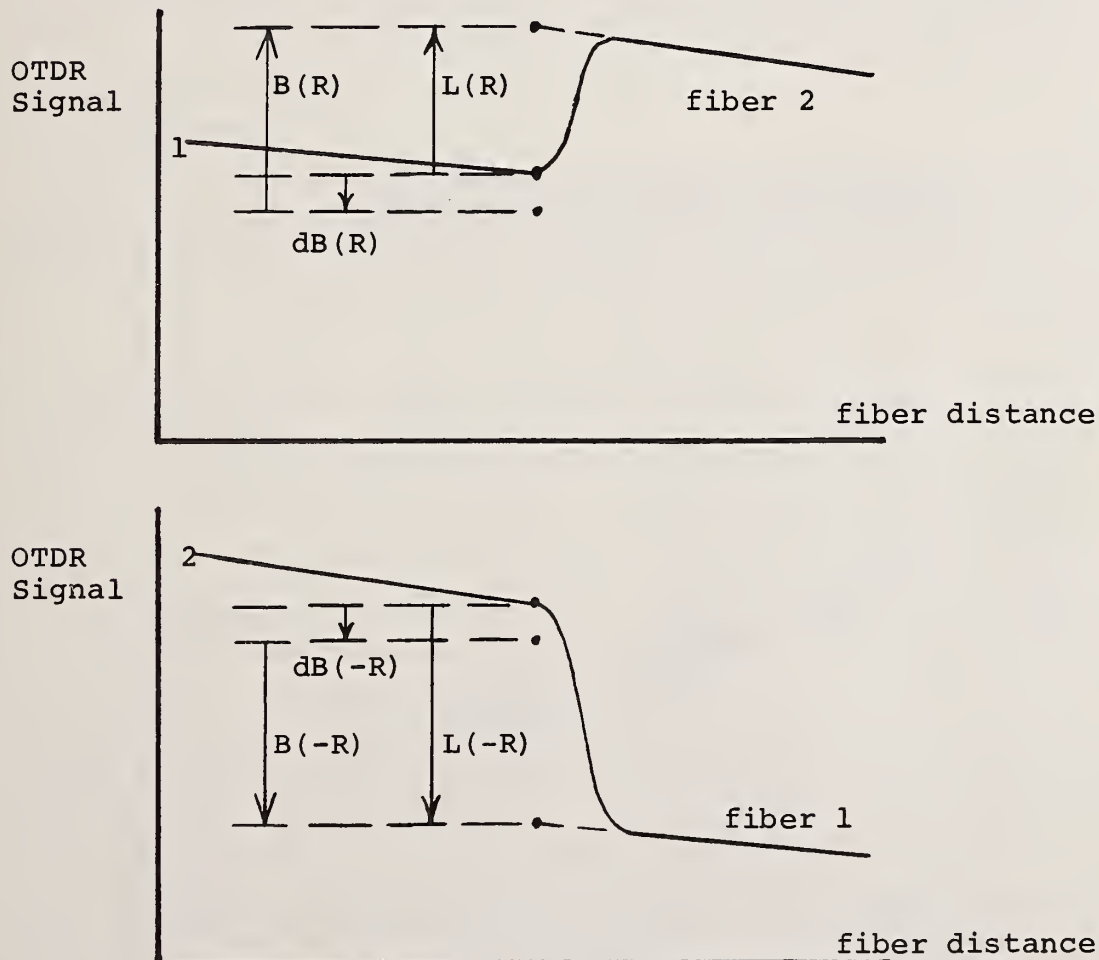


Figure 1. Schematic Bidirectional OTDR Splice Signals L with Mode Diameter Mismatch ( $w_1 > w_2$ ).

Shown are the contributions of true loss  $dB$  in (2) and backscatter ratio  $B$  in (3) to apparent loss  $L$  in (4).

Average Cutback Loss (dB)

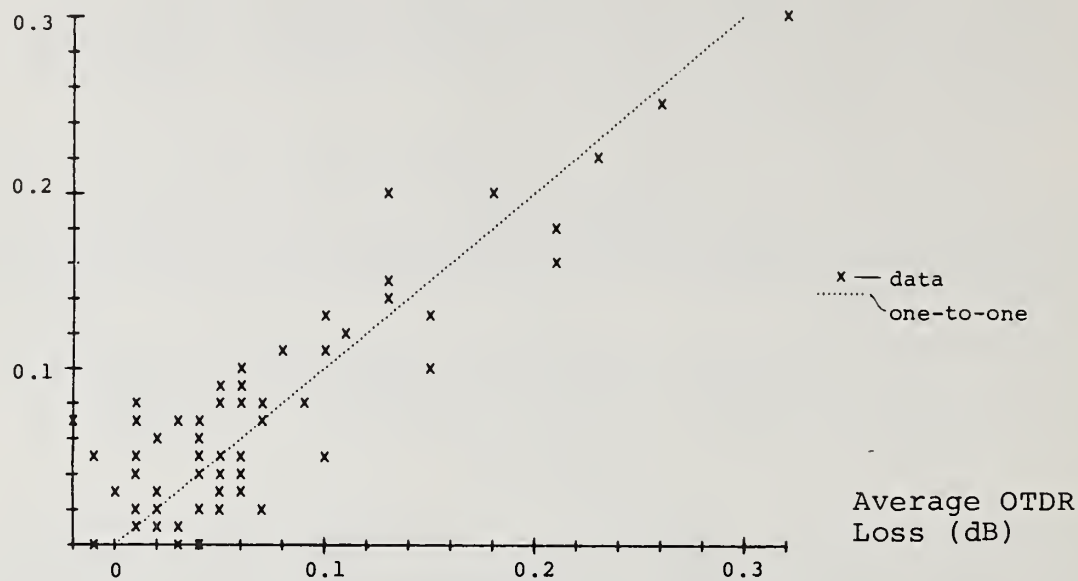


Figure 2. Correlation of Splice Losses  
Measured by Cutback and by OTDR.  
(Bidirectional averages are taken in each case; see (5))

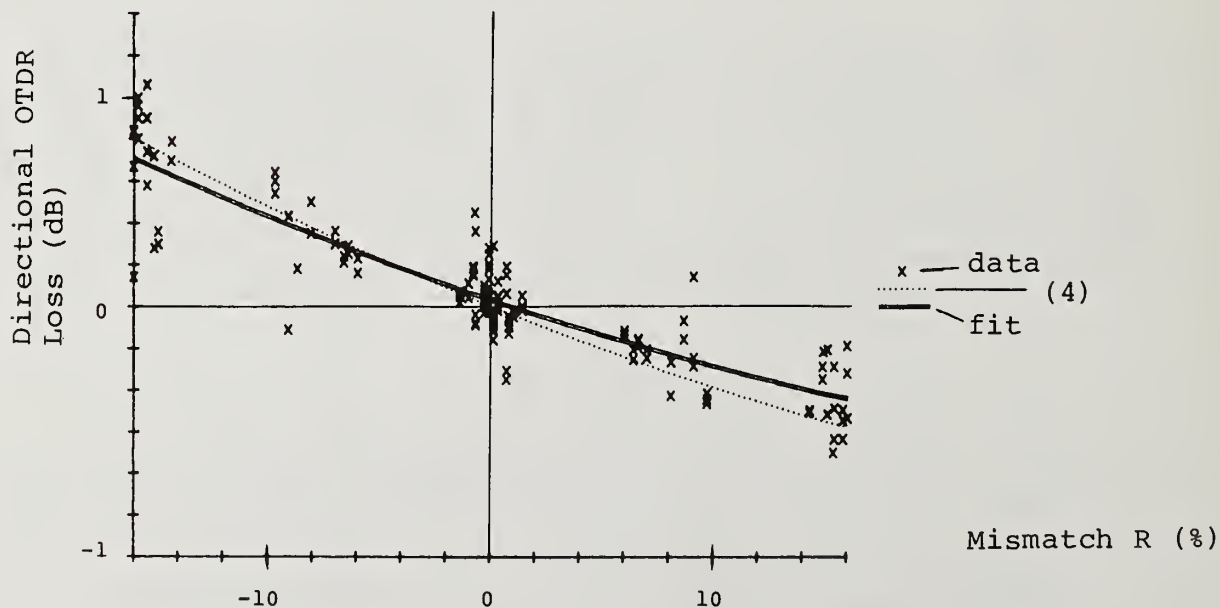


Figure 3. Directional OTDR Splice Apparent Loss  
vs Mode Diameter Mismatch

(best fit:  $L = 3.935R^2 - 3.607R + 0.030$ )

# MULTIMODE FIBER SYSTEMS CHARACTERIZATION

I.P. Vayshenker, D.R. Hjelme, and A.R. Mickelson  
Department of Electrical and Computer Engineering  
University of Colorado  
Boulder, Colorado 80309

## Introduction

When designing a multimode fiber system (MFS) one should take into consideration the mode-dependent properties of the components of the system. Lack of a design tool for fiber-optics networks makes the problem more difficult. However, one can describe a MFS using mode dependent matrices for each component of the system and obtain the system response as a product of these matrices and the input vectors [1]. This method has been used by Evers [2,3] to characterize couplers and connectors, and by Mickelson et al [4,5] for fusion splices and microbends. To our knowledge there exist no work on transmission matrices for fibers, but only mode dependent attenuation measurements [6]. The purpose of this paper is to give an accurate measurement technique to obtain the transmission matrix for arbitrary fiber optic connectors attached by multimode fibers, and apply these techniques to various connector/fiber combinations.

## Theoretical Relations

The mode transmission matrices can be obtained from power loss and near-field measurements. Using the mode continuum approximation [7], one can relate the near field,  $I(s)$ , to the modal power distribution  $p(R)$ . For an azimuthally symmetric fiber with arbitrary index

profile  $n^2 = n_1^2[1 - 2\Delta f(s)]$  this relation is  $I(s) = \frac{V^2}{\pi} \int_{f^{1/2}(s)}^1 p(R) R dR$  where  $s = r/a$  is the normalized radial coordinate,  $R^2 = \frac{1}{2\Delta} (1 - \beta^2/n_1^2 k^2)$  is the mode parameter and  $V = n_1 k a \sqrt{2\Delta}$ .

It should be mentioned that this approximation is valid provided that the linewidth,  $\delta\lambda$ , of the exciting source satisfy  $\delta\lambda/\lambda > \sqrt{2\Delta}/(ka N_1)$ , where  $N_1 = n_1 - \lambda \frac{dn}{d\lambda}$  is the material group index. The total power,  $P_i$ , in the modes with  $R$  values between  $R_i$  and  $R_{i+1}$  are given

by  $P_i = \int_{R_i}^{R_{i+1}} p(R) m(R) dR$  where  $m(R) = V^2 R [f^{-1}(R^2)/a]^2$  is the modal density. Dividing  $R$ -

space into  $n$  intervals, one can define a power vector  $P = [P_1, P_2, \dots, P_n]^T$  ( $T$  for transpose). The input,  $P^{(i)}$ , and output,  $P^{(0)}$ , vectors can then be related by the mode transmission matrix  $T$  [1] as  $P^{(0)} = T P^{(i)}$ . The diagonal elements of  $T$  represent the fraction of power incident on the system in the modes of one  $R$ -interval which remains in the same  $R$ -interval, and the off-diagonal elements represent the fraction of power coupled between the modes.

For a fiber,  $T$  would obviously be length dependent. In a fiber with only absorption and Rayleigh scattering it would be reasonable to assume  $T$  to be a diagonal matrix with elements  $T_{ii} = e^{-\gamma_i L}$ , where  $\gamma_i$  corresponds to the differential mode attenuation (DMA) coefficient  $\gamma(R)$  [6]. But as shown in [6], other mode dependent effects such as mode coupling and coupling to radiation modes gives  $\gamma$  a length dependence and worse, it is extremely hard to determine from measured data. These problems could be overcome if we define a length



independent matrix  $A$  as  $T = e^{-ZA}$  for the fiber.  $A$  would correspond to a two-variable DMA coefficient  $\gamma(R, R')$  as suggested in [6].

### Measurement of the Transmission Matrix

The transmission matrix contains in general  $n^2$  independent elements and to obtain these, one needs  $n^2$  independent measured quantities. This could be obtained using selective excitation to create  $n$  independent input vectors  $P_k^{(i)}$  and measure  $P_k^{(0)}$ . Then  $T$  is obtained from  $T = [P_1^{(0)}, \dots, P_n^{(0)}][P_1^{(i)}, \dots, P_n^{(i)}]^{-1}$ . The diffraction limit poses a severe restriction on how many independent inputs one can generate. Increasing  $n$  would then make  $T$  unstable, and there should be an optimal number of excitations,  $n$ . Some authors [2,3] recommend  $n = 3$  and others [4]  $n = 2$ . In this paper  $n = 2$  is used. It should be pointed out that the resulting matrix  $T$  is very sensitive to the power loss ratios  $|P_k^{(0)}|/|P_k^{(i)}|$ . The larger  $n$  and hence the less independent inputs, the more sensitive  $T$  is to this ratio.

The measurement set-up is shown in Fig. 1. Selective excitation is generated by varying the 3 parameters of the launch system. These parameters can be defined by  $u = \frac{r_s}{a}$ ,  $\rho = \frac{a_{\text{beam}}}{a}$ ,  $\tau = \frac{NA_{\text{beam}}}{NA_{\text{fiber}}}$  where  $r_s$  is radial launch position,  $a_{\text{beam}}$  is the beam radius,  $NA_{\text{beam}}$  is the effective numerical aperture of the launching system. In the experiment  $\rho = .14$ ,  $\tau = .68$ ,  $u = 0, .64$  were used. Fig. 2 shows the calculated (using the theory of [6]),  $p(R)$  and  $I(s)$  for these parameters. To find the input vector  $P_k^{(i)}$ , the measured near-field intensity of a short fiber, stripped for cladding modes, was used. Similarly for the connector a short fiber was used at the output end.

Beside errors in the power measurements and the near-field measurements, other error sources can affect the results. Among these are fiber end quality and alignment problems [8] and leaky modes [9, 10, 11]. According to Petermann [11], the leaky mode correction factor given in [9,10] is very sensitive to non-circular perturbations of the fiber. The correction therefore becomes very uncertain and in this work it is not used.

### Results

The following combinations were under test: Long fiber-connector-long fiber (lcl) and short fiber-long fiber (sl). Fig. 3 illustrates the measured near-fields and derived modal power distributions for the sl combination. To reduce the noise in the data, the measured near-fields were filtered using a fast-fourier transform and a properly chosen cut-off frequency. Next the filtered near-fields were fitted to a 12th order polynomial (only even powers of  $s$ ) and  $p(R)$  was calculated and the power vectors formed. The transmission matrix for the fiber is found from the sl combination to be

$$AL = \begin{bmatrix} .70 & -.13 \\ -.09 & .74 \end{bmatrix} \quad (*)$$

The total transmission matrix,  $T_{\text{lcl}}$ , for the lcl combination were found to be

$$T_{\text{lcl}} = \begin{bmatrix} .21 & .05 \\ .04 & .12 \end{bmatrix}$$

Using this matrix and the matrix for the fiber, the connector transmission matrix can be

found using the relation  $T_{lcl} = e^{-AL} T_c e^{-AL}$ . The resulting connector matrix becomes

$$T_c = \begin{bmatrix} .84 & .01 \\ .04 & .48 \end{bmatrix}$$

This matrix is in good agreement with the matrices found by Evers [3]. From the fiber transmission matrix  $A$  it is possible to find the steady-state distribution. We can write  $P^{(0)} = e^{-AL} P^{(i)} = \sum_{n=1}^2 \mu_k \cdot P^{(i)} \mu_k e^{-\lambda_k L}$  when  $\mu_k$  and  $\lambda_k$  are the eigenvectors and eigenvalues of  $A$ . After a long propagation distance only the vector corresponding to the smallest eigenvalue will survive, i.e., it is the steady state distribution [12]. The matrix (\*) has the following eigenvalues and eigenvectors

$$\mu_1 = \begin{bmatrix} 1.0 \\ .7 \end{bmatrix}; \quad \mu_2 = \begin{bmatrix} 1.0 \\ -1.0 \end{bmatrix} \quad L\lambda_1 = .61, \quad L\lambda_2 = .83.$$

The eigenvalue  $\lambda_1$  corresponds to a steady state loss of 2.63 dB/km. The corresponding power vector  $\mu_1$ , is in agreement with the steady state modal distributions found in [4,5].

#### Acknowledgment

This work is funded by a grant from AMP, Inc., Harrisburg, PA.

#### References

- [1] G.T. Holmes, "Estimation of concatenated system response based on measured transfer functions for low and high order modes," in Prod. Seventh European Conf. on Opt. Commun (Copenhagen, Denmark), Sept. 1981, pp. 3.4-1 - 3.4-4.
- [2] G. Evers, "Measurement of mode transition matrices of quasi-step-index optical fiber components," SPIE vol. 500, Fiber Optics: Short-Haul and Long-Haul measurements and application II, 1984.
- [3] G. Evers, "Mode transition matrices for fiber-optic connectors," El. Lett. 21, 401-2, 1985.
- [4] A.R. Mickelson, M. Eriksrud, S. Aamlid, N. Ryen, "Role of the Fusion Splice in the Concatenation Problem; J. Light Technology, Vol. LT-2, No. 2, pp. 126-138, 1984.
- [5] A.R. Mickelson, "Backscatter Readout from Serial Microbending Sensors," J. Light Tech., Vol. LT-2, pp. 700-09, 1984.
- [6] A.R. Mickelson and M. Eriksrud, "Mode-dependent attenuation in optical fibers," J. Opt. Soc. Am., vol. 73, No. 10, pp. 1282-1290, 1983.
- [7] A.R. Mickelson and M. Eriksrud, "Mode-continuum approximation in optical fibers," Opt. Lett., vol. 7, pp. 572-574, 1982.
- [8] D. Rittich, "Practicability of Determining the Modal Power Distribution by measured Near and Far Fields," J. Light Technology, Vol. LT-3, No. 3, pp. 652-661, 1985.
- [9] M.J. Adams, "Correction factors for the determination of optical-fiber refractive-index profiles by the near-field scanning technique," El. Lett. 12, pp. 281-83, 1976.
- [10] M.J. Adams, "Length-dependence effects due to leaky modes on multimode graded-index optical fibers", Opt. Commun. 17, pp. 204-09, 1976.
- [11] K. Petermann, "Uncertainties of leaky mode correction for near-square-low optical fibers," El. Lett. 18, pp. 513-14, 1977.
- [12] D. Marcuse, Theory of Dielectric Optical Waveguides, Academic Press, 1974.

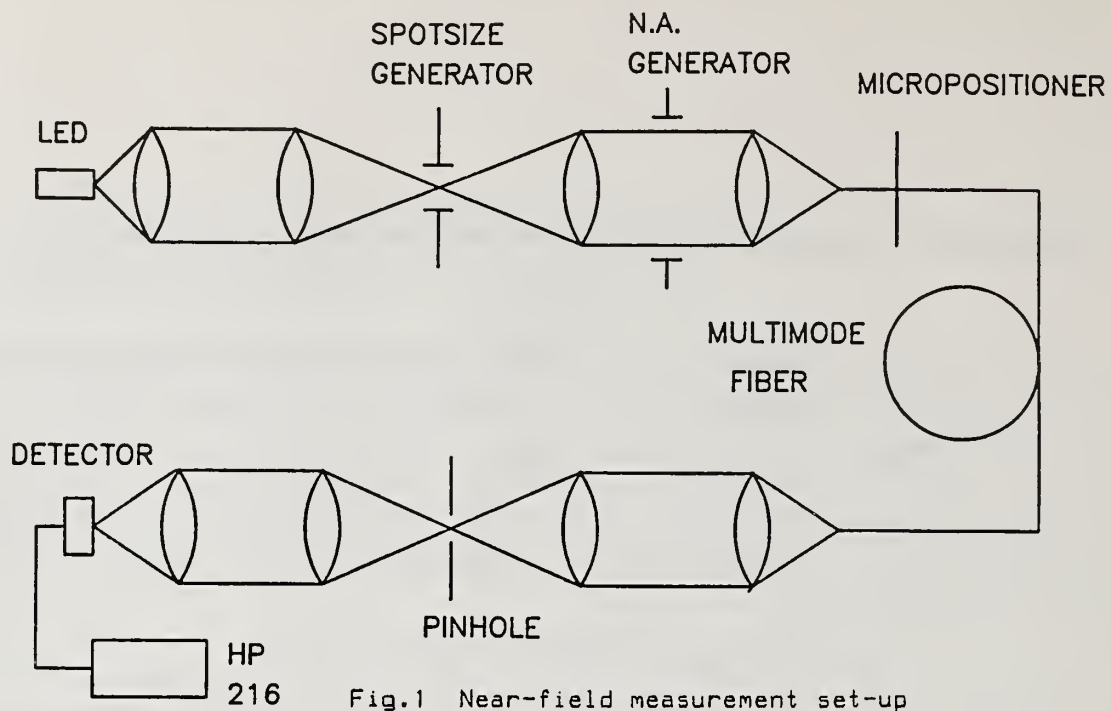


Fig.1 Near-field measurement set-up

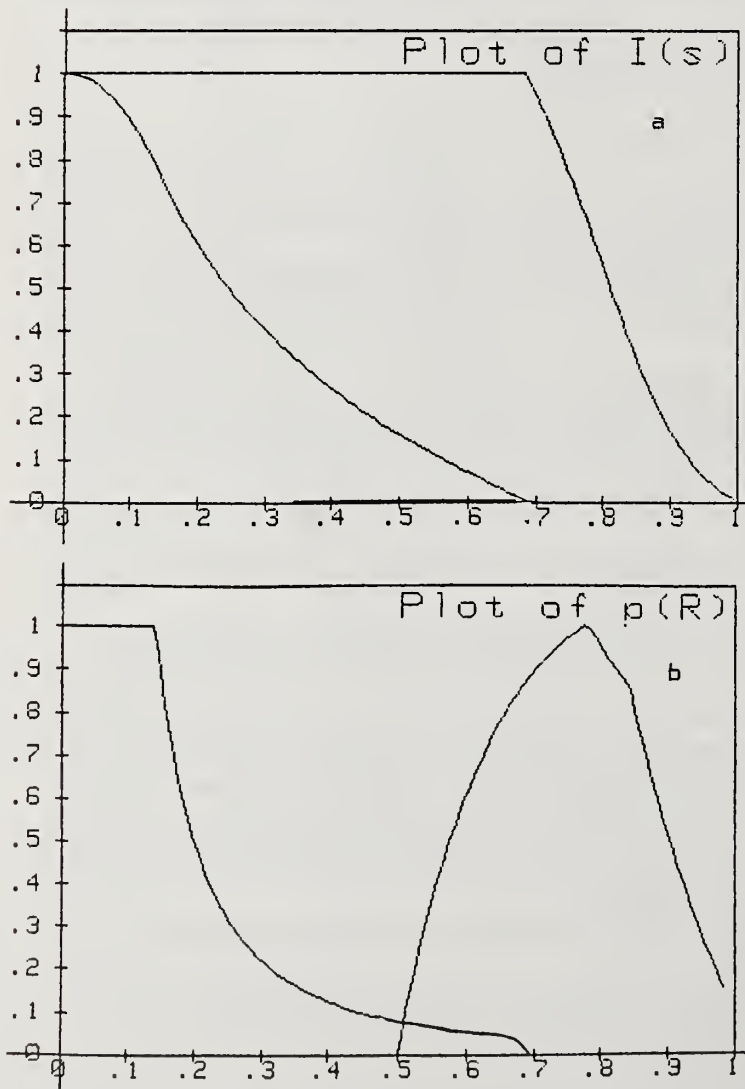


Fig.2 Theoretical  $I(s)$ -a and  $p(R)$ -b for the excitations used in the experiment

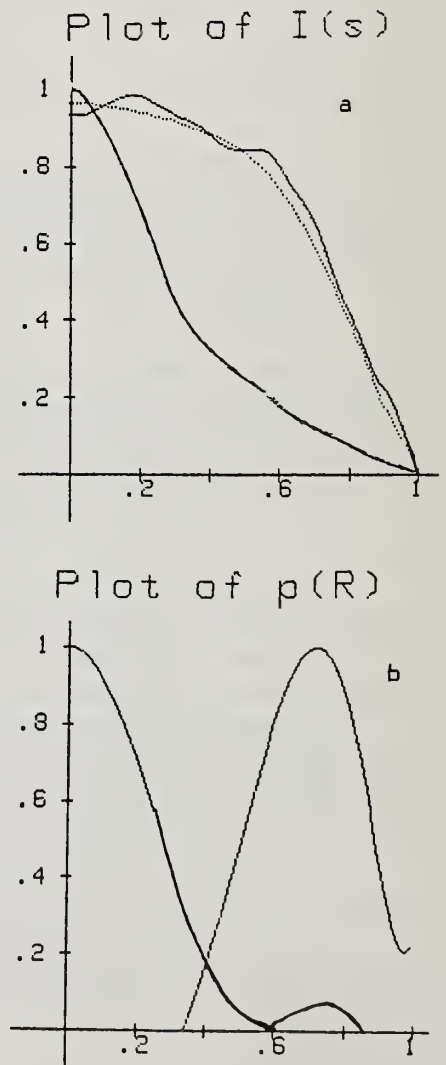


Fig.3 Measured  $I(s)$ -a and  $p(R)$ -b for the long fiber



# Single-Ended Bandwidth Measurement for Multimode Optical Fiber Using Far End Pulse Reflection

Shin-ichi Furukawa, Katsuya Yamashita, Mitsuhiro Tateda  
and Yahei Koyamada

NTT Electrical Communications Laboratories  
Tokai, Ibaraki, 319-11, Japan

## ABSTRACT

Single-ended bandwidth measurement using optical pulses reflected at the far end of a multimode optical fiber has been realized. This method makes it possible to measure the bandwidth of the optical fiber under test with measurement equipment located only at one end of the test fiber. Consequently, the time and manpower required for bandwidth measurement of installed fibers are extremely reduced.

## 1. Introduction

Usually, optical fiber bandwidth measurement requires to locate transmitting and receiving equipment at opposite ends of the fiber under test<sup>(1)</sup>. Recently, a remote-ended time domain bandwidth measurement technique has been proposed where both ends of the fiber can be separated by more than 10 km<sup>(2)</sup>. However, the situation where the transmitting and receiving equipment are located at both ends has not been changed. In the case of subscriber transmission lines, the subscriber ends of the fibers are distributed throughout many locations in the subscriber area, whereas the other ends are centered at the telephone office. If transmitting and receiving equipment need to be located at both ends, as usual, a large amount of time and manpower are required for bandwidth measurement. This paper describes a new bandwidth measurement method in which the transmitter and receiver are located at the same end of the test fiber, thus significantly reducing time and manpower.

## 2. Single-ended bandwidth measurement

The configuration of the single-ended bandwidth measurement is shown in Fig. 1. The test fiber ends are substantially clean, smooth and perpendicular to the fiber axis, so that Fresnel reflections at both ends can be expected. A train of nanosecond pulses is launched into the fiber under test through an optical directional coupler. The backward

pulses reflected from the far end of the test fiber are detected with an APD receiver through the optical directional coupler (ODC). Averaging of the received pulse waveforms is made with a sampling oscilloscope and transformation from the pulse waveform to baseband frequency response is accomplished with a mini-computer. The roundtrip return bandwidth  $BW_r$  of the test fiber is calculated from the ratio of the baseband frequency response obtained from the far end reflection to the one obtained from the input end reflection. The transmission bandwidth  $BW_t$  of the test fiber is estimated from the roundtrip return bandwidth using the equation

$$BW_t = BW_r \times 2^{\gamma}, \quad (1)$$

where  $\gamma$  is a correction coefficient for a roundtrip return pulse in the test fiber. The parameter  $\gamma$  is usually used to describe the bandwidth characteristics of concatenated fibers<sup>(1)</sup>.

A diagram of the optical power level is shown in Fig. 2, where the averaging of the received pulse waveforms in the sampling oscilloscope is not performed. 7 dB optical power loss is allowed for the test fiber. When 15 dB SNR improvement in optical power level can be obtained by averaging the pulse waveforms, it is possible to measure the bandwidth of an optical fiber having a one-way loss of up to 11 dB.

### 3. Experiment

An example of the baseband frequency response obtained from a single-ended bandwidth measurement is shown in Fig. 3. The insets in Fig. 3 represent pulse waveforms reflected from the input end and the far end of the test fiber. A test fiber about 12 km long was prepared by concatenating 4 pieces of fiber with a total loss of 8.5 dB. The peak optical power of the input pulse in the test fiber was about 12 dBm and its full width half maximum (FWHM) pulse width was 1.5 ns. The wavelength was 1.3  $\mu\text{m}$ . A standard 50/125  $\mu\text{m}$  graded-index multimode 10 meter long optical fiber cord was used to connect the test fiber to the optical directional coupler. The far end of the test fiber was prepared using a fiber cutting tool<sup>(3)</sup>. The average number of pulse waveforms in each train was 1024 providing an SNR improvement of about 15 dB in the optical power level. Deviation from the mean value of the single-ended bandwidth during 10 measurements under the same condition was less than 3 %.

### 4. Discussion

The measured bandwidth changes due to mode conversion when the cutting angle of the far endface is not perpendicular to the fiber axis.

Figure 4 shows the changes in the roundtrip return bandwidth  $BW_r$  when the far endfaces of fibers about 2 km long were polished at several angles. It was confirmed that the change in  $BW_r$  was less than 7 % when the angle variation was less than  $2^\circ$ . Usually, the cutting angle is as small as  $0.6^\circ$ <sup>(3)</sup>. Therefore, the influence of the cutting angle variation is negligibly small.

Figure 5 shows a comparison of the transmission bandwidth  $BW_t$  estimated from Eq. (1) with the measured transmission bandwidth for several test fibers having lengths from 1.5 km to 12 km. The transmission bandwidth measurement was performed by locating the receiving equipment at the far end of the test fiber without changing the launching condition. A value of 0.8<sup>(1)</sup> was used for the correction coefficient  $\gamma$  which was determined from several experimental results. Furthermore, it was experimentally confirmed that  $\gamma$  did not depend on the launching condition. The average difference between the estimated value and the measured value was as small as 9.2 % and the maximum was 19.5 %. This accuracy is considered to be sufficient for the bandwidth evaluation of fiber installed in the field.

## 5. Conclusion

A single-ended bandwidth measurement is proposed in which a transmitter and a receiver are located at the same end of a test fiber. With this method it is not necessary for technicians to go to or to carry measurement equipment to the far end of the test fiber. Consequently, a significant reduction in time and manpower can be achieved. By combining this measurement method with the conventional optical time domain reflectometer, attenuation and bandwidth, which are the two essential transmission characteristics in multimode optical fiber, can be measured at one end of the test fiber.

The authors would like to express their grateful appreciation to Fumihiro Nihei, Naoya Uchida and Nobuya Kojima for their encouragement.

## References

- (1) CCITT Recommendation ; "Characteristics of 50/125  $\mu$ m multimode graded index optical fiber cables", Vol. III, Fascicle III.2, Rec. G. 651 (1985)
- (2) A. Ahmad et al. ; "Remote-ended time domain bandwidth measurements on installed regenerator sections of multimode optical fiber cable in the british telecom network", Proceedings of the 32th IWCS, p.414 (1983)
- (3) M. Matsumoto et al. ; "A simple and practical cutting tool for optical fiber end preparation", Trans. IECE Japan, E66, 11, p.661 (Nov. 1983)



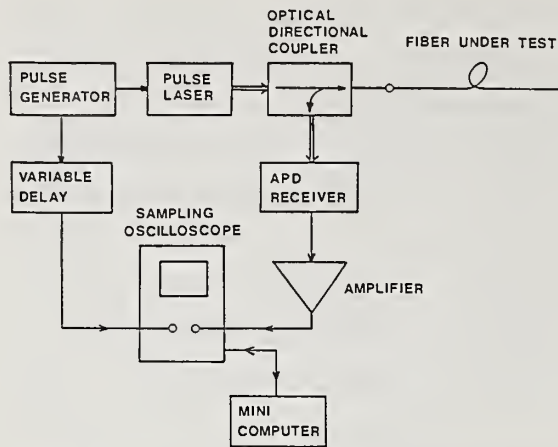


Fig. 1 Configuration of single-ended bandwidth measurement.

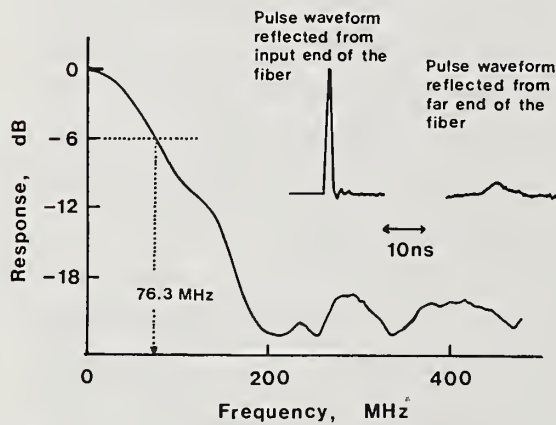


Fig. 3 An example of the baseband frequency response obtained from single-ended measurement (fiber length = 12 km).

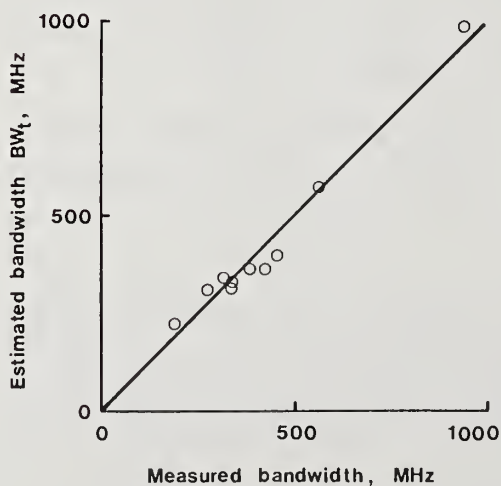


Fig. 5 Comparison of the estimated transmission bandwidth  $BW_t$  with the measured transmission bandwidth.

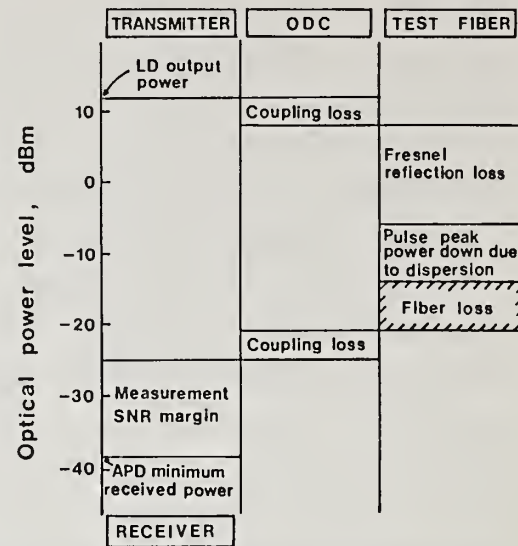


Fig. 2 Optical power level diagram for single-ended bandwidth measurement. Averaging of the received pulse waveforms is not performed. LD output power is 12dBm. APD minimum received power is -38dBm.

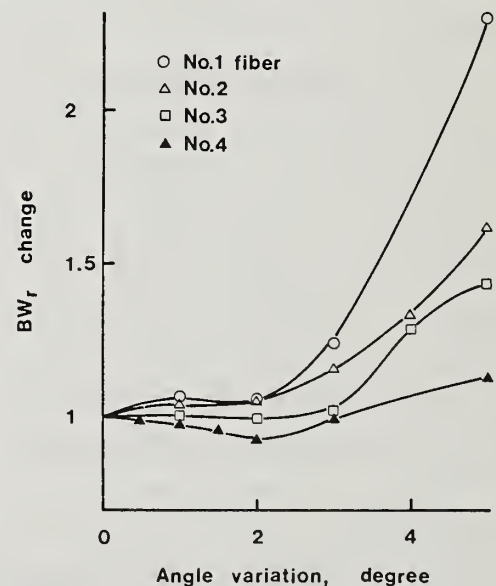


Fig. 4  $BW_r$  change with angle variation of the far endface.

## EFFECTIVE FIBER BANDWIDTHS IN LED BASED SYSTEMS

Dieter Schicketanz and William S. Jackman  
SIECOR Corporation, Hickory, N.C., USA, 28603

### INTRODUCTION

LED's create special problems in optical fiber systems when trying to predict system performance. With LED's operating close to the zero dispersion wavelength of the fiber system, not only are equations to predict fiber and system bandwidth complex, but measured bandwidths using LED's as sources are influenced by the inherent bandwidth limitations of LED's and are not easily used for system performance predictions.

Most predictive equations assume gaussian rolloffs and/or impulse responses to give baud to bandwidth ratios of 1.2 to 1.6 for specific power penalties and bit error ratios.\1\ While there is normally a "safety factor" built into bandwidth specifications to account for the non-gaussianity of modal bandwidth, the extreme non-gaussianity of the material component of fibers with LED sources operated near the zero dispersion wavelength overwhelm any reasonable "safety factor".

This paper uses the RMS pulse width of the output pulse to calculate an "effective" bandwidth to satisfactorily predict system performance with normal approximate gaussian assumptions. Since the "effective" bandwidth is not directly measurable, system rise times have been tested and compared to the predicted value indicated by the "effective" bandwidth. Excellent agreement has been observed.

### THEORY

Basic assumptions made in the calculations are: 1) The LED spectrum can be approximated by a gaussian  $[S(\lambda)]$  with the same "middle" wavelength  $[\lambda_m]$  and same RMS spectral width  $[\sigma_\lambda]$  as the real spectrum. And 2) The dispersion characteristics  $[M(\lambda)]$  of the fiber can be adequately defined by a Sellmeier equation with a zero dispersion wavelength  $[\lambda_0]$  and a slope at the zero dispersion wavelength  $[S_0]$ .

The impulse response  $[h(t)]$  of the fiber to an LED source can be derived, but is very involved. The RMS pulse broadening  $[\sigma_t]$  can be approximated by \2,3,4\:

$$(1) \sigma_t = L[M(\lambda)^2 \sigma_\lambda^2 + (S_0 \sigma_\lambda^2)^2 / 2]^{.5}$$

When  $\lambda_m = \lambda_0$ ,  $h(t)$  can be approximated by:

$$(2) h(t) = (\pi t S_0 L \sigma_\lambda^2)^{-.5} \exp[-t / (S_0 L \sigma_\lambda^2)]$$

with  $\sigma_t$  approximately equal to:

$$(3) \sigma_t = L S_0 \sigma_\lambda^2 / (2)^{.5}.$$

When  $|\lambda_c - \lambda_0| \gg \sigma_\lambda$ ,  $h(t)$  can be approximated by a gaussian:

$$(4) h(t) = \exp(-.5\{(t-t_0)/[M(\lambda)L\sigma_\lambda]\}^2)$$

with  $\sigma_t$  approximately equal to:

$$(5) \sigma_t = LM(\lambda)\sigma_\lambda.$$

Fourier transforms can be used to predict the frequency response rolloffs  $[H(f)]$  and the 3 dB optical bandwidths  $[BW]$ .

For  $\lambda_m = \lambda_0$  the transform of (2) is \5\:

$$(6) H(f) = (1+j2\pi f L S_0 \sigma_\lambda^2)^{-.5}$$

with magnitude:

$$(7) |H(f)| = (1+(2\pi f L S_0 \sigma_\lambda^2)^2)^{-.25}$$

3 dB optical ( $|H(f)| = .5$ )

$$(8) BW(\lambda_m = \lambda_0) = (15)^{.5} / (2\pi L S_0 \sigma_\lambda^2) = .616 / (L S_0 \sigma_\lambda^2) = .436 / \sigma_t$$

For  $|\lambda_m - \lambda_0| \gg \sigma_\lambda$  the transform of (6) is:

$$(9) H(f) = \exp(-.5(f/\sigma_f)^2) = \exp(-.5(f2\pi\sigma_t)^2) = \exp(-.5(f2\pi LM(\lambda)\sigma_\lambda)^2)$$

3 dB optical for  $|\lambda_m - \lambda_0| \gg \sigma_\lambda$

$$(10) BW(|\lambda_m - \lambda_0| \gg \sigma_\lambda) = (\ln(4))^{.5} / (2\pi\sigma_t) = .187 / \sigma_t = .187 / (LM(\lambda)\sigma_\lambda)$$

The effective material bandwidth is determined by using the rms pulse spreading found in (1) with the gaussian assumptions which are the basis of (10). Therefore the effective material bandwidth is:

$$(11) BW(\text{effective}) = .187 / (L(M(\lambda)^2 \sigma_\lambda^2 + S_0^2 \sigma_\lambda^4 / 2)^{.5})$$

The system bandwidth is a combination of the modal, material and LED responses. The measured bandwidth  $[BW(\text{measured})]$  using an LED source can be predicted by multiplying  $H(f)[\text{modal}]$  by  $H(f)[\text{material}]$  and  $H(f)[\text{LED}]$  and taking the half power point.  $H(f)[\text{Measured}]$  is non-gaussian and depending on the rolloff characteristics of the LED's, may not be comparable between LED's with the same optical characteristics.

The effective system bandwidth can be calculated using common gaussian assumptions as:



$$(12) 1/BW(\text{system effective})^2 = 1/BW(\text{modal})^2 + 1/BW(\text{effective material})^2$$

Limits to the accuracy of the effective system bandwidth occur when the system is long enough that spectral filtering significantly distorts the spectral output of the fiber or for extremely high performance or non-gaussian LED's. Spectral filtering could be accommodated if the spectral attenuation signature of the fibers to be used are sufficiently characterized and consistent. An "effective" middle wavelength and RMS pulse spreading could be calculated.

Because the effective system bandwidth is difficult to measure, to test the theory, rise times of systems were measured and compared to the predicted rise times using gaussian assumptions using the RMS pulse width, the same basic assumption behind the effective material bandwidth calculation.

Rise time calculations from the RMS pulse width start with a normalized gaussian impulse.

$$(13) h(t) = \exp(-.5(t/\sigma_t)^2)$$

The impulse rise time from  $h(t) = .1$  to  $h(t) = .9$  is:

$$(14) r_{ti} = ((-2\ln(.1))^{.5} - (-2\ln(.9))^{.5})\sigma_t = 1.6869 \sigma_t$$

The step response is related to the impulse response:

$$(19) \text{ Step response } h(t) = 1/(2\pi\sigma_t)^{.5} \int_{-\infty}^t \exp(-(t-t_0)^2/(2\sigma_t^2)) dt$$

The step rise time from  $h(t) = .1$  to  $h(t) = .9$  is:

$$(19) r_{ts} = 2.563\sigma_t$$

Measurements are easier to do for step rise times than impulse rise times. To measure the rise time of the fiber, it is necessary to deconvolve the effect of the transmitter and receiver from the actual measured rise time. Using Gaussian assumptions the system rise time is related to the component rise times by:

$$(22) r_{t_{\text{system}}}^2 = \sum r_{t_{\text{components}}}^2$$

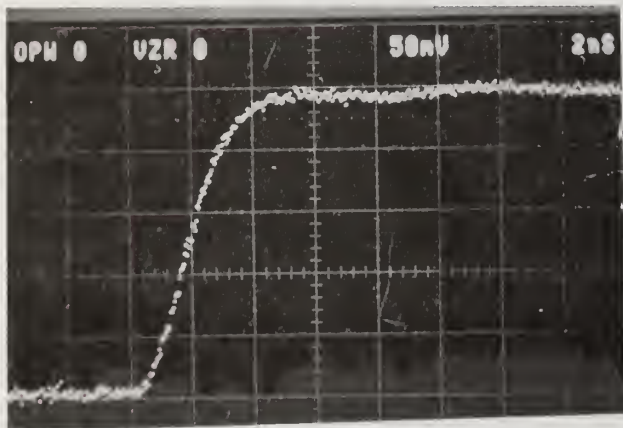
#### TEST PROCEDURE AND RESULTS

A Tautron 325 BER test set was used to drive a high performance LED,  $\lambda_m = 1290\text{nm}$  and  $\Delta\lambda = 135\text{nm}$ . A Ge avalanche diode ( $r_{ts} < 200\text{ps}$ ), 5 GHz amplifier, and a sampling oscilloscope completed the test set up. The system was first tested without a fiber to measure the test set up rise time. As shown in figure 1, The non fiber portions have a step rise time of 2.7 nanoseconds. Figure 2 includes a 2.3 km, 62.5  $\mu\text{m}$  core, .28 NA fiber,  $\lambda_0 = 1345\text{nm}$ ,  $S_0 = .1 \text{ ps/nm}^2\text{km}$ , with a modal bandwidth of 247 MHz

(800 MHz.km). Expected modal step rise time =1.4 ns. The predicted effective material bandwidth is 198 MHz, and the predicted material step rise time =2.413ns. The predicted total system step rise time was 3.9 nanoseconds. Figure 2 shows a measured step rise time of 4 nanoseconds.

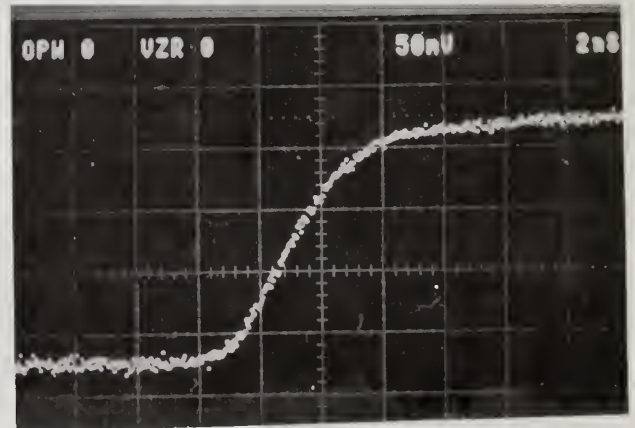
#### Literature:

- \1\ Personick, S. D.; "Receiver Design for Digital Fiber Optic Communications Systems, I"; The Bell System Technical Journal, Vol. 52, No 6; July-August, 1973; pages 843-875
- \2\ Marcuse, Dietrich and Lin Chinlon; "Low Dispersion Single-Mode Fiber Transmission- The Question of Practical versus Theoretical Maximum Transmission Bandwidth"; IEEE Journal of Quantum Electronics, Vol. QE-17, No. 6; June 1981; pages 869-878
- \3\ Geckler, S.: "Lichtwellenleiter für die optische Nachrichtenübertragen"; Berlin; Springer 1986, Chapter 3
- \4\ Gloge, D. "Effect of Chromatic Dispersion on Pulses of Arbitrary Coherence", Elec. Letters 21, 1979, pages 686-687
- \5\ Cohen, Leonard G., Mammel, Wanda L., and Lumish, Stan; "Dispersion and Bandwidth Spectra in Single-Mode Fibers"; IEEE Journal of Quantum Electronics, Vol QE 17, No 1, pages 49-53



LED rise time = 2.7 ns

Figure 1



LED + Fiber rise time = 4.0 ns

Figure 2 THEORETICAL = 3.9 ns

# MEASURING 825 NM TRANSMISSION ON 1300 NM SINGLE-MODE FIBERS

Catherine M. Ragdale\* and Felix P. Kapron

ITT Electro-Optical Products Division  
7635 Plantation Road  
Roanoke, VA 24019-0065

## Abstract

Standard single-mode fibers, designed for longwave transmission, are operated in the shortwave region well below the effective cutoff of the second-order mode group. The temporal and frequency responses are investigated.

## Introduction

The advantages of single-mode transmission are realized if the source wavelength is higher than the effective cutoff wavelength [1] of the fiber. This will not occur with 1300 nm transmission over short fiber lengths for which the second-order mode group is not fully attenuated, and modal noise can result [2]. However, here we examine operation at even shorter wavelengths where that mode group becomes less lossy, and study 825 nm fully bimodal transmission over longer lengths of single-mode fiber designed for 1300 nm operation.

## Second-Order Cutoffs

The fibers used were dispersion-unshifted (EIA fiber type IVa), with a nominal step-index matched-clad profile and a small central dip. The cutoff wavelength of the LP<sub>11</sub> second-order mode group was obtained by the standard power transmission procedure [3] for a 14-cm radius single turn and a 2-m length. We extended this procedure to wavelengths short enough to detect cutoff of the third-order LP mode group. Moreover, the effective cutoff wavelengths for 1.5 km lengths were obtained [4].

\* currently with Plessey Research, Caswell, Northants, U.K.



Figure 1 shows results for one particular fiber. For a simple ideal profile, the theoretical cutoff wavelength of the third-order mode group should be  $(2.405/3.832) = 62.8\%$  of the theoretical second-order mode group cutoff. Note that the measured third-order/second-order effective cutoff ratios are 68.6% and 68.4% for the short and long fibers, respectively, in reasonable agreement. Moreover, the long-length/short-length effective cutoff ratios are consistently 94.9% and 94.6% for the second-order and third-order mode groups, respectively.

The farfield patterns of Figure 2 were made with two light injection conditions. They show that at 825 nm, both mode groups are tightly bound over the full fiber length. The third-order group, which has a long-length effective cutoff of 836 nm, is comparatively weak.

### Bimodal Distortion

A time-domain measurement, done similarly to pulse broadening with multimode fiber, is shown in Figure 3. Differential mode delay is responsible for the pulse separation  $\Delta\tau = 3.65$  ns/km (assuming length linearity and negligible mode coupling). This agrees with the observed frequency periodicity  $\Delta f = 1/\Delta\tau = 275$  MHz-km in the Fourier-transformed baseband response  $A(f) \cdot \cos(2\pi f L \Delta\tau)$ .

We associate the larger and relatively delayed output pulse with the second-order and weakly guided third-order mode groups. This is consistent with the relative mode power degeneracy and with theoretical step-index group delays [5]. Chromatic dispersion causes the broadened pulses of Figure 3b compared to the input width in Figure 3a. It also causes the general frequency rolloff  $A(f)$  of Figure 3c. The extra broadening of the larger pulse is due to the weakly guided third-order mode group. This was confirmed by wrapping the fiber onto a smaller 13-cm diameter spool; this equalized the widths (but not heights) of both output pulses.

### Conclusion

Shortwave transmission in a fiber designed to be single-mode in the longwave region has been studied. Results are consistent with long-length bimodal operation around third-order mode cutoff. Such transmission can be useful for some bidirection WDM high/low bitrate applications.

### References

- [1] H. T. Nijhuis et al, Symp. O.F. Meas., NBS Special Pub. 683, 11 (Oct 1984)
- [2] D. G. Duff et al, paper TU01, Tech. Digest O.F. Comm. (Feb 1985), and references therein
- [3] EIA FOTP-80, CCITT Recommendation G.652
- [4] EIA FOTP-170
- [5] L. G. Cohen et al, B.S.T.J. 59, 1061 (July-Aug 1980)

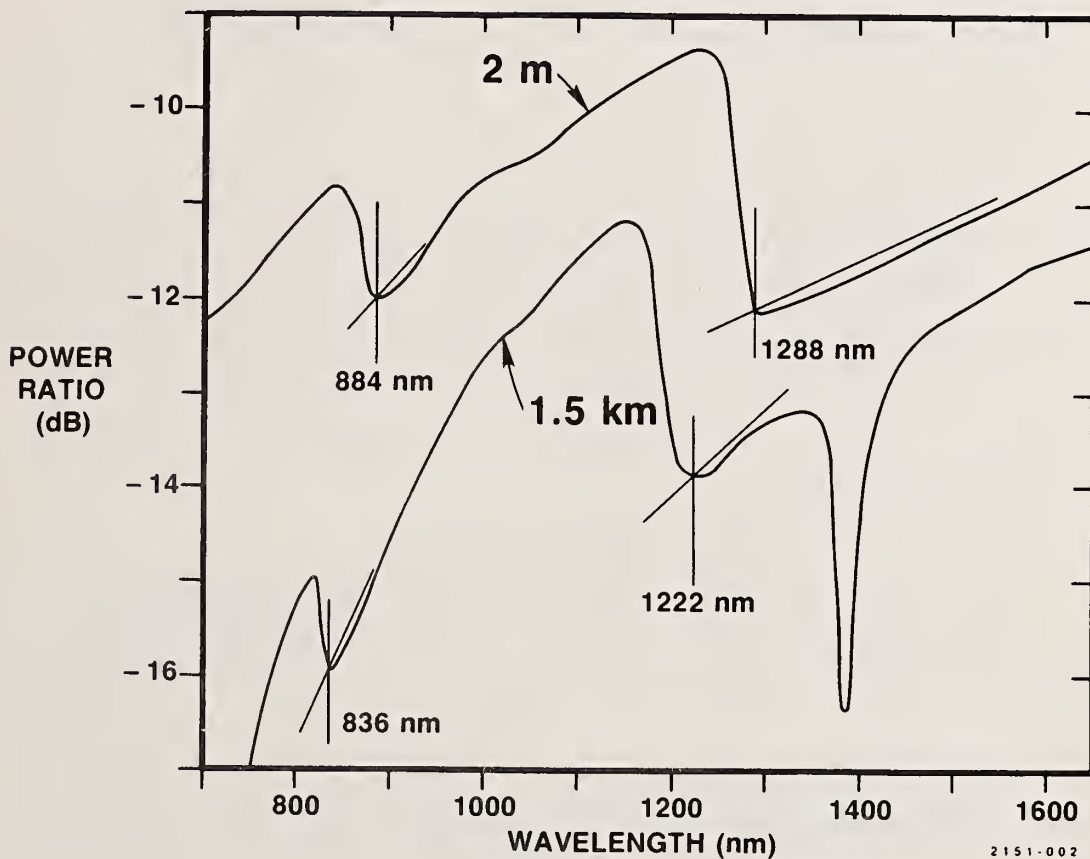


Figure 1. Measurement of short-length and long-length effective cutoff wavelengths for the second-order and third-order mode groups. Power transmitted through the single-mode fiber is ratioed to power through 2 m of multimode fiber.

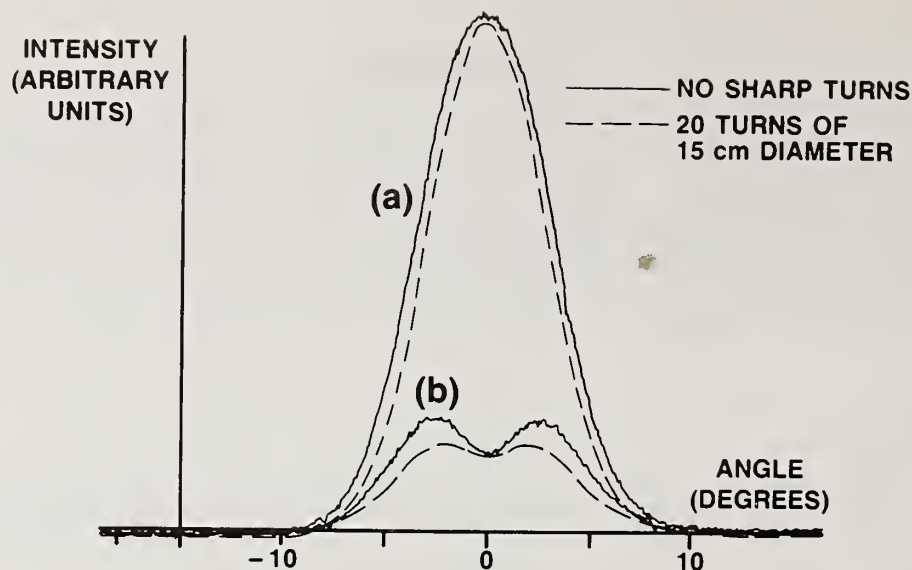


Figure 2. Far-field patterns obtained by butting the 1.5 km test fiber to a similar fiber pigtailed to an 825 nm laser diode: (a) injection of all modes; (b) transverse offset injection of mainly the second-order and third-order mode groups. The dashed curves were taken with 20 turns around a mandrel of 15-mm diameter.

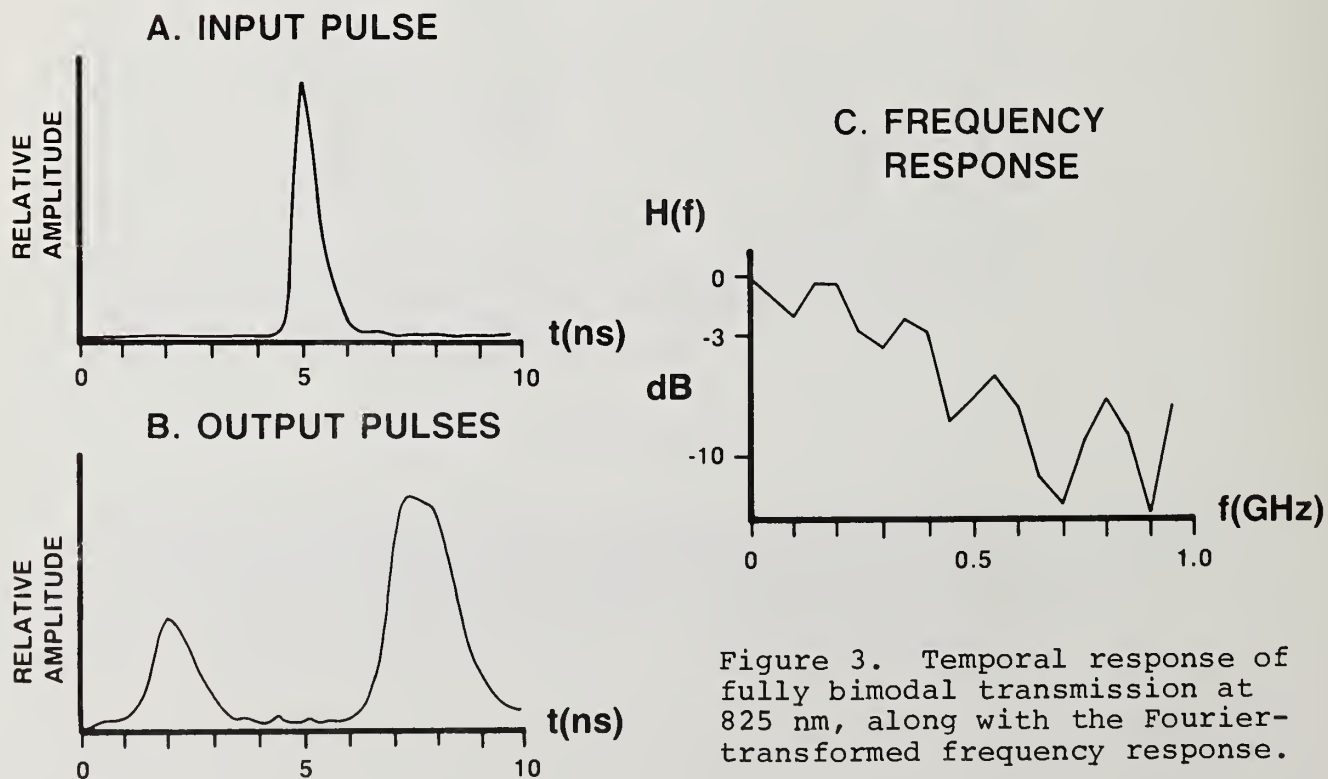


Figure 3. Temporal response of fully bimodal transmission at 825 nm, along with the Fourier-transformed frequency response.



# CHARACTERIZATION OF SOURCES AND DETECTORS FOR OPTICAL FIBER SYSTEMS

T. ITO\* and K. KURUMADA\*\*

NTT ELECTRICAL COMMUNICATION LABORATORIES

\*1-2356 Take, Yokosuka-shi, Japan

\*\* 3-1 Wakamiya, Morino-sato, Atsugi-shi, Japan

## 1. INTRODUCTION

Fiber optics are now playing an important role in telecommunication networks that include inter-city trunks, undersea transmission lines and subscriber loops. Present fiber optic communication systems utilize an intensity-modulation direct-detection scheme. However, advanced lightwave technology using coherent light is expected to go beyond the limit of present fiber optic communication systems. Optical device characterization is key technology in the development of new fiber optic communication systems.

This paper describes the present state of semiconductor light source and photodetector characterization technologies, while reviewing the progress made in the development of fiber optic communication systems at NTT.

## 2. TRUNK TRANSMISSION

400 Mbit/s single-mode fiber trunk lines are now connecting major cities in Japan. The following items are important in designing high-speed long haul transmission systems.

### 2.1 LD transversal mode

Stable single transversal mode oscillation is indispensable to obtain large a signal-to noise ratio. The LD transversal mode stability is estimated from a kink of LD I-L characteristics, i.e. a multi-mode LD has a kink in the I-L characteristic curve.

The mode stability and single mode oscillation characteristics are closely related to LD structures. Among the LD structures proposed thus far, especially the index-guide LDs including a buried heterostructure (BH) LD have shown excellent mode stability.

### 2.2 LD spectrum

A multi-longitudinal mode Fabry-Perot LD restricts transmission distance by signal waveform degradation due to

the mode partition noise. The degradation is evaluated from an LD spectrum shape. The LD spectrum, changing with a LD structure and an operating condition, is not unique. One is a single-peak shape ; another a double-peak shape. In general it can be said that, for Gaussian shape spectrum, the transmission distance limited by this degradation is given as :

$$L_m = 350 / w m f_0 \text{ (km)},$$

where  $w$  is an LD average spectrum width (nm),  $f_0$  the transmission bit rate (Gbit/s), and  $m$  the single-mode fiber dispersion ( psec/km nm) (1).

### 2.3 Longitudinal submode suppression

A single transversal mode DFB LD solves the mode partition noise degradation. In this case, wavelength (optical frequency) chirping inherent in a DFB LD modulation restricts the transmission distance. A streak camera, then, is a powerful tool to examine the dynamic chirping behaviour. The transmission length restricted by the frequency chirping is given as :

$$L_m = 120 / \Delta\lambda \quad m f_0 \text{ (km)},$$

where  $\Delta\lambda$  is an average spectrum width of frequency chirping(nm),  $f_0$  the transmission bit rate (Gbit/s), and  $m$  the single-mode fiber dispersion ( psec/km nm) (2).

The modulated LD characteristics are evaluated from the submode suppression ratio. A suppression ratio of more than 30 dB is required to eliminate the submode effect on transmission characteristics.

Some sophisticated DFB LDs proposed thus far have already met this requirement. An asymmetric laser cavity structure is a promising way to suppress the submode. This structure is realized by forming an anti-reflection (AR) coating on one face of a DFB LD chip. Since a low reflectivity face provides more output power than the other face, light from the coated face is usually coupled into the transmission fiber. However, the AR coating significantly increases the backscattering effect on an LD's characteristics. An optical isolator having more than a 25 dB isolation ratio is able to eliminate the reflected wave noise.

### 2.4 Modulation waveform

The LD modulation waveform, for high speed modulation in particular, depends on bias and modulation conditions.

In a practical transmission system design, the modulated waveform is specified as masked waveform pattern.

## 2.5 Reliability

Undersea transmission requires extremely high device reliability. For an NTT 400 Mbit/s undersea transmission system (FS-400M system), Fabry-Perot Buried Heterostructure (BH) LDs are selected by a threshold current screening test and then undergo more than 1500 hour in an aging test to determine that the LDs have more than a 25 year average lifetime and a failure rate of less than 50 fit (3).

## 2.6 APD characteristics

Quantum efficiency, the dark current excess noise factor, maximum multiplication coefficient, and the bandwidth are major parameters in system design. An InGaAs APD, when compared with a Ge APD, displays a low dark current level, small excess noise factor and longer wavelength responsibility. Therefore, higher speed transmission systems such as a 1.6 Gbit/sec system (F-1.6G system) and 1.5  $\mu\text{m}$  systems use InGaAs APDs.

## 3. COHERENT TRANSMISSION TECHNOLOGY

Coherent transmission, accompanied with control of wave's fundamental properties such as frequency, phase and amplitude, aims at full utilization of broad lightwave frequency band up to several hundred THz. While several barriers, listed below, stand in the way of this technology, there have been enthusiastic research into these area for the past several years.

### 3.1 Lightsource phase noise

Microwave or millimeter wave single tone oscillator spectrum width (phase noise) is less than 1 Hz and , in practice, the oscillator phase noise does not affect transmission characteristics. However, in a lightwave region, it is difficult to obtain the same absolute spectrum width as in a radio wave region, since the lightwave frequency is so high that oscillator requirement becomes relatively restrictive.

The required spectrum width, which depends on a modulation and demodulation scheme, is between  $10^{-10}$  -  $10^{-11}$  times transmission speed for heterodyne/homodyne detection. A wider spectrum width results in an error rate floor phenomena. The most accurate one among LD spectrum width measurement tools is a delayed self heterodyne/homodyne technique with an accuracy of about 1 kHz (4).



### 3.2 Lightsource modulation bandwidth

The lightsource spectrum width can be reduced by inserting an external cavity. However, the external cavity reduces an LD's modulation performance, i.e. its FM characteristics. Heavily doped LDs and multi-quantum well (MQW) LDs are promising lightsources for coherent high speed systems.

### 3.3 Lightsource frequency stability

Although present intensity modulation fiber optic communication has, compared with radio systems, larger transmission capacity, the present fiber optic system frequency utilization efficiency is in the order of 10 - 10%. The improvement of LD frequency stabilization for optical frequency division multiplexing (optical FDM) will permit the full use of a broad lightwave frequency band up to several hundred THz. At present, LD relative frequency stabilization is less than 1 MHz. However, highly accurate optical frequency measurements and semiconductor crystal growth processes for highly frequency controlled LDs are required to control absolute optical frequency so that more than one hundred channel optical FDM transmission can be realized.

### 3.4 Photodiode bandwidth

Higher speed transmission requires a broader bandwidth photodiode. For example, a heterodyne/homodyne detection demands photodetectors 1.5 - 2 times as broad as its transmission speed. A wideband photodiode frequency response over 10GHz is evaluated by the beat of two laser diodes having slightly different frequencies (5).

## 4.SUBSCRIBER LOOP APPLICATIONS

For subscriber loops, there are multiple choices among the combination of lightsources, photodetectors and fibers. Here as an example, multimode fiber analog modulation systems will be discussed, because either multimode fiber analog baseband or FM modulation has been a key economic factor in fiber optic field trials. In multimode fiber systems, S/N degradation due to modal noise is a significant problem. Basically there are two ways to solve this problem :

- (1) The employment of modulation schemes, such as FM, squared wave FM, PFM, which can resist the modal noise.
- (2) The reduction of lightsource coherency to suppress modal noise.

In terms of economy, an LED is one of the promising solutions in constructing simple and stable systems. With regard to the LED systems, keen attention has been paid to the following items.

#### 4.1 LED wavelength-division-multiplexing

At various NTT subscriber system trials, wavelength division multiplexing (WDM), which makes subscriber system more flexible and more economical, has used 0.78 - 1.55  $\mu\text{m}$  wavelength. The shortest wavelength for practical silica fiber subscriber loops is 0.78  $\mu\text{m}$ .

Since an LED has a broad spectrum width of 30-100 nm, it is necessary to reduce interchannel optical interference by optical filters in optical multi/demultiplexers.

#### 4.2 LED nonlinear distortion

Analog modulation, in comparison with digital modulation, demands LED modulation high linearity. LED modulation characteristics are usually compensated by an LED driving circuit. The nonlinear distortion caused in a PIN-photodiode or in an APD is much smaller than that in an LED. The nonlinear distortion affects video signals remarkably. Video transmission specifications are usually described in terms of differential gain (DG) and differential phase (DP). The requirement for NTSC video transmission is a DG of less than 10% and a DP of less than  $4^\circ$  (6).

#### Acknowledgement

The authors would like to express their sincere thanks to Dr. K. Nosu, Dr. M. Saruwatari and Mr. E. Yoneda for their fruitful discussion. They also would like to express their thanks to Dr. H. Kimura, Dr. S. Shimada, Dr. M. Fujimoto and Dr. T. Ikegami for their encouragement.

#### References

- (1) Y. Kobayashi et al., "Non-repeatered submarine optical transmission terminal equipment," Rev. of ECL, 31, 6, pp.844-850 (Nov. 1983)
- (2) K. Iwashita et al., "Error rate performance of high-speed optical fiber transmission systems using single-longitudinal mode laser diodes," Trans. IECE Japan, J67-B, 12, pp.1415-1422 (Dec. 1984)
- (3) Y. Nakano et al., "Screening method for laser diodes with high reliability," Electron. Lett., 20, 10, pp.397-398

(May 1984)

- (4) S.Kawanishi et al., "Wideband frequency response measurement of photodetectors using optical heterodyne detection technique," Electron. Lett., 22, 6, pp.337-338 (Mar. 1986)
- (5) T.Okoshi et al., "Novel method for high resolution measurement of laser output spectrum," Electron. Lett., 16, 16, pp.630-631 (July 1980)
- (6) J.Yamagaka et al., "Development of fiber optic broadband interactive distribution network", to be presented at ISSLS 86, Sep. 29-Oct.3, 1986, Tokyo.



## CHARACTERISATION OF SPECIALITY FIBRES AND COMPONENTS

D.N.Payne\*, S.B.Poole\*, M.P.Varnham<sup>†</sup>, R.D.Birch\*

\* Optical Fibre Group,  
Southampton University,  
Southampton,  
England.

+ British Aerospace plc  
Six Hills Way,  
Stevenage,  
England.

Optical fibres are making ever increasing inroads into areas traditionally satisfied by older, more established technologies. One of the prime vehicles for this trend is the proliferation of specially-tailored fibres designed for specific applications<sup>1</sup>. Since these applications are diverse (especially in the sensor field<sup>1</sup>) and the required fibre characteristics often subtle, measurement of the fibre response frequently presents a challenge. On occasions it is even necessary to resort to indirect measurements by observing the performance of the fibre in the intended application, from which its characteristics can be implied. A particular example here is the fibre gyroscope, where signal processing techniques have progressed to such an extent that the gyro itself provides the ideal environment for high-accuracy measurements of fibre polarisation performance.

It is the intention of this paper to review some of the many speciality fibres currently available or being developed, the selection being made to emphasise topical measurement issues. A summary of different fibre types, their applications and associated measurement problems is given in Table 1.

**Dispersion-Tailored Fibres** were among the first speciality fibres to be investigated and a number of techniques have been developed to measure the chromatic dispersion. Despite this, questions remain concerning which curve-fitting routines should be used to reduce measurement noise. This is particularly true for dispersion flattened fibres, since no a priori knowledge of the shape of the dispersion curve can be assumed.

**Polarisation-Maintaining Fibres:**<sup>2,3</sup> Controversy exists as to whether these should be characterised by the polarisation holding h-parameter<sup>4</sup> (which is the polarisation cross-talk per unit length), or by the intrinsic modal-birefringence B. The h-parameter measures the actual cross-talk present when the fibre is subject to uncontrolled random external perturbations, for example by winding on a drum. It therefore reveals more about the quality of the winding or fibre coating than it does about the

fibre. The modal birefringence, on the other hand, describes the resistance of the fibre polarisation state to cross coupling (externally induced in all but the worst fibres) and is therefore an intrinsic fibre property. The problem is complicated by the fact that the modal fields are not plane polarised<sup>5</sup>, but are actually curved, with the orthogonally-polarised minor-field components present at levels ranging from -32 to -45 dB. Thus with state-of-the-art fibres providing h-parameters ranging from  $10^{-5}$  to  $10^{-6} \text{ m}^{-1}$  (cross-talk of -20 to -30dB after 1 km), it is necessary to use long lengths of fibre in order to obtain a reliable measurement of h. In this case, the measurement is usually dominated by external perturbations.

Since the modal birefringence is an intrinsic fibre property, it would appear to be a better measure of fibre characteristics than the h-parameter<sup>6</sup>. Perhaps the best solution, however, would be a measurement of h-parameter with the fibre subject to controlled perturbations, such as mandrel bends and twists. In this way the fibre resistance to cross-talk could be directly specified, since the measurement would automatically include the resistance of the fibre and buffer coating to cross-talk caused by microbends and pressure.

Single Polarisation Fibres<sup>7,8</sup> rely on the differential-mode attenuation which occurs in depressed-cladding, stress-birefringent fibres when operated at low V-values ( $V \sim 1.8$ ). Figure 1 shows the spectral differential attenuation for the two orthogonally-polarised modes in a conventional Bow-Tie fibre and a polarising Bow-Tie fibre having the same beat length. It is clear that the polarising fibre has sharper microbending edges and a wider polarising bandwidth. To obtain reliable measurements, care must be taken to reduce the effects of stray light and polarisation dependence within the monochromator.

The performance of a polariser can only be fully specified by including cross-talk terms in the form of an intensity transfer matrix,  $I$ , between the input and output polarised modes<sup>9</sup>. This matrix has been measured for a coil polariser with broadband light from a laser diode, and the results are as follows:

$$I = \begin{pmatrix} T_{XX} & T_{XY} \\ T_{YX} & T_{YY} \end{pmatrix} = T_{XX} \cdot \begin{pmatrix} 1 & R_2 \\ R_1 & R_2 R_3 \end{pmatrix} = \begin{pmatrix} -2 & -44 \\ -44 & -64 \end{pmatrix} \text{ dB}$$



where  $T_{xx}$ ,  $T_{yy}$  are the transmission ratios of the x and y polarised modes and  $T_{xy}$ ,  $T_{yx}$  are the cross-coupled power between the modes. First  $T_{xx} = -2$  dB is measured using a cut-back technique. X-polarised light is then launched and the output extinction ratio  $R_1 = T_{yx}/T_{xx} = -42$  dB measured with a prism polariser. Similarly, the output extinction ratio  $R_2 = T_{yy}/T_{xy}$  transmission ratio  $R_3 = (T_{xy} + T_{yy})/(T_{xx} + T_{yx}) = -42$  dB is measured using the prism polariser at the input.

The measurement of  $T_{yx}$  in the above may have been limited by the minor-field components<sup>5</sup>. This is not a limitation for the other terms because the source has the wrong spatial symmetry to launch a mode via its minor-field components. A similar principle can be used to advantage in mode extinction-ratio measurements, since a conventional monomode fibre will spatially filter (to 50 - 60 dB) the minor-field components which pass through a prism analyser. Following the analyser with a short length of monomode fibre reduces the minor field components to -80 to -100dB. Thus the measurement is now limited by the prism polariser (typically 50-60dB), not the minor field components.

**Circularly Birefringent Fibres**<sup>10</sup> (Fig.2) are fabricated by rapidly spinning a preform containing an offset core. A nondestructive method to measure the polarisation beat length  $L_p$  of such a helical-core fibre is to launch linearly-polarised light and to cross an analyser with respect to the emerging linear polarisation. The birefringence of the fibre is then perturbed by moving a pressure-point along its length and counting the nulls in the cross-coupled power. These occur when the polarisation vector is parallel or perpendicular to the direction of the force. Thus if N nulls are counted in length L, then  $L_p = 2L/N$ . A similar method has been used to measure  $L_p$  in a linearly-birefringent fibre<sup>11</sup>.

A novel feature of the helical-core fibre, is that the fibre is effectively monomode at high V-values. This is because the higher-order modes cannot survive the fibre curvature. A simple demonstration of the effect can be seen in a fibre where the spin pitch has been gradually reduced along its length. When light is launched into the fibre, bright bands appear along its length showing where successively lower-order modes are reaching their effective cut-offs.

**Metal/Glass Composite Structures** are formed by introducing metal into



longitudinal holes close to the core of a silica optical fibre (Table 1). The fibres make ideal low-loss polarisers utilising the absorption of one of the polarisation states in the metal layer<sup>12</sup>. The measurement requirements are similar to those for coiled fibre polarisers, but with reduced errors from minor-field components. However, owing to their very high extinction ratio (>52dB), the optical quality of the crystal analyser and dynamic range of the spectral loss measurement system become the limiting factors. Further improvements in measurement dynamic range may be achieved using a gyroscope configuration<sup>13</sup>.

By incorporating two metal electrodes on either side of the fibre core a fibre modulator can be constructed based on the Kerr effect<sup>14</sup>. Here care must be taken in separating the phase modulation produced by the Kerr effect from that caused by electrostriction.

**Rare-Earth Doped-Fibres** containing small (<0.25%) quantities of rare-earth impurity ions (e.g.  $\text{Nd}^{3+}$ ) in the fibre core<sup>15</sup> are of great interest as fibre lasers and amplifiers<sup>16</sup>. To this end, a knowledge of their absorption and fluorescence characteristics is required. Measurement of the absorption spectra of these fibres poses a number of problems owing to the difficulty of measuring losses which vary by several orders of magnitude across the spectrum (Fig.3). However, a multiple cut-back technique in combination with attenuation equipment optimised for dynamic range (>48dB in single-mode fibres with 2nm spectral resolution c.f. 35dB in most systems) may be used to overcome these difficulties. Various fibre lengths must be measured, depending upon the regions of the spectrum under test and the results may then be re-scaled and combined to give absorption spectra with extremely high dynamic ranges. Care must also be taken to avoid fluorescence effects.

The fluorescence spectra of the fibres may itself be measured using similar equipment, but with the fluorescence excited by pumping the fibre with a laser matched to one of the impurity absorption bands. Examples of fluorescence spectra for a fibre containing 450ppm  $\text{Tb}^{3+}$ , 30ppm  $\text{Nd}^{3+}$  and 10ppm  $\text{Er}^{3+}$  ions are shown in Fig.4.

Fibre lasers present a number of measurement problems in their own right. Apart from threshold, gain and output power, the spectral output characteristics are of particular interest for potential applications such as a broad-band source for the fibre gyro, or as a narrowband optical communications source. Measurements are complicated by the fact that the

axial mode spacing may be only a few MHz, owing to the length of the laser cavity (up to 300m). Results on  $\text{Nd}^{3+}$  (0.9 and 1.08  $\mu\text{m}$ ),  $\text{Pr}^{3+}$  (1.07  $\mu\text{m}$ ) and  $\text{Er}^{3+}$  (1.55  $\mu\text{m}$ ) will be presented.

**Acknowledgements:** The authors would like to thank past and present members of the Optical Fibre Group in the University of Southampton who have made and are continuing to make significant contributions in this field. Particular thanks are due to L.S.Li. A Readership (DNP) and a Fellowship (SBP) were provided by Pirelli General plc. Some of this work was supported under the DTI/JOERS programme.

#### References:

1. D.N.Payne, Proc. OFS, pp.353-360, Stuttgart, 1984.
2. R.H.Stolen et al., Appl. Phys. Lett., 33, pp.699-701, 1978.
3. R.D.Birch et al., Electron. Lett., 18, pp.1036-1038, 1982.
4. S.C.Rashleigh, J.Lightwave Technol., LT-1, pp.312-331, 1983.
5. M.P.Varnham et al., Electron. Lett., 20, pp.55-56, 1984.
6. F.Payne et al., Proc. ECOC, Barcelona 1986.
7. J.R.Simpson et al., Proc. OFC, p.32, New Orleans, 1983.
8. M.P.Varnham et al., Electron. Lett., 19, pp.246-247, 1983.
9. M.P.Varnham et al., Opt.Lett., 9, pp.306-308, 1984.
10. M.P.Varnham et al., Proc. ECOC, pp.135-138, Venice, 1985.
11. N.Chinone and R.Ulrich, Opt. Lett., CITS, pp.16-18, 1981
12. L.Li et al., Proc. ECOC, Barcelona, 1986.
13. R.A.Bergh et al., Opt.Lett., 5, pp.479-481, 1980.
14. L.Li et al., Electron. Lett. to be published
15. S.B.Pcole et al., J. Light. Tech., LT-4, July 1986.
16. L.Reekie et al., ibid. July 1986.

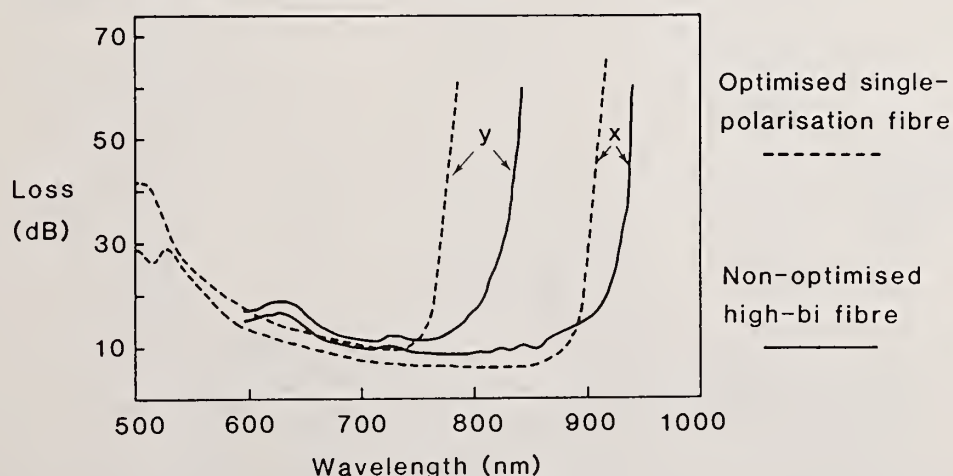


Fig.1. Spectral Attenuation of Bow-Tie fibres showing differential loss between X- and Y-polarised modes. Note wider polarising window for fibre with optimised design.

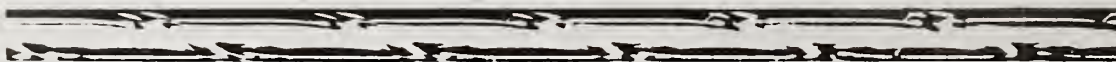


Fig.2. Transverse view of helical-core circularly-birefringent fibre.

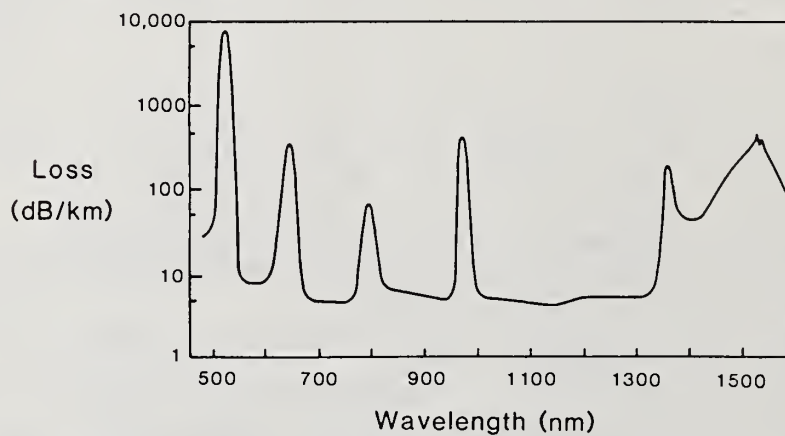


Fig.3. Spectral attenuation of a single-mode fibre doped with 10ppm  $\text{Er}^{3+}$ . Note very large measurement dynamic range required.

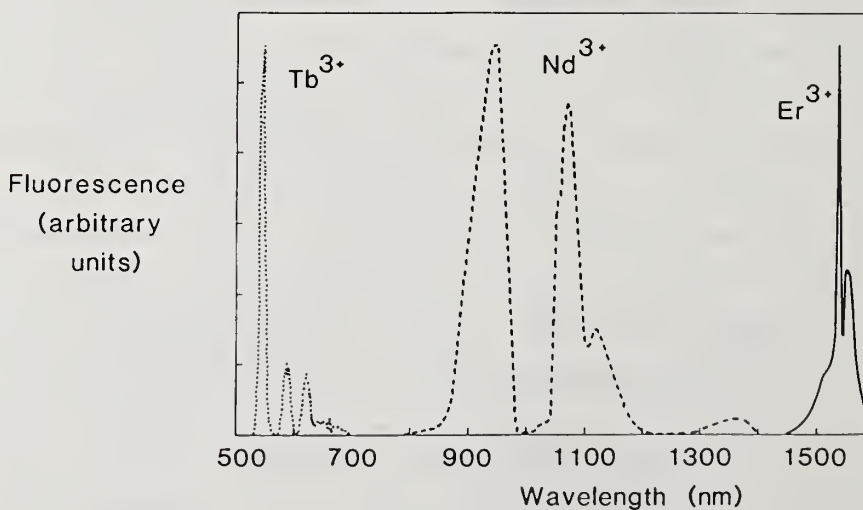


Fig.4. Fluorescence spectra of fibres containing  $\text{Tb}^{3+}$ ,  $\text{Nd}^{3+}$  and  $\text{Er}^{3+}$  ions.









FIBRE TYPE	APPLICATIONS	MEASUREMENTS REQUIRED	POSSIBLE MEASUREMENT PROBLEMS
Dispersion-tailored	Telecommunications Non-linear effects	Dispersion, $\lambda_0$	Wide Spectral range for measurement Appropriate Fitting routines Dynamic range
Ultra-low Birefringence	Sensors Isolators Non-linear effects	Birefringence	External Effects - e.g. Temp., Banding, Stress
Highly-Birefringent e.g. Bow Tie 	Sensors (e.g. Gyros) Interferometers Coherent Communications	Birefringence Beat Length Polarisation mode-dispersion Polarisation Holding Temperature Variation of Parameters	Minor Field Component h - parameter Vs Birefringence
Single Polarisation 	Fibre Polarisers	Extinction Ratio including Spectral Dependence Matrix Measurements Temperature Variation of Parameters	Minor-Field Component Monochromator Performance
Circular Birefringent 	Current sensors Coherent communications	Mode Cut-off Birefringence Temperature Variation	Mode Coupling Circular Birefringence Vs Rotating Linear Birefringence.
Metal/glass fibre polarisers 	Fibre Polarisers	Extinction Ratio including Spectral Dependence	Monochromator Performance, Minor Field Components
Metal/glass fibre modulators 	Electro-Optic Modulators	Modulation Transfer Function	Separation of Kerr and Electro-strictive effects
Rare-Earth Doped 	Fibre Lasers Fibre Amplifiers Sensors Non-linear Optics	Absorption Spectra Fluorescence Spectra and Temporal Characteristics Verdet Constant Non-linear Coefficients Saturation/Bistability Effects Temperature dependence of above	Measurement system performance Saturation/Multiphoton Absorption/ Excited State Absorptions Low fluorescence intensities

Table 1. Measurement requirements for specialty fibres.



Measurement Requirements for  
Waveguide Electro-Optic Devices

R. C. Alferness

AT&T Bell Laboratories

Holmdel, New Jersey 07733

Abstract

Electro-optic waveguide devices, including modulators, switches and tunable filters provide important control functions for future lightwave networks. The technology as well as the application of these devices to high performance research systems has made rapid progress in the last several years. Indeed, waveguide modulators in limited quantities are now available commercially. In this talk we will discuss the optical and electro-optic measurements required to support this rapidly growing and potentially broadly applicable technology.

Introduction

Waveguide electro-optic devices, including switches, modulators and electrically tunable wavelength filters have been the subject of research for more than fifteen years.<sup>1</sup> Significant advances toward making these devices practical components to provide essential control functions for lightwave systems and signal processing have been achieved in the last several years. This progress, which includes the demonstration of low insertion-loss, fiber pigtailed high-speed modulators and complex switch arrays, has been stimulated by the rapid growth in single-mode lightwave



systems.<sup>2</sup> The current interest in extending single-mode fiber into the loop is particularly important. Such applications require low cost components which is potentially achievable with mass produced electro-optic waveguide devices using photolithographic techniques.

Several technologies for electro-optic waveguide devices are currently being researched. They are the epitaxially grown waveguides based upon the semiconductor materials GaAs and InP in which complete monolithic opto-electronic integration is possible and the more developed titanium diffused lithium niobate ( $\text{Ti:LiNbO}_3$ ) waveguide technology. Indeed, commercial  $\text{Ti:LiNbO}_3$  modulators for research applications have been announced by several companies.<sup>3</sup> Measurements -both optical and electro-optical - are required to evaluate and support the manufacture of this new technology. In this talk we will review the important device parameters and measurement requirements. For clarity we consider the titanium diffused lithium niobate technology, but the measurement concepts apply to the semiconductor based technologies as well.

### Fabrication

The fabrication steps to fabricate  $\text{Ti:LiNbO}_3$  waveguides are shown in Fig. 1. Briefly, the photolithographically defined titanium device pattern of thickness  $\tau$  and width  $W$  is deposited, either by electron beam, RF sputtering or a resistively heated evaporator, on a clean, polished crystal. The crystal is then placed in a diffusion furnace and heated at a temperature,  $T$ , for  $t$  hours. After diffusion, an intermediate insulating layer,

typically  $\text{SiO}_2$ , is deposited over the crystal. Control electrodes - typically aluminum or, for high-speed devices, gold-are then deposited over the waveguides. Finally, fiber pigtails are aligned to the waveguides and attached using UV curable epoxy. Typical parameter values are:  $W = 6 - 10\mu\text{m}$ ,  $\tau = 500 - 1000\text{\AA}$ ,  $T = 1000^\circ\text{C} - 1050^\circ\text{C}$  and  $t = 4 - 10$  hours. The metal diffuses in as an oxide with an error function profile where the characteristic depth depends upon the diffusion temperature and time. The waveguide substrate index difference,  $\Delta n$ , is proportional to the titanium concentration with a peak value that depends upon the titanium thickness, and the diffusion time and temperature. The titanium density is also important and may depend upon the deposition technique.

The important waveguide parameters are the optical mode shape and size, which is important for fiber-waveguide coupling and switch voltage, and the propagation loss. For some devices the effective index may also be of interest.

### Electro-Optic Devices

A large family of electro-optically controlled waveguide devices has been demonstrated. Examples include the switch/modulators, frequency shifter, tunable filter, polarization filter or controller. Obviously special measurements are required depending upon device function. However, the most important devices currently are the Y - branch interferometric modulator and the directional coupler switch/modulator, both shown schematically in Fig. 2. The transmitted or cross-over efficiency in the two cases, respectively, varies in response to

applied voltage through the electro-optic effect as shown also in Fig. 2. The required switch voltage, an important device parameter, depends upon the material electro-optic coefficient, wavelength, electrode length, electrode gap and the overlap,  $\Gamma$ , between the applied electric field and optical mode. All these parameters are well known or photolithographically defined except,  $\Gamma$ , which depends upon the diffusion process and electrode alignment. However, for good electrode alignment,  $\Gamma$ , can be inferred from the optical mode profile. A typical voltage  $\times$  length product figure of merit for  $\text{Ti:LiNbO}_3$  switch/modulator is 6 volt  $\cdot$  cm for  $\lambda = 1.3 \text{ } \mu\text{m}$ .

These devices can be operated at very high speeds by using a traveling-wave electrode. Therefore, the electrical frequency response must also be measured. For  $\text{Ti:LiNbO}_3$  traveling-wave switch/modulator the figure-of-merit for the 3dB bandwidth  $\Delta f$  is a bandwidth  $\times$  length product of  $\sim 10 \text{ GHz} \cdot \text{cm}$ . Broad bandwidth devices are particularly attractive for high bandwidth lightwave systems. A schematic diagram of the measurement system for high-speed measurements in both the time and frequency domain is shown in Fig. 3.

### Measurements

A somewhat simplified measurement pyramid that summarizes the important parameters to be measured from substrate material, to fabrication, through the chip stage to the final packaged device. A discussion of current research measurement techniques as well as the challenges for future manufacture-compatible methods will be discussed in the talk.<sup>4-7</sup>



## References

1. For an overview of guided-wave technology, see, for example, R. C. Alferness, "Guided-Wave Devices for Optical Communications", IEEE J. of Quantum Electron., QE-17, p. 946 1981; or R. C. Alferness, "Optical Guided-Wave Devices", Science, to be published.
2. For applications in lightwave systems see, for example, S. K. Korotky, et al., "4 Gb/s Transmission Experiment over 117 Km of Optical Fiber Using a Ti:LiNbO<sub>3</sub> External Modulator", IEEE J. Lightwave Tech., LT-3, pp. 1027-1031, 1985; or L. McCaughan and G. Bogert, "4x4 Ti:LiNbO<sub>3</sub> Integrated-Optical Crossbar Switch Array, Appl. Phys. Letts., 47, pp. 348-350, 1985.
3. See, for example, "Lithium Niobate Devices Finally Make It to Market", W. R. Iversen, Electronics, J. p. 20, January 13, 1986.
4. Substrate Index Measurement: G. E. Peterson, S. R. Lunt, R. J. Holmes, Y. S. Kim, "Refractive Index Measurements of Lithium Niobate Integrated Optical Substrates", Proceedings of SPIE, vol. 578, p. 31, 1985.
5. Optical Mode Profile: C. Y. Chen and S. Wang, "Near-field and Beam-Waist Position of Semiconductor Laser", Applied Physics Letters, 37, p. 257, 1980.
6. Fiber-Coupled Insertion Loss: R. C. Alferness, V. Ramaswamy, S. K. Korotky, M. D. Divino and L. L. Buhl, "Efficient Single-Mode Fiber to Titanium Diffused Lithium Niobate Waveguide Coupling for  $\lambda = 1.32\mu\text{m}$ ", IEEE J. Quant. Electron., QE-18, p. 1807, 1982.
7. High-Frequency Response: S. K. Korotky, G. Eisenstein, R. C. Alferness, J. J. Veselka, L. L. Buhl, G. T. Harvey, and P. H. Read, "Fully Connectorized High-Speed Ti:LiNbO<sub>3</sub> Switch/Modulator", IEEE J. of Lightwave Tech., LT-3, p. 1, 1985.

# Ti-DIFFUSED LITHIUM NIOBATE WAVEGUIDES

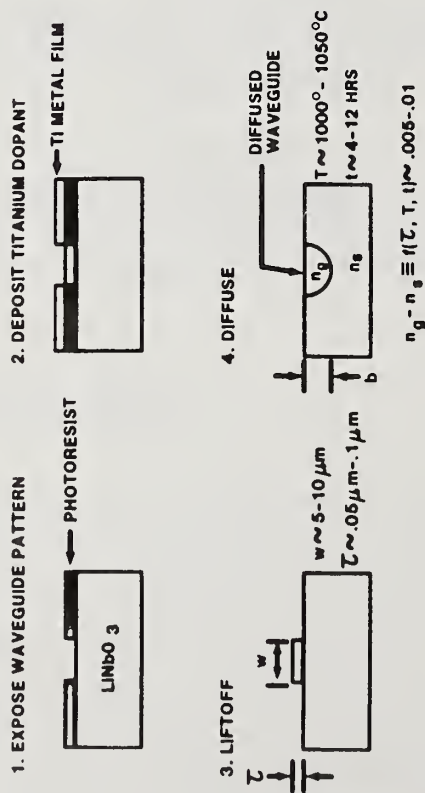


FIGURE 1

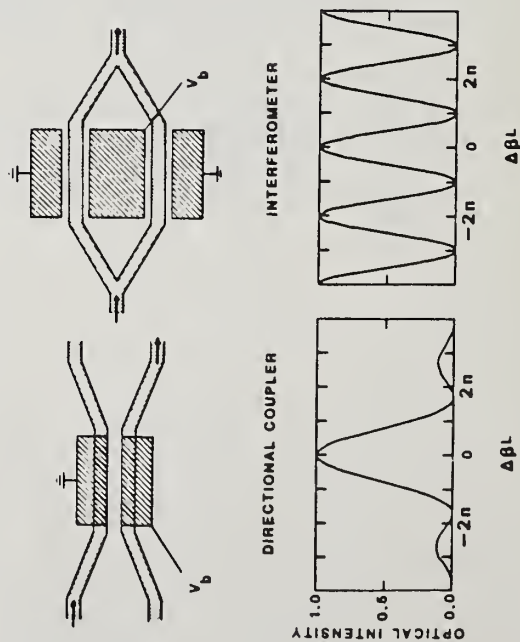


FIGURE 2

# HIGH-SPEED DEVICE EVALUATION

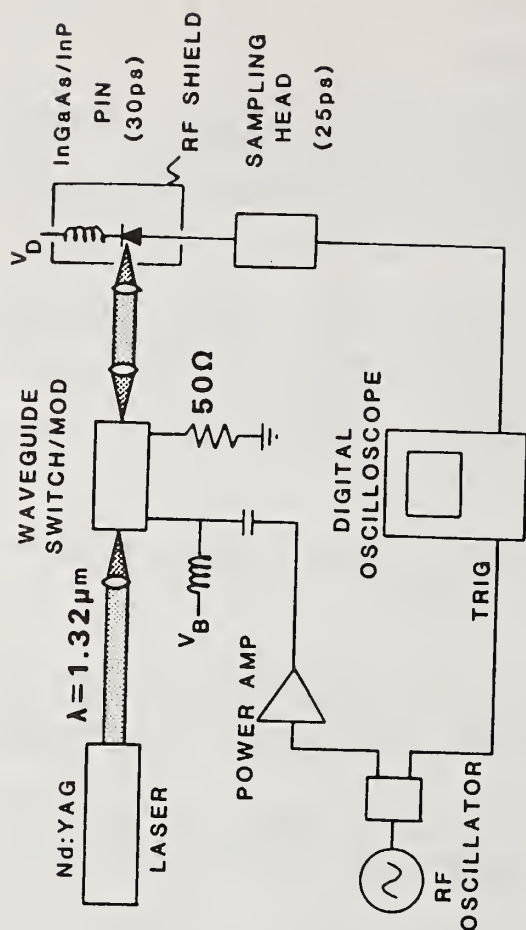


FIGURE 3

# ELECTRO-OPTIC WAVEGUIDE-DEVICES: MEASUREMENT PYRAMID

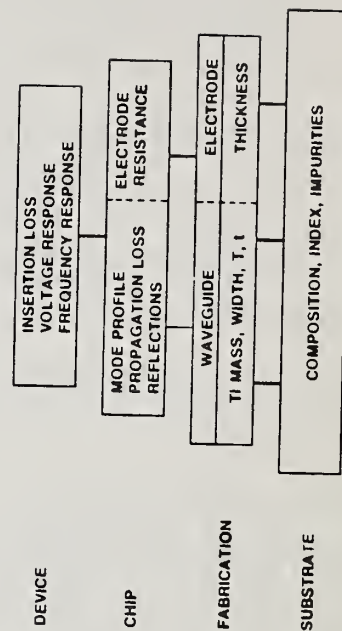


FIGURE 4

Practical Upper Limits to Cutoff Wavelength  
for Different Single Mode Fiber Designs

L. Wei\*, C. Saravanos and R.S. Lowe  
Northern Telecom Canada Limited  
Optical Systems Division  
8 Colonnade Road  
Nepean, Ontario, CANADA K2E 7M6

Recently, a number of studies [1-3] have been conducted in an effort to establish upper limits for the  $LP_{11}$  cutoff wavelength of single-mode fibers designed for 1300nm operation. A value of 1350nm has been quoted for a depressed cladding fiber design based on a modal noise analysis [1]. To date, little work has been done to determine how this upper cutoff value may be affected by fiber design. In this paper, we utilize the measured length dependence of cutoff wavelength together with applicable modal noise constraints to determine the upper limits of cutoff wavelength for both matched and depressed cladding fibers. For these calculations, we have not used the wavelength dependent loss of the  $LP_{11}$  mode [3] due to the sensitivity of this measurement to fiber layout condition. However, by relating the  $LP_{11}$  mode loss to the length dependence of cutoff wavelength, this experimental problem has been avoided.

The attenuation of the  $LP_{11}$  mode can be approximated by the following equation [2][3]

$$\alpha_{11} L = 19.4 X \frac{\lambda - \lambda_c(L)}{10} \quad (1)$$

where  $\lambda_c(L)$  is the cutoff wavelength measured on a length of fiber  $L$  and  $X$  is a constant related to the fiber index profile. Comparing Eq. (1) with the widely accepted empirical formula for the length dependence of cutoff wavelength [4] viz:

$$\lambda_c(L_2) = \lambda_c(L_1) + C \log \frac{L_2}{L_1} \quad (2)$$

where  $C$  is a constant we can relate  $C$  and  $X$  if the cutoff condition of 19.4 dB is assumed:

$$C = -10/\log X \quad (3)$$

\* On leave from Research Inst. of Telecomm. Transmission, PTT, Beijing, P.R. China.



Therefore, by evaluating C the wavelength dependent attenuation of the  $LP_{11}$  mode can be determined.

Measurements of cutoff wavelength length dependence for different fiber designs have been carried out employing the transmitted power method. For matched and depressed cladding fibers, (referred to as fiber types I and II in Table 1) the parameters C were -22 and -55nm/decade with corresponding X values of 2.82 and 1.51, respectively. The latter compare with a value of X = 1.43 as calculated from Anderson's C value of -65nm/decade [4] for a fiber with a more heavily depressed cladding (fiber type III in Table 1). A direct measurement of the wavelength dependent attenuation of the  $LP_{11}$  mode was performed by a technique described elsewhere [3][5] and, as shown in Figure 1, good agreement with the calculated  $LP_{11}$  mode loss is obtained.

The upper limit of cutoff wavelength is conventionally fixed at the minimum operating system laser wavelength in order to eliminate propagation of the  $LP_{11}$  mode in the fiber. In fact, from the system point of view, there is no rationale for this restriction because, providing the modal noise penalty is kept small enough, operating in the two mode region does not impose a practical limit to system performance. If Eqs. (1) and (3) are combined, with  $L_1$  equal to the standard measurement length for cutoff wavelength and  $L_2 = L$ , the following relation is obtained:

$$\lambda_c(L_1) = \lambda_c(L) + C \log \frac{\alpha_{11} L_1}{19.4} \quad (4)$$

If the modal noise penalty [2] is chosen assuming reasonable worst case system parameters for a particular bit rate, the loss parameter  $\alpha_{11}$  can be determined for the shortest unspliced fiber length L (e.g. 10 meters). Using this value of  $\alpha_{11}$ , the cutoff wavelength  $\lambda_c(L_1)$  at the factory test length  $L_1$  can be calculated from Eq. 4 if  $\lambda_c(L)$  is set equal to the minimum operating laser wavelength,  $\lambda_s$ .  $\lambda_c(L_1)$  becomes the maximum allowable factory cutoff wavelength. The variation of maximum cutoff wavelength with modal noise penalty is shown in Fig. 2. For  $\Delta P = 0.5$  dB,

$\lambda_c$  (2m) for fiber types I, II and III are 1305nm, 1335nm and 1345nm, respectively. Typical results at different mode partition noise values (K), corresponding to different bit rates, are given in Table 1. Experimental confirmations of these results utilizing a 2 Gbits/s system will be presented at the conference.

In conclusion, it has been found that by using the measured length dependence of cutoff wavelength together with appropriate modal noise considerations, upper limits to the cutoff wavelength of single-mode fibers as measured on a 2 meter sample are established. It has been shown that this limit depends strongly on the particular fiber design. For matched cladding fibers, the maximum cutoff wavelength is shown to be 30 to 40nm lower than for depressed cladding fiber in order to meet the same modal noise penalty.

#### References

- [1] N.K. Cheung and P. Kaiser, ECOC '84, P. 242, 1984.
- [2] D.G. Duff, et al., OFC '85, TU01, P. 52, 1985.
- [3] F.M. Sears, et al., OFC '86, TUL19, P. 66, 1986.
- [4] W.T. Anderson and T.A. Lenahan, IEEE, Journal of Lightwave Technology, Vol. LT-2, No. 3, P. 238, 1984.
- [5] K.A.H. Van Leeuwen and H.T. Nijhuis, Optics Letts., Vol. 9, No. 6, 1984.

Table 1: Maximum cutoff wavelengths for different mode partition noise values (K)

K		0.4	0.6	0.8	1.0
Fiber Type					
I	$\Delta^+ = 0.25\%$ $\Delta^- = 0\%$	1312	1307	1305	1302
II	$\Delta^+ = 0.2\%$ $\Delta^- = 0.09\%$	1355	1342	1335	1332
III	$\Delta^+ = 0.2\%$ $\Delta^- = 0.15\%$	1365	1350	1345	1340

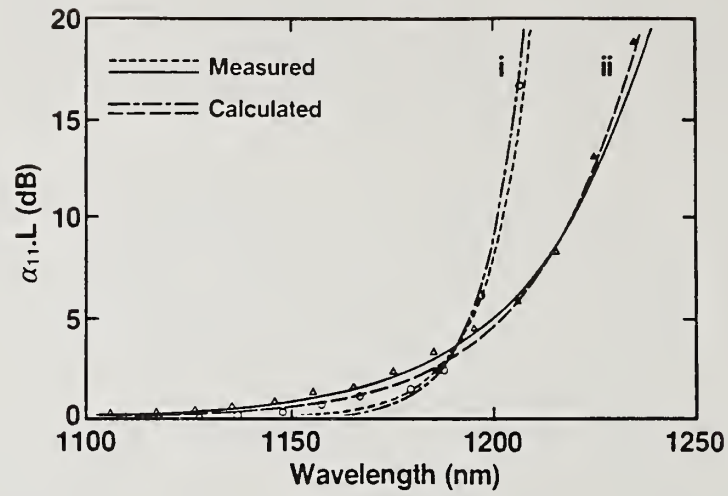


Fig. 1: Comparison of measured and calculated  $LP_{11}$  mode attenuation. Calculated values are derived from the length dependence of cutoff wavelength.

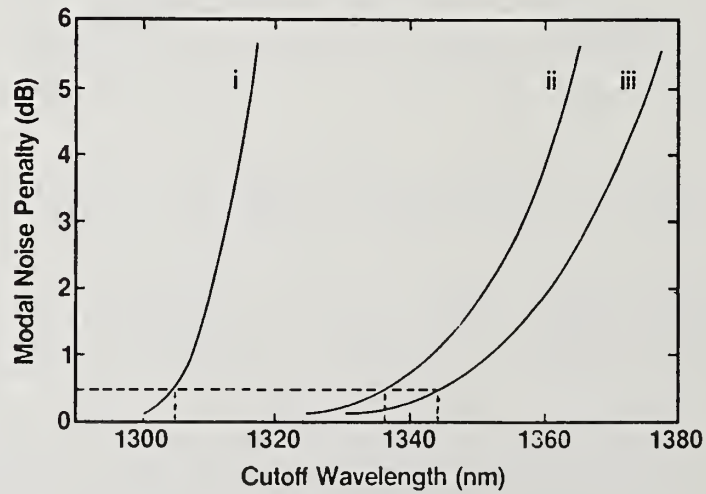


Fig. 2: Variation of upper cutoff wavelength limit with modal noise penalty for 3 fiber designs. System parameters used are  $K = 0.8$ ,  $N = 1$  dB,  $L = 10$  m, and  $\lambda_s = 1285$  nm.



## New Measurement Technique for Measurement of Microbend Losses in Single Mode Fibers

A. O. Garg and C. K. Eoll  
Siecor Corporation

### Introduction

Microbending is very important to the performance of various fiber optic devices. Until now, however, the authors have not found a repeatable method for measuring microbend losses in single mode optical fibers. Various techniques have been suggested and are in use for multimode fibers. Though these techniques give usable results for multimode fibers, they are not particularly reliable in the single mode case. One technique is the sand paper test. This method has the disadvantage that measurements with two different sandpapers of the same nominal grit size can give different results. Similarly the grit is not necessarily uniform over the whole sandpaper, and this introduces further randomness in the measurement. We have found a new measurement technique which avoids much of this uncertainty, and which gives results which are more repeatable. One can use theory to predict results of this new measurement technique. We use ASTM standard sieves of various sizes to give different types and amounts of microbending. This report describes the methodology and also presents some of the results obtained using the new technique.

### Methodology & Theory

One form of microbending in single mode fibers is caused by deformations of a fiber in the range from 0.1 to 0.3 mm in length. Microbend losses in single mode fibers due to this kind of perturbation show up as an increase in attenuation across a wide band of wavelengths; the extra attenuation at 1300 nm, for example, can be comparable to that at 1550 nm. Increasing the length of the

perturbations beyond 1mm results in the familiar microbending edge similar to a bending edge, where losses are very wavelength dependent i.e. where losses increase dramatically as the wavelength increases. ASTM standard sieves can be obtained with wire diameters of 100um and above with respective spacings of 100um and above. We used three different sieves with the designation of #100, #70 and #50. The wire dimensions and the spacing between the wires are presented in Table 1. The set-up is shown in Figure 1. Two slots were made in the bottom rim of each of sieve such that a fiber may be laid parallel to one of the sets of wires in the inverted sieve. This set-up is placed between the launch and receiving optics of a spectral attenuation measurement system. Care is taken to confirm the wire mesh is well supported from underneath so that the mesh does not give way or flex under weight of the loads. The fiber to be measured is installed in the slots in the sieve and a reference measurement is made. The fiber is then loaded with standard weights of 1 kg each. These weights are each a smooth 1" x 2" block of steel with a protective coating on one side (The protective coating prevents the fiber from being cut by the corners of the steel plate). Additional spectral scans are made and compared to the reference scan to give microbend losses due to the respective loads.

## Results

Single mode optical fibers with varying deltas and cutoff wavelengths were evaluated for microbending using this technique. The increase in attenuation depends on the load on the fiber, type of mesh and sensitivity of the fibers to microbending losses (i.e. how low the delta and cutoff wavelength were).

Mesh #70 seems to give the most discriminating results with the single mode fibers tested; bends are not too sharp and attenuations are not overly high. The results presented in this report show effects of Mesh #70 with loads upto 4 kg varying in steps of 1 kg load.

Mesh #100 on single mode fibers did not yield any increase in attenuation. The mesh wires are extremely small and close together. Apparently the effect of the force exerted by the wires is absorbed by the coating. The effect is as if two smooth plates were squeezing the fiber. Interestingly this does not change the attenuation of the fiber. Further tests are planned to evaluate the effect due to Mesh #100 and other meshes on bare/ uncoated fibers.

#### Further Experiments

Microbend analysis using this setup will also be performed on multimode fibers. These results will be presented at the conference. A correlation between the current results and microbend analyses in earlier technical papers will also be attempted.

#### References

- 1) Furuya and Suematsu (Applied Optics, Vol. 19, p. 1493, 1980)
- 2) J.Auge, P.Dupont, L.Jeunhomme (Bending and Microbending Loss Sensitivity of Step Index Single Mode Fibers, 1984 Symposium on Optical Fiber Measurements, Boulder, Colorado).
- 3) Proposed EIA Test procedure FOTP-68 (Microbend Test Procedure).

TABLE 1

Mesh Wire Dimensions and Spacing

Mesh #	Wire diameter	Spacing
1) #100	110 um	150 um
2) #70	152 um	212 um
3) #50	215 um	300 um



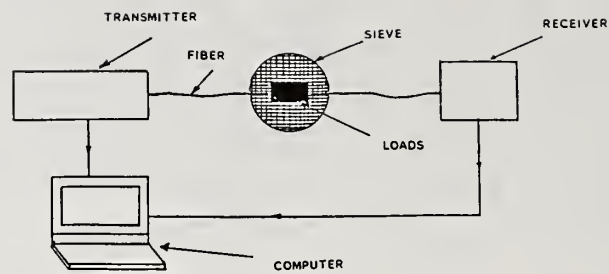


Figure. 1

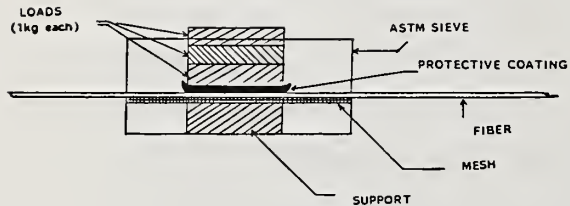


Figure. 2

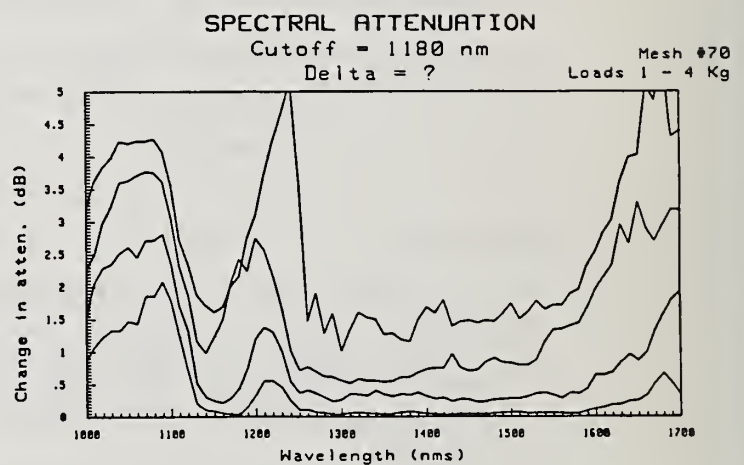


Figure. 3

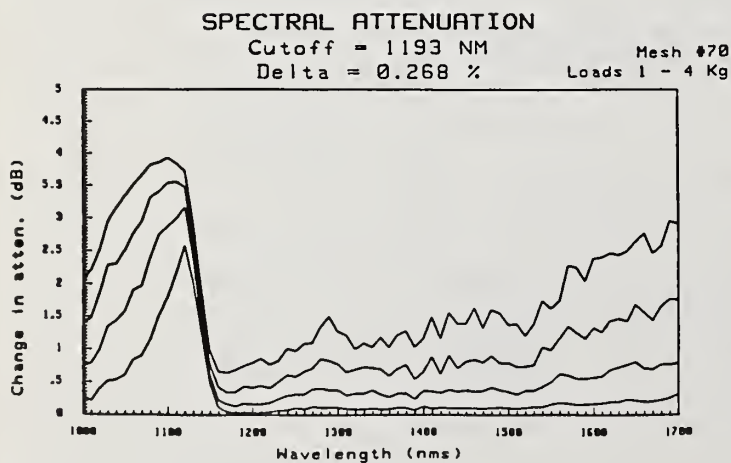


Figure. 4

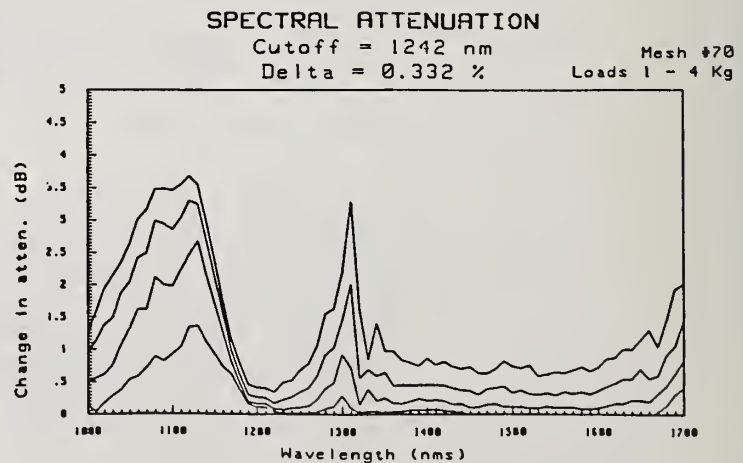


Figure. 5

## PREDICTING MICROBENDING LOSSES IN SINGLE-MODE FIBERS

Neil Kamikawa

Naval Ocean Systems Center, P.O. Box 997, Kailua, HI 96734-0997

Ching-Ten Chang

San Diego State University and Naval Ocean Systems Center,  
San Diego, CA

**INTRODUCTION.** Conventional techniques for evaluating microbending resistance in single-mode fibers using basketweave [1], pin [2], drum [3], and sandpaper tests depend on excess loss measurements. These tests can evaluate one fiber against another, but the stresses induced in the fiber may not be representative of cable structures or other environments. An alternative evaluation method involves predicting excess losses using a model based on Petermann's microbending theory [4], which depends on mode-field radius, and geometry of the microbends. This method is demonstrated by predicting the excess losses in two precision-wound spools of fiber.

**MODEL.** The model shown below for periodic, Gaussian-shaped microbends that are separated by a distance  $L$  was derived from Petermann's theory. It relates excess loss in dB/km to fiber specifications and microbend geometry.  $Y_0$  is the maximum amplitude and  $A$  is average half-width at the  $1/e$  amplitude, as shown in Figure 1. Variations in the half-width values can be described by a standard deviation,  $\sigma$ . The electric field distribution of the fundamental mode is also approximated by a Gaussian function with a radius  $W$ , which is defined at the  $1/e$  value.

$$\alpha = \frac{13.644 Y_0^2}{LW^2} \left[ \frac{A^2 B^3}{(B^2 + \sigma^2)^{5/2}} + \frac{\sigma^2 B}{2(B^2 + \sigma^2)^{3/2}} \right] \exp \left[ \frac{-A^2}{(B^2 + \sigma^2)} \right]$$

where  $B = knW^2/\sqrt{2}$   
 $k = 2\pi/\lambda$   
 $n$  = refractive index of the core

RESULTS. To demonstrate the model excess losses were calculated and measured in two precision-wound spools of fiber described in Table 1. Precision winding of fibers produces crossovers that can be approximated by the Gaussian-shaped microbends. Each layer of the precision-wound spool forms a helix with a lay angle nearly 90 degrees with respect to the axis of the mandrel. The next layer forms a helix in the opposite direction. As a result the fiber crosses over a fiber beneath it twice per turn so that the period of the microbends are equal to half the circumference of the mandrel ( $L = \pi \times 5.72$  cm). The crossovers cause perturbations on the fiber axis and coupling of the fundamental mode to the lossy higher-order mode. This is assumed to be the primary physical mechanism for the microbending loss.

Table 1. Fiber and winding specifications

	Fiber 1	Fiber 2
LP <sub>11</sub> cutoff $\lambda$ ( $\mu\text{m}$ )	1.135	1.209
Mode-field radius ( $\mu\text{m}$ )		
@ $\lambda = 1.3 \mu\text{m}$	4.87	4.73
@ $\lambda = 1.5 \mu\text{m}$	5.65	5.32
@ $\lambda = 1.55 \mu\text{m}$	5.96	5.55
Delta (%)	0.27	0.30
Fiber OD ( $\mu\text{m}$ )	125	127
Coating OD ( $\mu\text{m}$ )	243	241
Length (km)	2.2	2.0
Mandrel diameter (cm)	11.43	11.43
Crossover amplitude ( $\mu\text{m}$ )	35	35
Winding tension (grams)	200	200
Average crossover		
half-width, A (mm)	1.05	1.05
Standard deviation $\sigma$ (mm)	0.201	0.210

The fibers were wound onto 11.43-cm-OD mandrels in 17 layers under 200 grams of tension. Figures 2 and 3 illustrate the measured losses in the fibers before and after winding. Fiber 2



exhibits better microbending resistance at long wavelengths due to tighter mode confinement.

$Y_0$  was calculated to be 35  $\mu\text{m}$  based on the fiber OD, and A was estimated to be 1.05 mm for both fiber spools by visual observation. The standard deviation values,  $\sigma$ , are 201  $\mu\text{m}$  and 210  $\mu\text{m}$  for fibers 1 and 2, respectively. These values were chosen for the best match between calculated and measured excess losses at 1.3, 1.5 and 1.55  $\mu\text{m}$ . Table 2 compares the excess losses calculated using the model and measured excess losses at the three wavelengths. Errors in the calculated values are tentatively attributed to measurement errors in the mode-field radius, and visual observation of A. Winding imperfections also contributed to measurement and prediction errors.

Table 2. Calculated and measured excess losses in dB/km  
(Measurement errors are in parentheses.)

	1.3 $\mu\text{m}$	1.5 $\mu\text{m}$	1.55 $\mu\text{m}$
Fiber	calc/measured	calc/measured	calc/measured
1	.017/.001 ( $\pm$ .013)	.090/.086 ( $\pm$ .015)	.220/.202 ( $\pm$ .023)
2	.031/.008 ( $\pm$ .015)	.067/.044 ( $\pm$ .022)	.110/.110 ( $\pm$ .031)

**CONCLUSION.** Prediction of excess losses as a method to evaluate microbending resistance of single-mode fibers is a viable alternative to the other testing methods. Efforts are underway to improve the predictive capabilities of the model by including mechanical bending properties of the fiber.

#### REFERENCES.

1. A. Tomita, P.F. Glodis, D. Kalish, P. Kaiser, Technical Digest - Symposium on Optical Fiber Measurements, Boulder, CO, p 89-92, 1982.
2. V.A. Bhagavatula, IOOC '81, paper TUK5, San Francisco, CA, 27-29 April 1981.
3. D. Gloge, Bell System Technical Journal, p 245-262, Feb, 1975.
4. K. Petermann, Opt. and Quant. Elect., p 167-175, Sept, 1977.

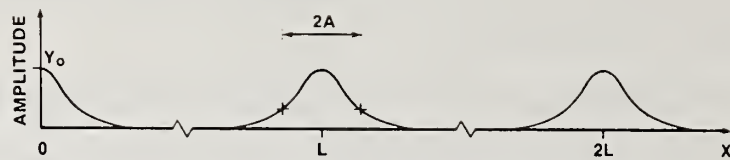


Figure 1. Gaussian-shaped microbends

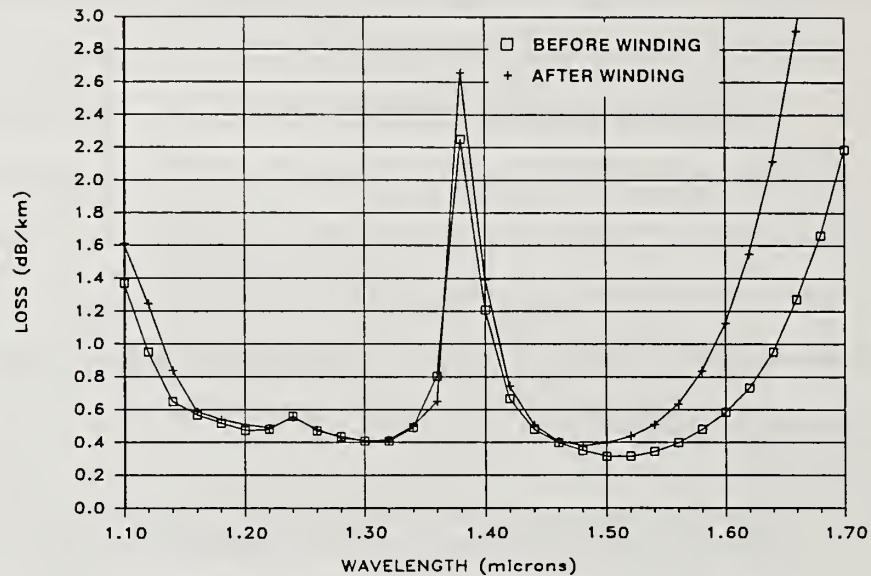


Figure 2. Spectral attenuation for fiber 1

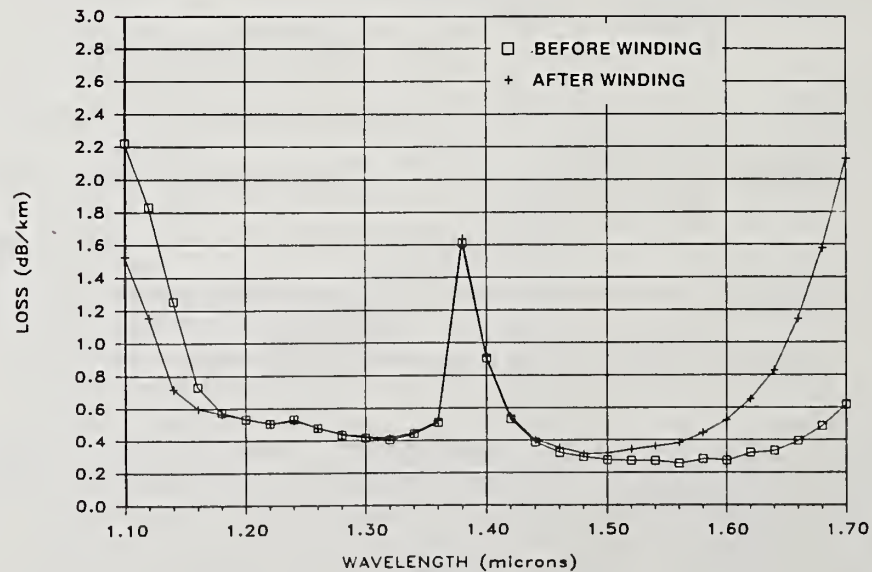


Figure 3. Spectral attenuation for fiber 2

# ON THE NUMERICAL APERTURE OF A SINGLE-MODE FIBER

*D. N. Christodoulides*

*L. A. Reith*

*M. A. Saifi*

Bell Communications Research

Murray Hill, New Jersey 07974

Light-emitting diodes (LEDs) coupled to single-mode fibers (SMFs) may become the first generation lightwave system to be deployed in the local distribution network.<sup>1</sup> The concept of the fiber numerical aperture (NA) which originates from geometrical optics is commonly employed to estimate the coupling efficiency of an LED to a multimode fiber. For a step-index fiber,  $NA = (n_1^2 - n_2^2)^{1/2}$ , where  $n_1$  and  $n_2$  are respectively the refractive indices of the fiber core and cladding. However, the problem of an LED coupled to a SMF falls within the frame of wave optics and therefore the concept of SMF NA must be reconsidered. In this paper the NA of a SMF is revised so as to incorporate the wave nature of the coupling process. This is done by interpreting the results of electromagnetic theory from a geometrical point of view.

We envision the LED light emitting surface as an ensemble of classical radiators, radiating in a mutually incoherent fashion. The power collecting ability of a SMF is then investigated by embedding one of these radiators in an infinite SMF. Let this radiator be a simple current dipole located at a distance  $r$  from the fiber axis as shown in Fig. 1. Under steady-state propagation, the dipole supplies power to the fundamental mode  $LP_{01}$ , in both the forward  $P_{0+}$  and backward direction  $P_{0-}$ . In order to convert the wave picture to a geometrical one, it is assumed that the elementary dipole provides the power  $P_{0\pm}$  to the  $LP_{01}$  mode only through a "cone" of angle  $\hat{q}$  whose axis is parallel to that of the fiber. The electric field within the SMF is described using the Gaussian approximation<sup>2</sup>, i.e.,  $E = \exp(-r^2/2r_0^2)$ , where  $r_0$  is the mode field radius. It can then be shown that<sup>3</sup>



$$\bar{\theta}_t = \frac{\lambda_0}{n_1 \pi r_0} \exp(-r^2/2r_0^2). \quad (1)$$

When the dipole is located outside the fiber, the maximum "acceptance angle" can be obtained from Snell's law, i.e.,  $\bar{\theta}_m = (\lambda_0/\pi r_0) \exp(-r^2/2r_0^2)$ . We identify  $\bar{\theta}_m$  as the numerical aperture  $\tilde{NA}$  of a SMF

$$\tilde{NA} = \frac{\lambda_0}{\pi r_0} \exp\left(-\frac{r^2}{2r_0^2}\right) = \frac{\lambda_0}{\pi r_0} \exp\left[-\frac{(x^2+y^2)}{2r_0^2}\right]. \quad (2)$$

For step-index SMFs, the quantity  $\lambda_0/\pi r_0$  is very close to the geometrical optics NA. Unlike multimode fibers whose NA depends on the index distribution, in the case of a SMF,  $\tilde{NA}$  is only a function of wave parameters such as wavelength  $\lambda_0$  and mode field radius  $r_0$  and also a function of radial position  $r = (x^2+y^2)^{1/2}$ .

Using (2), the coupling efficiency of an LED butt-coupled to a SMF can be obtained from

$$\eta = T \frac{\int_{-\infty}^{\infty} \int_{-\infty}^{\infty} dx dy \int_0^{2\pi} \int_0^{\bar{\theta}_m(x,y)} B(x,y;\phi,\theta) \sin \theta d\theta d\phi}{\int_{-\infty}^{\infty} \int_{-\infty}^{\infty} dx dy \int_0^{2\pi} \int_0^{\pi/2} B(x,y;\phi,\theta) \sin \theta d\theta d\phi} \quad (3)$$

where  $T = 4n/(1+n)^2$  is the Fresnel transmission coefficient and  $B$  is the radiance of the LED.

Butt-coupling efficiencies were measured at  $\lambda_0 = 1.3 \mu\text{m}$  using an edge-emitting LED and a surface emitting LED. The fiber used was a step-index fiber whose mode field radius at  $\lambda_0 = 1.3 \mu\text{m}$  was  $3.5 \mu\text{m}$ .

The measured butt-coupling efficiency for the edge-emitting LED was -19.4 dB, which compared to a calculated value of -18.6 dB using (3). If the center of the edge-emitting

LED is located at  $(\alpha, \beta)$  in the Cartesian system whose origin coincides with the fiber axis, then equation (3) can be used to predict the coupling sensitivity due to misalignment. The  $Y$  axis is perpendicular to the junction plane of the edge-emitter. Figure 2 shows the coupling sensitivity  $S_x$  and  $S_y$  as a function of displacement  $\alpha$  and  $\beta$  respectively. The solid dots represent the experimental results. Note that the  $S_y$  curve is a result of the wave nature of the numerical aperture.

The butt-coupling efficiency for the surface-emitting LED was found to be -35 dB as compared to -34.8 dB evaluated using (3).

## REFERENCES

- [1] J. L. Gimlet, M. Stern, R. S. Vodhanel, N. K. Cheung, G. K. Chang, H. P. Leblanc, P. W. Shumate and A. Suzuki, "Transmission experiments at 560 Mbit/s and 140 Mbit/s using single-mode fiber and 1300 nm, LEDs", *Electron. Lett.*, vol. 21, pp. 1198-1200, 1985.
- [2] D. Marcuse, "Gaussian approximation of the fundamental modes of graded-index fibers", *J. Opt. Soc. Am.*, vol. 68, pp. 103-109, 1978.
- [3] D. N. Christodoulides, L. A. Reith and M. A. Saifi, "Theory of LED coupling to single-mode fibers", to be published.

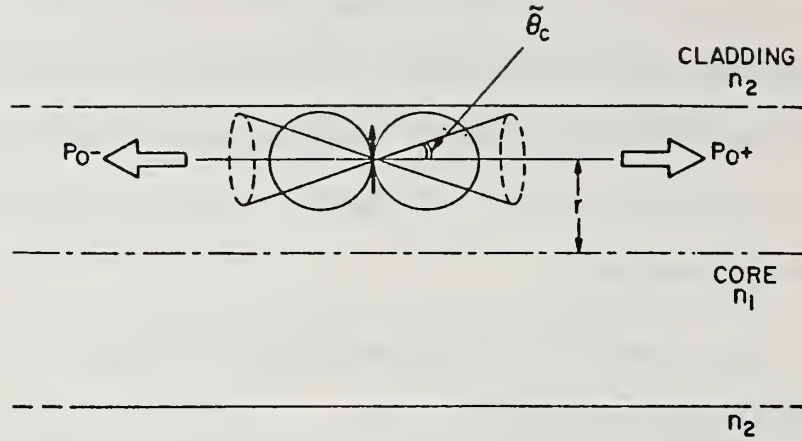


Fig. 1. A current dipole within a single-mode fiber.

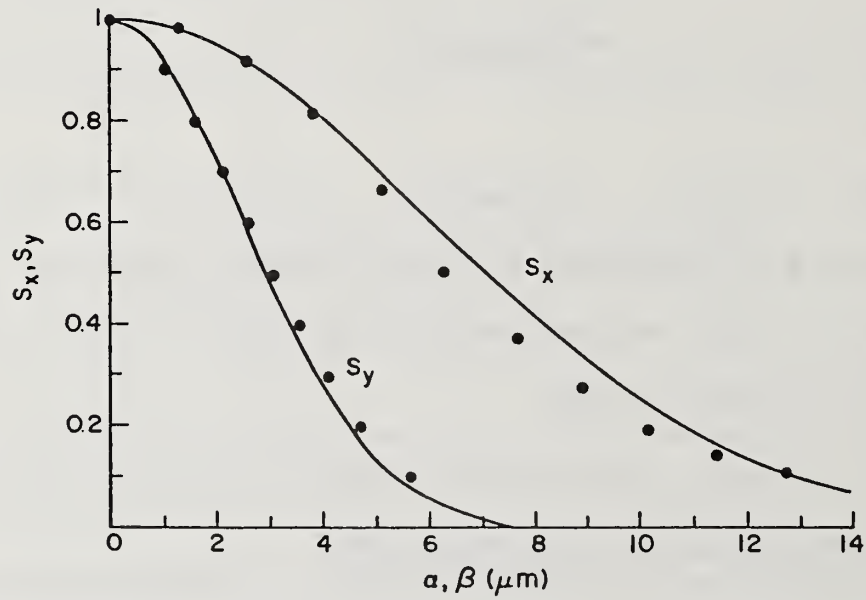


Fig. 2. Coupling sensitivities  $S_x$  and  $S_y$  as a function of displacements  $\alpha$  and  $\beta$  respectively. The solid curves represent their behavior as predicted by eq. (3) and the solid dots the experimental results.



# OPTICAL FIBRE FAR FIELD ESI DETERMINATION USING THE EQUALISATION WAVELENGTH

A C Boucouvalas, S C Robertson and J Walker

GEC Research Limited Hirst Research Centre East Lane Wembley Middlesex HA9 7PP United Kingdom

## ABSTRACT

It is shown that measurement of the equalisation wavelength, ( $\lambda_e$ ) instead of the LP<sub>11</sub> mode cut-off wavelength ( $\lambda_c$ ), can be used to calculate a more reproducible and reliable value for the equivalent step index profile parameter. Unlike  $\lambda_c$ ,  $\lambda_e$  is virtually independent of fibre bending.

## INTRODUCTION

When a single mode optical fibre is operated in the dual mode regime, with an off-axis launch, power is guided in both the LP<sub>01</sub> and LP<sub>11</sub> modes. Provided the group time delay difference, T, between the modes is less than the coherence time of the light  $\tau$ , (where  $\tau < \frac{\lambda^2}{c\delta\lambda}$ ,  $\delta\lambda$  is the line width, c

the speed of light in a vacuum, and  $\lambda$  the wavelength) then modal interference will be observed [1,2].

The equalisation wavelength,  $\lambda_e$ , of the dual mode fibre is the wavelength at which the group velocities of the two interfering modes are the same. When observing the fibre in the near field, it is possible to measure  $\lambda_e$  of the fibre precisely [3], by varying wavelength, and recording the intensity oscillation of the two LP<sub>11</sub> lobes. This effect has already been used [4,5] in fibre optic measurements to relate  $\lambda_c$ , the cutoff wavelength, to  $\lambda_e$ , and further to determine the V-value of fibres. In this work we extend this technique to the determination of reliable ESI fibre parameters using  $\lambda_e$ , as an alternative to the current practice of using  $\lambda_c$  for ESI measurements [6,9].

## FAR FIELD METHOD

We have examined the possibility of using the far field intensity distribution measurement data in conjunction with  $\lambda_e$  as an alternative method to the cutoff wavelength,  $\lambda_c$ , for determination of the fibre ESI parameters.

The method utilises the far field radiation pattern to determine the ESI core radius.

Using:

$$U = \frac{(1+\sqrt{2})V}{1+(4+V^4)^{1/4}},$$

or Newmann's approximation with  $V=V_e\lambda_e/\lambda$ , ( $V_e = 3.04$ ) together with the far field intensity distribution:

$$|\psi|^2 = \left[ \frac{U^2 W^2}{(U^2 - \alpha^2)(W^2 + \alpha^2)} \{ J_0(\alpha) - \alpha J_1(\alpha) \} \frac{J_0(U)}{U J_1(U)} \right]^2$$

the only unknown ESI core radius can be found by a best fit of the above formula to the measured data. Hence the ESI parameters can be calculated.

A typical best fit to the far field data using the above formula is shown in Figure 1. The fibre has matched cladding and a small axial dip. The far

field pattern was measured for a number of wavelengths and the ESIs obtained were shown in Table 1 showing the insensitivity of the ESI measurements to the wavelength used.

We can now write Petermann's spot size [9] for a step index fibre in terms of  $\lambda_e$  as follows:

$$\frac{\omega_p}{a} = 0.634 + 0.30545 \left( \frac{\lambda}{\lambda_e} \right)^{3/2} + 0.003648 \left( \frac{\lambda}{\lambda_e} \right)^6 - 0.0006506 \left( \frac{\lambda}{\lambda_e} \right)^7$$

This allows us to determine the dispersion of the fibre, (knowing  $a$ , and  $\lambda_e$ ). Figure 2 shows the measured and computed dispersion results for this fibre type. The agreement is good considering that the fibre is quasi step index. The zero material dispersion wavelength is predicted to within 5 nm.

### Insensitivity of $\lambda_e$ to bends

It is well known that  $\lambda_c$  is dependent on the state of the fibre, i.e. bending [5], affects the cutoff wavelength significantly. Since bends are normally unavoidable, we have decided to examine the dependence of  $\lambda_e$  to bending. For this, one turn of fibre was wound on cylinders of different diameters.

Light from a Raman laser was launched into the fibre, after it has been filtered by a monochromator, and the emerging light at the output (near field) was displayed on a TV monitor. The oscillation of the LP<sub>11</sub> mode pattern was observed as the wavelength of the monochromator was scanned. The wavelength positions for minima of one of the lobes was noted. Figure 3 shows the results plotted for a variety of cylinder diameters. We can see that as the bend radius decreases, the visibility of the oscillations is gradually lost for long wavelengths. We have found in this case that  $\lambda_e = 1.064 \mu\text{m}$  and this remains constant to within 1 nm for bends down to 3.5 cm diameter. Below this measurement of  $\lambda_e$  is not possible. The results show, that compared to  $\lambda_c$  the measured value of  $\lambda_e$  is quite insensitive to bends.

### Profile dependence of $V_e/V_c$

It was considered necessary to determine how the ratio of  $\lambda_c/\lambda_e$  is dependent on the core refractive index profile. This was determined computationally using graded index core profile ( $\alpha$  value profile). Figure 4 shows the results of the ratio  $V_e/V_c$  versus  $\alpha$ , the profile grading power. It is clear that the ratio is insensitive to the  $\alpha$  value so long as  $\alpha > 5$ . In the case of  $\alpha = 5$ , the change in the ratio from that of  $\alpha = \infty$ , (step index) is 10%. Since the manufactured fibres have  $\alpha$  values  $>> 4$ , (non-dispersion shifted), the change of the ratio improves drastically.

This indicates that the measurement of  $\lambda_e$  is sufficient for the accurate prediction of the theoretical  $\lambda_c$  even for graded index profiles.

### CONCLUSIONS

A technique of determining the ESI parameters based on the measurement of the equalisation wavelength of the LP<sub>11</sub> and LP<sub>01</sub> modes has been developed. The fibre dispersion is shown to be in good agreement with the measured results for quasi step index core fibres. The technique has the advantage that the measurement of  $\lambda_e$  is more accurate than the measurement of  $\lambda_c$  (which can be predicted from  $\lambda_e$  for  $\alpha$  values  $> 4$ ).

This method is therefore more reliable than determining the ESI parameters by measurement of the cutoff wavelength of the LP<sub>11</sub> modes.

## ACKNOWLEDGEMENT

Part of this work was supported by DTI under JOERS.

## REFERENCES

- 1 PLANAS, S.A., BOCHOVE, E., and SRIVASTA, R.: 'Geometrical characterisation of liquid core fibres by measurement of thermally induced mode cutoffs and interferece', Applied Optics, August 1982, Vol 21, No 15, pp 2708-2715.
- 2 SHIBATA, N., TATEDA, M., SEIKAI, S., and UCHIDA, N.: 'Spatial technique for measuring modal delay differences in a dual-mode optical fibre', Applied Optics, May 1980, Vol 19, No 9, ppM1489-1492
- 3 McMILLAN, J.L.: 'Novel techniques for measurement of wavelength of zero relative delay between modes of a dual-mode optical fibre', Electronics Letters, 1983, Vol 19, pp 240-42
- 4 McMILLAN, J.L. and ROBERTSON, S.C.: 'Cutoff wavelength determination in single mode optical fibres by measurement of equalisation wavelength', Electronics Letters, 1984, Vol 20, pp 689-699
- 5 MCMILLAN J.L. and ROBERTSON, S.C.: 'Characterisation of single-mode optical fibres by measurement of equalisation wavelength', Electronics Letters, 1985, Vol 21, pp 295-296
- 6 MARCUSE, D.: 'Loss analysis of single mode fibre splices', Bell Systems Tech., 1977, Vol 56, p 703
- 7 MILLAR, C.A.: 'Direct method of determining equivalent-step-index profiles for monomode fibres', Electronics Letters, 1981, Vol 17, pp 458-460
- 8 ANDERSON, W.: 'Consistency of measurement methods for the mode field radius in a single mode fibre', IEEE Journal of Lightwave Technology, April 1984, LT-2, pp 191-197
- 9 HUSSEY, C.D. and MARTINEZ, F: 'Approximate analytic forms for the propagation characteristics of single-mode optical fibres', Electronics Letters, November 1985, 21, pp 1103-1104

FIGURE 1

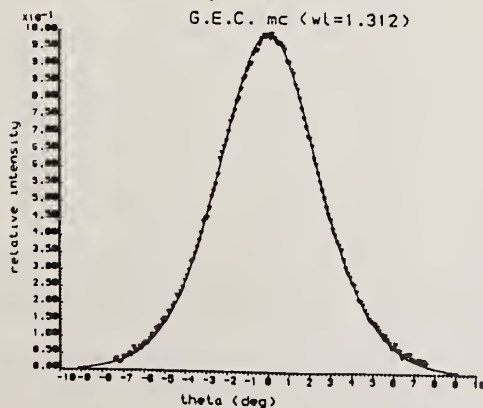


TABLE 1

Fibre: GECMC

Wavelength (nm)	aESI ( $\mu\text{m}$ )	NAESI
1312	4.15	0.1256
1409	4.09	0.1274
1555	4.05	0.1287
1700	4.03	0.1293



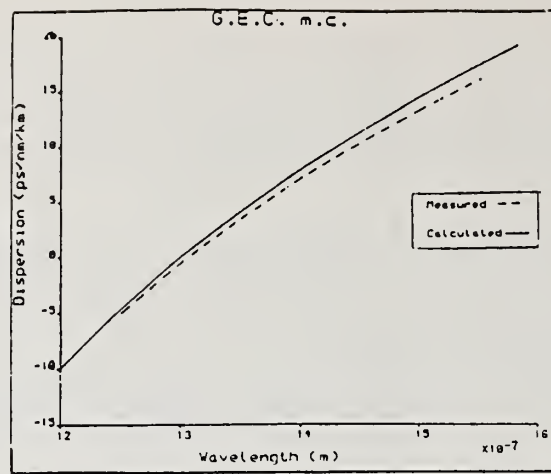


Figure 2

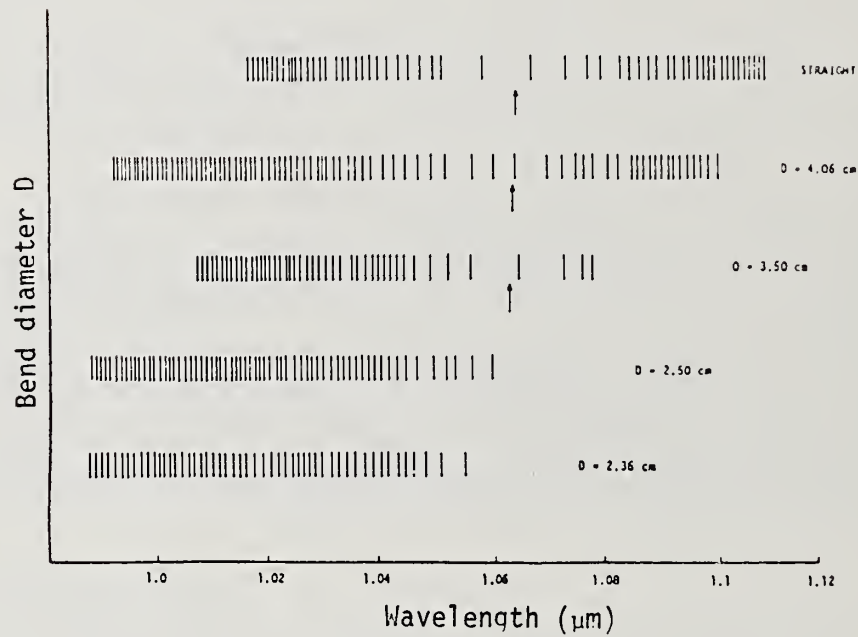


Figure 3

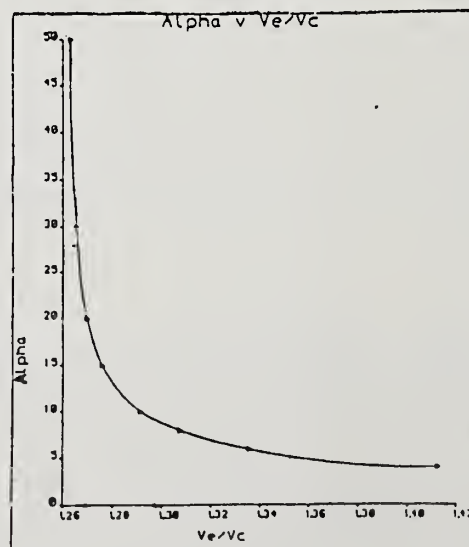


Figure 4

# Impact of Reflection on the Performance of Single-Mode Fiber Optic Systems

*Shuenn Jyi Wang*

Bell Communications Research, Morristown, NJ 07960

## 1. Introduction

The effect of reflection on a laser's characteristics has been discussed in many papers, but only a few articles address the impact of reflection on the performance of fiber optic systems [1,2]. Reflecting surface and laser facet form a cavity that acts as an external resonance cavity for the laser. The resonance cavity changes the laser's lasing wavelength, linewidth, and threshold current, as well as enhances low and high frequency noise[3,4]. All these effects result in output power fluctuation or undulation, mode hopping, and hence degrade signal-to-noise ratio [5-7]. For a single-mode fiber optic system, large reflections can be introduced by connectors that have an air-gap [1,6]. The maximum reflectivity on such connectors is  $4r$  [6], where  $r$  is the single-reflection coefficient between air and the fiber end. For a silica fiber with a refractive index of 1.46,  $r = 3.5\%$ . Therefore, the reflectivity of connectors can vary from 0 to 14% depending on the length of the air-gap. To examine the effect of reflection on fiber optic systems, we introduce different amounts of reflection into the systems, and then measure the systems bit-error-ratio (BER). Twenty-two transmitters operating at various bit rates and employing different kinds of laser diodes were checked. The result shows that the power penalty due to reflection for single-mode fiber optic systems operating up to 570Mb/s could be as high as 1.9 dB for the lasers tested.

## 2. Experiment

Figure 1 illustrates the configuration of the fiber optic systems for the BER measurements. The transmitter usually includes the multiplexers that multiplex several DS3 channels, each corresponding to 44.736 Mb/s, and some overhead bits. The multiplexed signal is scrambled and coded for a 50% duty cycle. The scrambled signal then drives a laser diode that operates either in multi-longitudinal mode at  $1.3\ \mu\text{m}$  or in single-longitudinal mode at  $1.55\ \mu\text{m}$ . A specially designed and calibrated reflection generator is used to control the amount of intended reflection [8]. The reflection generator is made with an attenuator and a segment of fiber with dielectric coating on one end face (see Figure 1). It is then connected directly to the output of the transmitter by a fiber jumper cable three meter in length. The adjustment of the reflection generator changes the reflection amount as well as the forward attenuation. Hence, we use a low reflection attenuator to compensate the adjustment of the reflection generator and control the received power for the BER measurement. To minimize the discrepancy in the power reading due to connect and disconnect, we used a coupler that was characterized before being connected to the power meter and the receiver. Also, the coupler was held stationary until the measurement for a transmitter was finished. During the measurement period, only the knobs of the attenuators were touched so that the polarization and the phase condition could be

preserved. For each transmitter measurement, some arbitrarily chosen DS3 channels are monitored. The performance of these channels were not exactly the same. However, the difference of the BERs was not significant and was consistent during the measurements.

The reflection amount was set at 1%, 6.3%, 15.9% and 22.4% (corresponding to 20, 12, 8, and 6.5 dB of return loss, respectively) in the BER measurement for those transmitters with multi-longitudinal-mode lasers operating at 1.3  $\mu\text{m}$ . The 15.9% reflection is to simulate the case of an air-gap connector near the transmitter. We also took some transmitters' optical spectra corresponding to the above reflection setting to verify the lasing wavelength's drift and the spectral width's change. For one transmitter, we inserted a 40 kilometer fiber between the attenuator and the coupler to produce dispersion result. The measured BER then included the effect of the mode-partition noise that is induced by reflection. For the transmitter with a distributed feed back (DFB) laser working at 1.55  $\mu\text{m}$  region, we measured the BER versus the received power with the reflection set at 1%, 6.3%, and 10%.

### 3. Results

Figure 2 shows the typical BER curves for a single-mode fiber optic system with reflections. Comparing the data for the 15.9% and 1% reflection, we find about 0.05 to 1.9 dB power penalty for various transmitters. We did not control the polarization or the phase of the reflected field in the measurements. For those transmitters that experience less power penalty, the phases or the polarizations of the reflected field and the field in the laser cavity could be less matched. The leftmost curve in Figure 2 is the BER curve without intended reflection, and is measured by removing the reflection generator. We find that, for some transmitters, the system performance with 1% intended reflection is better than that without reflection. A potential cause is that the polarization and/or the phase mismatch between the reflected field and the field in laser cavity results in a weak optical feedback. The weak feedback then reduces some noise and narrows the linewidth of each individual longitudinal mode. It was decided not to compare the data for the system with and without intended reflection, because of the different physical configurations for these two measurements.

Although the root-mean-square (RMS) spectral width and the central wavelength for the systems using a multi-longitudinal mode laser are changed by reflection, these changes are too trivial to affect the dispersion power penalty. On the other hand, the mode-partition noise induced by reflection could be serious [5,9]. Using a long fiber, it is expected to see more dispersion power penalty caused by the induced mode-partition noise. Figure 3 shows 0.45 dB power penalty for a 405 Mb/s single-mode fiber optic system with 15.9% intended reflection and an additional 0.6 dB power penalty when using a 40 kilometer fiber.

All the measured data is summarized in Figure 4. The power penalty due to reflection is defined as the difference between the received powers for a fiber optic system operating at  $\text{BER} = 10^{-8}$  with 1% and 15.9% of reflection. For the system using a DFB laser, the data of 0% and 10% reflections is compared (see Figure 5).



#### 4. Conclusion

It is found that reflection does affect the system performance for a single-mode fiber optic system. From the data it is concluded that;

- a. Different type laser diodes may respond to reflection differently [1]. However, for the same laser diode, the power penalty due to reflection is determined primarily by the condition of "polarization" and "phase" of the reflected field.
- b. The central wavelength's drift and the spectral width's change due to reflection for a multi-longitudinal-mode laser are insignificant. However, the mode-partition noise induced by reflection is not negligible.
- c. For the fiber optic systems operating at higher bit rates, the degradation of the system performance due to reflection becomes more serious.

*Acknowledgment:* The author would like to thank David S. Burpee and Nim K. Cheung for their stimulating discussions, William C. Young for making and calibrating the reflection generator, Edward Cherkassky, Garvey C. Ince, Sunil G. Joshi, and Dan L. Lucas for their help in collecting the data.

#### REFERENCES

1. N. K. Cheung, *SPIE Conference*, Arlington, Virginia (1984).
2. V. J. Mazurczyk, *Electron. Lett.* 17, 143 (1981).
3. M. Fujiwara, K. Kubota and R. Lang, *Appl. Phys. Lett.* 38, 217 (1981).
4. K. Kikuchi and T. Okoshi, *Electron. Lett.* 18, 10 (1982).
5. N. A. Olsson, W. T. Tsang, H. Temkin, N. K. Dutta, and R. A. Logan, *J. Lightwave Technol.* LT-3, 215 (1985).
6. R. E. Wagner and C. R. Sandahl, *Appl. Opt.* 21, 1381 (1982).
7. G. A. Acket, D. Lenstra, A. J. denBoef and B. H. Verbeek, *IEEE JQE-20*, 1163 (1984).
8. W. C. Young et al, to be published.
9. G. P. Agrawal and T. M. Shen, *J. Lightwave Technol.* LT-4, 58 (1986).

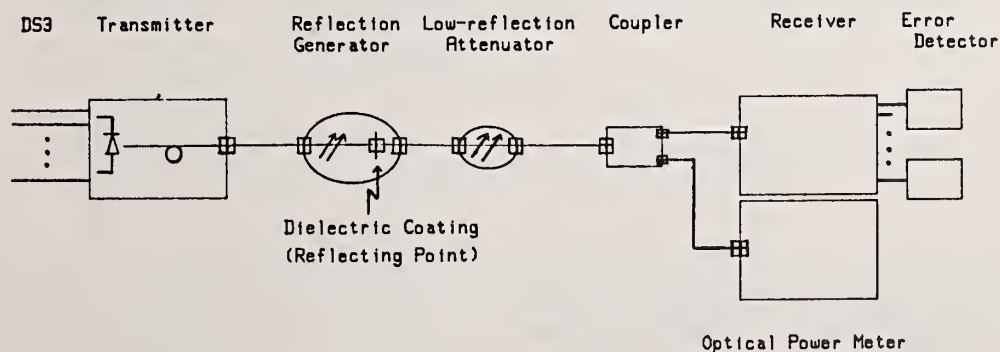


Figure 1

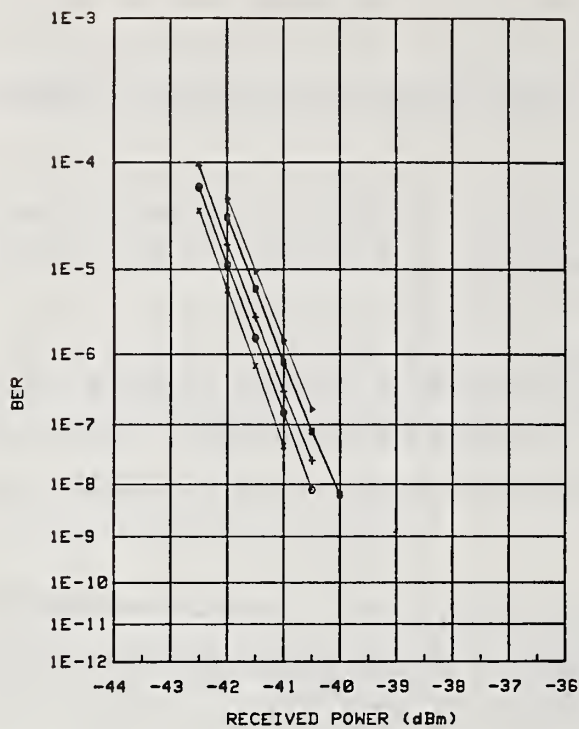


Fig. 2 A typical fiber optic system with 0%(X), 1%(O), 6.3%(+), 15.9%(■), and 22.4%(▲) reflections.

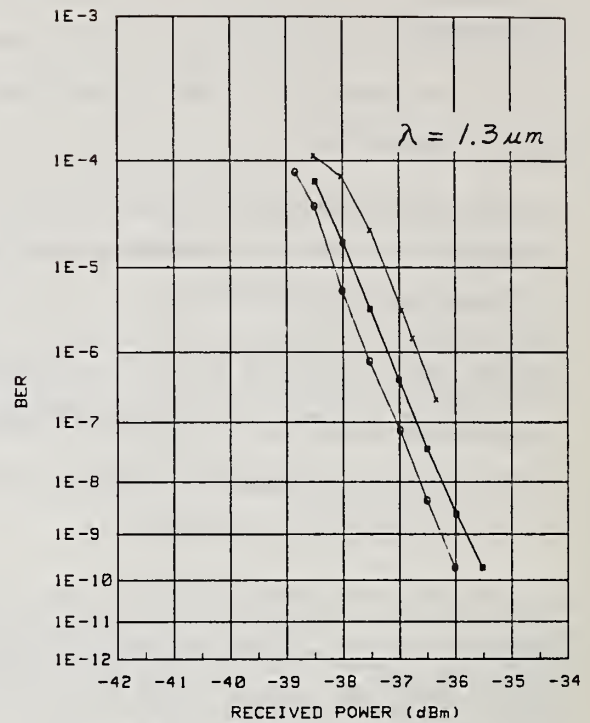


Fig. 3 A 405 Mb/s fiber optic system with 1%(O) and 15%(■) reflections, and (X) using a 40 Km fiber (15.9% reflc.)

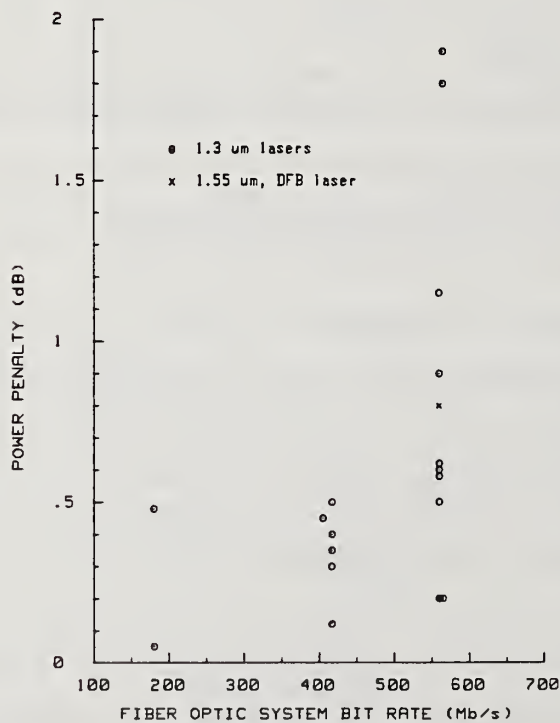


Fig. 4 The power penalty due to reflection for single-mode fiber optic systems.

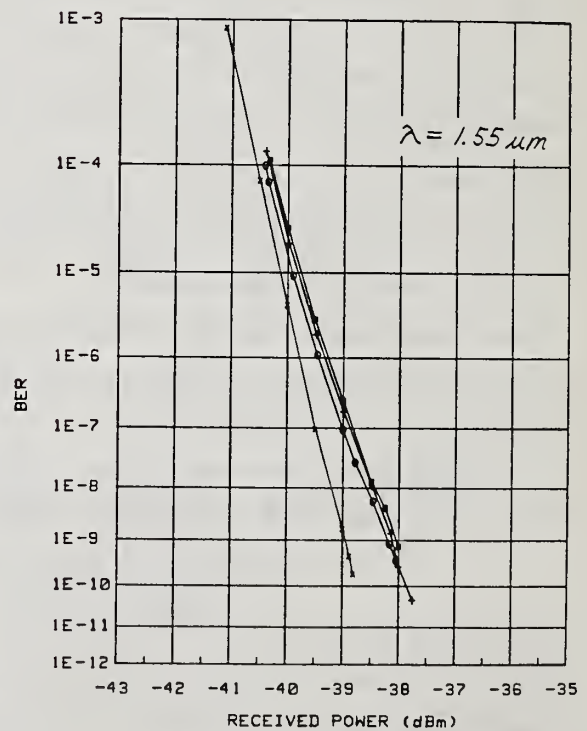


Fig. 5 The fiber optic system using DFB laser with 8%(X), 1%(O), 6.3%(+), and 10%(■) reflections.

## Spurious Edge Elimination for Accurate Glass Geometry Measurements

Devon R. McIntosh and David A. Hall  
Corning Glass Works

One method of performing glass geometry measurements on optical waveguides is to digitize the near-field image of the fiber end using a gray scale analyzer. By defining a certain percentage level of the gray scale value as the transition threshold, fiber image edge coordinates can be determined. These edge coordinates are the data points used in the calculation algorithms suggested by CCITT for glass geometry measurements using such a raster scan. Clad diameter is determined by the diameter of the best-fit circle to the clad edges. Non-concentricity is determined as the distance between best-fit circle centers of the clad and the core; and the radii from these centers are used for noncircularity calculations.

In single mode fibers, due to the step-like changes of the index of refraction, any percentage threshold level can theoretically be used. In practice, the 50% threshold level has given the best results. In multimode fibers, with their associated graded index profile, glass geometry parameters for the core must be defined close to the baseline of the nearfield intensity patterns. At such a low threshold a significant number of spurious edges are detected due to noise or foreign matter causing an unwanted threshold crossing. These edges must be identified and discarded before applying the calculation algorithms in order to maintain acceptable accuracy and repeatability.

A method of identifying these spurious edges has been developed which compares edge locations to a mathematical model of the fiber end and its interaction with the measurement system. This model is based on the following assumptions:

1. The number of edges belonging to the fiber image is more than the number of spurious edges.
2. The image's deviation from circular is either elliptical or oval or some combination of both. (Although the mathematics is derived using this assumption, the results can be used to eliminate spurious edges from other somewhat circular shapes.)
3. This deviation can be modeled by some combination of sinusoids having a period of  $\pi$  and  $2\pi$ .
4. The location of the center of the best-fit circle at the 50% threshold level is a close approximation to the center at the measured level.

Using the above assumptions, all edges belonging to the image of the multimode core can be analyzed for their conformity to the mathematical model. Measurement system error estimates are used to determine the tolerance around the model parameters. Since these parameters can be calculated for each edge; any edge parameter falling outside the tolerance can be discarded.



The mathematical model for determining edge parameters is derived as follows:

Given a data distribution for the core edges as shown in fig. 1 and using the center as stated in assumption 4, the distribution of radii is mapped and the best determined radius,  $R_b$  is determined as shown in fig. 2. For each data point:

$$\text{Let: } f(\theta) = R(\theta) - R_b \text{ (Local deviation from the circle of radius } R_b) \quad (1)$$

$$\text{and: } f'(\theta) = (R(\theta) - R(\theta')) / (\theta - \theta') \text{ (Local slope of the data)} \quad (2)$$

where  $R(\theta)$  and  $R(\theta')$  are adjacent radii and  $(\theta - \theta')$  is the angle separating them in radians.

For purely oval deviations (modeled as a sinusoid with period  $2\pi$  and maximum amplitude  $A_1$ ):

$$f(\theta) = A_1 \sin \theta$$

$$\text{and } f'(\theta) = df(\theta) / d\theta = A_1 \cos \theta.$$

$$\text{Since } (A_1 \sin \theta)^2 + (A_1 \cos \theta)^2 = A_1^2$$

$$\text{then } (f(\theta))^2 + (f'(\theta))^2 = A_1^2. \quad (3)$$

For purely elliptical deviations (sinusoid of period  $2\pi$  and max. amplitude  $A_2$ )

$$f(\theta) = A_2 \sin 2\theta$$

$$\text{and } f'(\theta) = df(\theta) / d\theta = 2A_2 \cos 2\theta.$$

As above:

$$((A_2 \cos 2\theta) / 2)^2 + (A_2 \sin 2\theta)^2 = A_2^2$$

$$\text{and } (f'(\theta) / 2)^2 + (f(\theta))^2 = A_2^2. \quad (4)$$

Since non-circularity deviations will be a linear combination of ellipticity (of maximum magnitude  $a_2$ ) and ovality (of maximum magnitude  $a_1$ ) separated by a phase angle ( $\phi$ );

$$f(\theta) = a_1 \sin \theta + a_2 \sin (2(\theta + \phi)) \quad (5)$$

$$\text{and } f'(\theta) = a_1 \cos \theta + 2a_2 \cos (2(\theta + \phi)) \quad (6)$$

Eqn. (3) then becomes:

$$(f'(\theta))^2 + (f(\theta))^2 = A_1^2(\theta) \quad (7)$$

and Eqn. (4) becomes:

$$(f'(\theta) / 2)^2 + (f(\theta))^2 = A_2^2(\theta) \quad (8)$$

It is important to note that there are now two different definitions for  $f(\theta)$  and  $f'(\theta)$ . Eqn's (1) and (2) give the physically measured definition and Eqn's (5) and (6) give the mathematically modeled definitions. This in turn gives two different definitions for  $A_1^2(\theta)$  and  $A_2^2(\theta)$ . To avoid confusion the subscript m will be used for the mathematically modeled definitions and the subscript p will be used for the physically measured definitions.

An average of  $A_{1p}^2(\theta)$  and  $A_{2p}^2(\theta)$  is needed with which to compare each individual parameter. Therefore let  $A_{1p}^2$  and  $A_{2p}^2$  be the averages of  $A_{1p}^2(\theta)$  and  $A_{2p}^2(\theta)$  respectively.

Spurious edges may now be eliminated by determining the tolerance around  $A_{1p}^2$  and  $A_{2p}^2$  through the propagation of system error estimates.  $A_{1p}^2(\theta)$  and  $A_{2p}^2(\theta)$  must be within this tolerance for an associated edge coordinate to be retained.  $a_1$  and  $a_2$  in Eqn's (5) and (6) are needed for this calculation and are determined as follows:

$$\text{Let: } A_{1m}^2 = 1/2\pi \int_0^{2\pi} A_{1m}^2(\theta) d\theta \quad (\text{Average of } A_{1m}^2(\theta)) \quad (9)$$

$$\text{and } A_{2m}^2 = 1/2\pi \int_0^{2\pi} A_{2m}^2(\theta) d\theta \quad (\text{Average of } A_{2m}^2(\theta)) \quad (10)$$

After substituting Eqn's (5) and (6) into Eqn's (7) and (8), and then into Eqn's (9) and (10), and then integrating; the following results are obtained:

$$a_1^2 = 4.44 (A_{2m}^2 - .4 A_{1m}^2)$$

$$a_2^2 = 1.11 (A_{1m}^2 - 1.6 A_{2m}^2)$$

Given a correspondence between  $A_{2m}^2$  and  $A_{2p}^2$ , and between  $A_{1m}^2$  and  $A_{1p}^2$ , the following is also true:

$$a_1^2 = 4.44 (A_{2p}^2 - .4 A_{1p}^2)$$

$$a_2^2 = 1.11 (A_{1p}^2 - 1.6 A_{2p}^2)$$

The expected tolerance around  $A_{1p}^2$  and  $A_{2p}^2$  comes primarily from three sources; edge detection errors, the estimation of  $R_b$  (Fig. 1 and Fig. 2), and the functional dependence of  $A_{1p}(\theta)$  and  $A_{2p}(\theta)$  on  $\theta$ . The first two sources are measurement errors and can be estimated. The third source can be analytically determined from Eqn's (9) and (10). All three are propagated through the mathematical model (defined by  $a_1$  and  $a_2$ ) to determine tolerances for  $A_{1p}^2$  and  $A_{2p}^2$ .

Let:  $T_{A1}$  = Tolerance around  $A_{1p}^2$   
 $T_{A2}$  = Tolerance around  $A_{2p}^2$

Every retained edge has to satisfy the following inequalities:

$$A_{1p} - T_{A1} \leq A_{1p}(\theta) \leq A_{1p} + T_{A1}$$

$$A_{2p} - T_{A2} \leq A_{2p}(\theta) \leq A_{2p} + T_{A2}$$

Glass geometry parameters are then computed for the cleaned image using the standard algorithms. Repeatabilities on the same order as for single mode fiber have been obtained on multimode fiber using this technique.

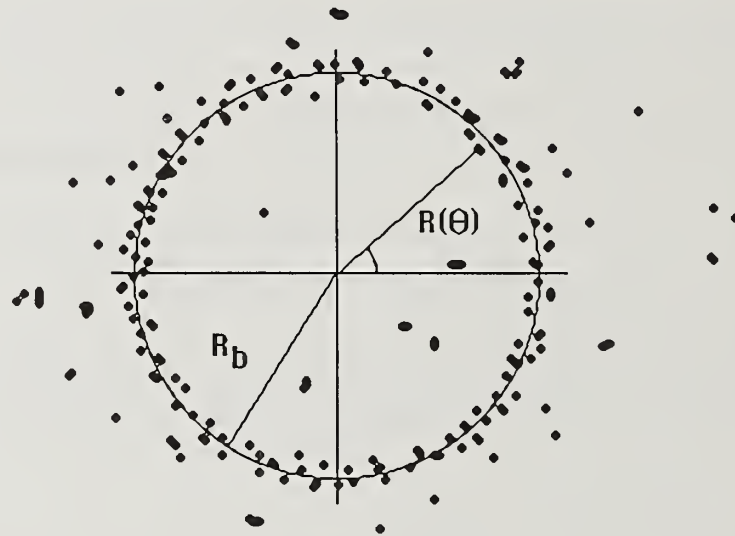


Fig. 1 Collection of core edges at a low threshold level with best determined radius ( $R_b$ ).

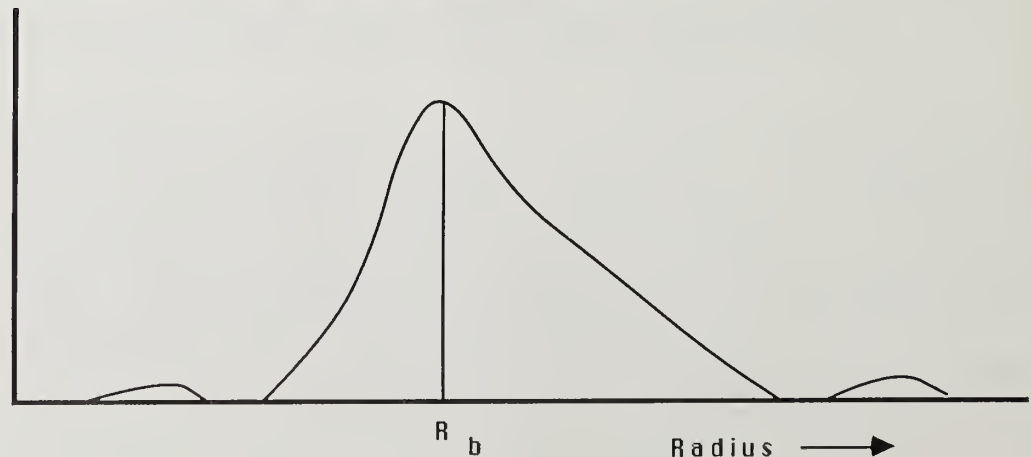


Fig. 2 Distribution of radii with best determined radius ( $R_b$ )



# INDEX OF AUTHORS

W. T. Anderson.....	1,49,65	W. F. Love.....	11
R. C. Alferness.....	115	R. S. Lowe.....	121
R. D. Birch.....	107	P. D. Ludington.....	61
L. Bosselaar.....	15	F. Martinez.....	77
A. C. Boucouvalas.....	137	P. Matthijsse.....	15
M. C. Brain.....	73	D. R. McIntosh.....	145
E. L. Buckland.....	31	E. McNair.....	43
L. Button.....	11	A. R. Mickelson.....	85
M. Calzavara.....	53	F. Mogensen.....	23
C.-T. Chang.....	129	Y. Namihira.....	19
D. N. Christodoulides.....	133	M. Nishimura.....	31
G. Coppa.....	35,53	D. N. Payne.....	77,107
E. A. Cottrell.....	73	D. L. Philen.....	7,27
R. Crotts.....	81	S. B. Poole.....	77,107
L. Curtis.....	57,69	M. Potenza.....	35
H. Damsgaard.....	23	Catherine M. Ragdale.....	97
P. Di Vita.....	35,53	M. R. Ramadas.....	39
C. K. Eoll.....	125	W. A. Reed.....	7
R. Engel.....	43	L. A. Reith.....	133
M. E. Fermann.....	77	S. C. Robertson.....	137
S. Furukawa.....	89	M. A. Saifi.....	133
A. O. Garg.....	125	C. Saravanos.....	121
D. A. Hall.....	145	D. Schickentanz.....	93
O. Hansen.....	23	V. Shah.....	57,69
W. H. Hatton.....	31	M. R. Shenoy.....	39
R. M. Hawk.....	11	M. Tateda.....	89
D. R. Hjelme.....	85	E. A. Thomas.....	65
T. Ito.....	101	K. Thyagarajan.....	39
Y. Iwamoto.....	19	J. F. van Luijk.....	15
W. S. Jackman.....	93	M. P. Varnham.....	107
A. J. Johnson.....	65	I. P. Vayshenker.....	85
Neil Kamikawa.....	129	J. Walker.....	137
F. Kapron.....	81,97	Shuenn Jyi Wang.....	141
J. P. Kilmer.....	49,65	L. Wei.....	121
Y. Koyamada.....	89	Ian A. White.....	61
C. Kozikowski.....	81	Katsuya Yamashita.....	89
G. Kuijt.....	15	W. C. Young.....	57,69
K. Kurumada.....	101		

U.S. DEPT. OF COMM. <b>BIBLIOGRAPHIC DATA SHEET</b> <i>(See instructions)</i>	1. PUBLICATION OR REPORT NO.  NBS / SP-720	2. Performing Organ. Report No.	3. Publication Date  September 1986
4. TITLE AND SUBTITLE  Technical Digest, Symposium on Optical Fiber Measurements, 1986			
5. AUTHOR(S) G. W. Day and D. L. Franzen, Editors			
6. PERFORMING ORGANIZATION <i>(If joint or other than NBS, see instructions)</i>  NATIONAL BUREAU OF STANDARDS DEPARTMENT OF COMMERCE WASHINGTON, D.C. 20234			7. Contract/Grant No.  8. Type of Report & Period Covered
9. SPONSORING ORGANIZATION NAME AND COMPLETE ADDRESS <i>(Street, City, State, ZIP)</i>  Sponsored by the National Bureau of Standards, in cooperation with the IEEE Optical Communications Committee and the Optical Society of America			
10. SUPPLEMENTARY NOTES  Library of Congress Catalog Card Number 86-600563  <input type="checkbox"/> Document describes a computer program; SF-185, FIPS Software Summary, is attached.			
11. ABSTRACT <i>(A 200-word or less factual summary of most significant information. If document includes a significant bibliography or literature survey, mention it here)</i>  This digest contains summaries of 34 papers presented at the Symposium on Optical Fiber Measurements, held September 9-10, 1986, at the National Bureau of Standards, Boulder, Colorado.			
12. KEY WORDS <i>(Six to twelve entries; alphabetical order; capitalize only proper names; and separate key words by semicolons)</i>  fiber optics; instrumentation; measurements; optical fiber; reviews			
13. AVAILABILITY  <input checked="" type="checkbox"/> Unlimited <input type="checkbox"/> For Official Distribution. Do Not Release to NTIS <input type="checkbox"/> Order From Superintendent of Documents, U.S. Government Printing Office, Washington, D.C. 20402.  <input checked="" type="checkbox"/> Order From National Technical Information Service (NTIS), Springfield, VA. 22161			14. NO. OF PRINTED PAGES  158  15. Price







# NBS *Technical Publications*

## *Periodical*

---

**Journal of Research**—The Journal of Research of the National Bureau of Standards reports NBS research and development in those disciplines of the physical and engineering sciences in which the Bureau is active. These include physics, chemistry, engineering, mathematics, and computer sciences. Papers cover a broad range of subjects, with major emphasis on measurement methodology and the basic technology underlying standardization. Also included from time to time are survey articles on topics closely related to the Bureau's technical and scientific programs. Issued six times a year.

## *Nonperiodicals*

---

**Monographs**—Major contributions to the technical literature on various subjects related to the Bureau's scientific and technical activities.

**Handbooks**—Recommended codes of engineering and industrial practice (including safety codes) developed in cooperation with interested industries, professional organizations, and regulatory bodies.

**Special Publications**—Include proceedings of conferences sponsored by NBS, NBS annual reports, and other special publications appropriate to this grouping such as wall charts, pocket cards, and bibliographies.

**Applied Mathematics Series**—Mathematical tables, manuals, and studies of special interest to physicists, engineers, chemists, biologists, mathematicians, computer programmers, and others engaged in scientific and technical work.

**National Standard Reference Data Series**—Provides quantitative data on the physical and chemical properties of materials, compiled from the world's literature and critically evaluated. Developed under a worldwide program coordinated by NBS under the authority of the National Standard Data Act (Public Law 90-396).

NOTE: The Journal of Physical and Chemical Reference Data (JPCRD) is published quarterly for NBS by the American Chemical Society (ACS) and the American Institute of Physics (AIP). Subscriptions, reprints, and supplements are available from ACS, 1155 Sixteenth St., NW, Washington, DC 20056.

**Building Science Series**—Disseminates technical information developed at the Bureau on building materials, components, systems, and whole structures. The series presents research results, test methods, and performance criteria related to the structural and environmental functions and the durability and safety characteristics of building elements and systems.

**Technical Notes**—Studies or reports which are complete in themselves but restrictive in their treatment of a subject. Analogous to monographs but not so comprehensive in scope or definitive in treatment of the subject area. Often serve as a vehicle for final reports of work performed at NBS under the sponsorship of other government agencies.

**Voluntary Product Standards**—Developed under procedures published by the Department of Commerce in Part 10, Title 15, of the Code of Federal Regulations. The standards establish nationally recognized requirements for products, and provide all concerned interests with a basis for common understanding of the characteristics of the products. NBS administers this program as a supplement to the activities of the private sector standardizing organizations.

**Consumer Information Series**—Practical information, based on NBS research and experience, covering areas of interest to the consumer. Easily understandable language and illustrations provide useful background knowledge for shopping in today's technological marketplace.

*Order the above NBS publications from: Superintendent of Documents, Government Printing Office, Washington, DC 20402.*

*Order the following NBS publications—FIPS and NBSIR's—from the National Technical Information Service, Springfield, VA 22161.*

**Federal Information Processing Standards Publications (FIPS PUB)**—Publications in this series collectively constitute the Federal Information Processing Standards Register. The Register serves as the official source of information in the Federal Government regarding standards issued by NBS pursuant to the Federal Property and Administrative Services Act of 1949 as amended, Public Law 89-306 (79 Stat. 1127), and as implemented by Executive Order 11717 (38 FR 12315, dated May 11, 1973) and Part 6 of Title 15 CFR (Code of Federal Regulations).

**NBS Interagency Reports (NBSIR)**—A special series of interim or final reports on work performed by NBS for outside sponsors (both government and non-government). In general, initial distribution is handled by the sponsor; public distribution is by the National Technical Information Service, Springfield, VA 22161, in paper copy or microfiche form.

**U.S. Department of Commerce**  
National Bureau of Standards  
Gaithersburg, MD 20899

Official Business  
Penalty for Private Use \$300